

# **For Reference**

---

**NOT TO BE TAKEN FROM THIS ROOM**



Ex LIBRIS  
UNIVERSITATIS  
ALBERTAENSIS







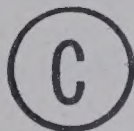






THE UNIVERSITY OF ALBERTA  
LIQUID AND GAS PHASE MASS TRANSFER COEFFICIENTS  
AT BUBBLE FORMATION

by



SUBHASH S. AGGARWAL, B.Tech.

A THESIS

SUBMITTED TO THE FACULTY OF GRADUATE STUDIES  
IN PARTIAL FULFILLMENT OF THE REQUIREMENTS FOR THE DEGREE  
OF MASTER OF SCIENCE IN CHEMICAL ENGINEERING

DEPARTMENT OF CHEMICAL AND PETROLEUM ENGINEERING

EDMONTON, ALBERTA

SPRING, 1971





## UNIVERSITY OF ALBERTA

## FACULTY OF GRADUATE STUDIES

The undersigned certify that they have read, and recommend to the Faculty of Graduate Studies for acceptance a thesis entitled "Liquid and Gas Phase Mass Transfer Coefficients at Bubble Formation" submitted by Subhash S. Aggarwal, B.Tech., in partial fulfillment of the requirements for the degree of Master of Science in Chemical Engineering.





ABSTRACT

Average liquid and gas phase mass transfer coefficients during bubble formation have been determined using the carbon dioxide-water and the ammonia-nitrogen-water systems respectively. The value of the mass transfer coefficient for the CO<sub>2</sub>-water system was found to be about 47 cm./hr. at 25°C which is lower than the values reported for the bubble rise period.

The gas phase mass transfer coefficient for an ammonia-nitrogen feed containing 19 percent by volume ammonia was found to increase with the bubble frequency. The range of frequencies studied was 3 - 10 bubbles/second and the transfer coefficient ranged from 0.25 gm-moles/hr-cm<sup>2</sup>-atm. at 3 bubbles/sec. to 0.32 gm-moles/hr-cm<sup>2</sup>-atm. at 10 bubbles/second.

The geometry of the growing bubble was evaluated in terms of its surface area and volume as a function of time by taking high speed motion pictures of the bubble at 600 frames/second and subsequently using a numerical integration method to calculate the area and volume from the coordinates of a number of points on the bubble periphery. The results obtained were accurate to within  $\pm 2\%$ . The surface area of the growing bubble could be approximated by an equation of the form,

$$A = A_0 + k't$$

where A and A<sub>0</sub> are the surface area of the bubble at time t and time zero respectively, and k' is an empirical constant.





A theoretical model based on the penetration theory and which makes use of the experimentally observed area-time relationship gives a reasonable estimate of the mass transfer occurring under liquid phase controlling conditions during the bubble formation period.





ACKNOWLEDGEMENTS

The author would like to express his appreciation of the critical guidance given by Dr. F. D. Otto who supervised this investigation.

Indebtedness is felt to Mr. H. Kalra from whom much of the experimental technique involved was inherited.

Gratitude is felt towards Mr. D. Sands of Photographic Services, University of Alberta, who helped in developing the photographic technique.

The author is grateful to the staff of the Chemical and Petroleum Engineering Department for their cooperation at all times.

Without the financial aid of the National Research Council of Canada and the Department of Chemical and Petroleum Engineering of University of Alberta this work would not have materialised.





## TABLE OF CONTENTS

<u>TITLE</u>	<u>Page No.</u>
<u>ABSTRACT</u>	(i)
<u>ACKNOWLEDGEMENTS</u>	(iii)
<u>LIST OF FIGURES</u>	1
<u>LIST OF TABLES</u>	2
1. <u>INTRODUCTION</u>	4
2. <u>LITERATURE REVIEW</u>	7
2.1 Effect of Variables on Bubble Behaviour	7
2.1.1 Effect of Gas Flow Rate	8
2.1.2 Effect of Orifice Characteristics	11
2.1.3 Effect of Chamber Volume	12
2.1.4 Effect of Liquid Seal Height	13
2.1.5 Effect of Physical Properties of the Liquid	14
2.1.6 Effect of Liquid Velocity	15
2.2 The Bubble Shape During Growth	15
2.3 Mass Transfer in Continuous Phase	18
2.3.1 Transfer During Bubble Rise	18
2.3.1.1 Experimental Data	18
2.3.1.2 Theoretical Analyses	18
2.3.2 Transfer During Bubble Formation	23
2.4 Mass Transfer in Dispersed Phase	27
2.4.1 General Models	27
2.4.2 Studies During Bubble Formation	32



2.4.3 Mechanisms for Mass Transfer During Drop Formation	34
---	----

### 3. THEORY

3.1 General Theories of Interphase Mass Transfer	36
3.1.1 The Film Theory	36
3.1.2 The Penetration Theory	37
3.2 Continuous Phase Controlled Mass Transfer	40
3.2.1 Mass Transfer Through the Stretching Surface	40
3.2.2 Mass Transfer Through an Interface Expanding by the Formation of Fresh Elements	50

### 4. EXPERIMENTAL

4.1 Choice of Systems	56
4.2 Basis of the Experimental Method	56
4.3 Experimental Set-up	57
4.3.1 Carbon Dioxide-Water System	57
4.3.2 Ammonia-Nitrogen-Water System	60
4.4 The Photographic Technique	60
4.5 The Experimental Procedure	64
4.5.1 The Preparation for Runs	65
4.5.2 The Calibration Run with Air-Water	67
4.5.3 The Photographic Procedure	68
4.5.4 Mass Transfer Runs with Carbon Dioxide-Water System	69
4.5.5 Mass Transfer Runs with Ammonia-Nitrogen-Water System	69
4.5.6 Sample Data Sheets	70





	<u>Page No.</u>
4.6 Analysis of Results	70
4.7 Precautions	78
5. <u>EXPERIMENTAL RESULTS</u>	
5.1 General	81
5.2 Calibration Runs with Air-Water	81
5.3 Mass Transfer Runs with Carbon Dioxide-Water	83
5.4 Mass Transfer Runs with Ammonia-Nitrogen-Water	95
6. <u>DISCUSSION OF RESULTS</u>	
6.1 Carbon Dioxide-Water System	108
6.1.1 Volume of Detached Bubbles	108
6.1.2 Area-Time Relationship for the Growing Bubble	108
6.1.3 Volume-Time Relationship for the Growing Bubble	112
6.1.4 Liquid Phase Mass Transfer Coefficient	112
6.2 Ammonia-Nitrogen-Water System	118
6.2.1 Volume of Detached Bubbles	118
6.2.2 Area-Time Relationship for the Growing Bubble	119
6.2.3 Volume-Time Relationship for the Growing Bubble	119
6.2.4 Gas Phase Mass Transfer Coefficient	119
7. <u>CONCLUSIONS</u>	
7.1 General	123
7.2 Carbon Dioxide-Water System	123
7.3 Ammonia-Nitrogen-Water System	124
<u>NOMENCLATURE</u>	126
<u>BIBLIOGRAPHY</u>	130
A. <u>APPENDIX</u>	





A.1	Calibration of Liquid Flow Rotameters	A-1
A.2	Calibration of Gas Flow Rotameter	A-1
A.3	Calculations for Determining $k_L$ from CO <sub>2</sub> -Water Data	A-1
A.4	Calculations for Determining $k_L$ from NH <sub>3</sub> -N <sub>2</sub> -Water Data	A-7
A.5	Bubble Area and Volume vs. Time Data for the CO <sub>2</sub> -Water System	A-9
A.6	Mass Transfer Coefficients for the NH <sub>3</sub> -N <sub>2</sub> -Water System	A-17



LIST OF FIGURES

<u>TITLE</u>	<u>Page No.</u>
1. Photographs of Bubble Behaviour	16
2. Flowsheet for Carbon Dioxide-Water System	58
3. Flowsheet for Ammonia-Nitrogen-Water System	61
4. Photographic Arrangement	62
5. Typical Curves for Area of a Growing Bubble	91
6. Typical Curves for Volume of a Growing Bubble	94
7. Area of a Growing Bubble for $\text{NH}_3\text{-N}_2\text{-H}_2\text{O}$ System	101
8. Volume of a Growing Bubble for $\text{NH}_3\text{-N}_2\text{-H}_2\text{O}$ System	103
9. Variation of Detached Bubble Volume with Frequency for $\text{NH}_3\text{-N}_2\text{-Water}$ System	105
10. $k_G$ vs. Bubble Frequency for $\text{NH}_3\text{-N}_2\text{-Water}$ System	107
11. Comparison of Areas During Formation for Run M8	110
12. Comparison of Areas During Formation for Run M11	111
13. Liquid Flow Rotameters Calibration Curves	A-3
14. Gas Flow Rotameter Calibration Curve	A-4





LIST OF TABLES

<u>TITLE</u>	<u>Page No.</u>
1. Summary of Available Data on the CO <sub>2</sub> -Water System During Bubble Rise	19
2. Sample Data Sheet for Air-Water System (Run A-2)	71
3. Sample Data Sheet for CO <sub>2</sub> -Water System (Run M-8)	72
4. Sample Data Sheet for NH <sub>3</sub> -N <sub>2</sub> -Water System (Run N-2)	73
5. Results of Calibration Runs	82
6. Initial Mass Transfer Runs With CO <sub>2</sub> -Water	84
7. Range of Variables Studied for CO <sub>2</sub> -Water	86
8. Data for CO <sub>2</sub> -Water Runs	87
9. Results of CO <sub>2</sub> -Water System	88
10. Surface Area of Detached Bubbles for CO <sub>2</sub> -Water System	89
11. Volume of Detached Bubbles for CO <sub>2</sub> -Water System	90
12. Range of Variables Studied for NH <sub>3</sub> -N <sub>2</sub> -Water System	96
13. Data for Ammonia-Nitrogen-Water Runs	97
14. Results of Runs on NH <sub>3</sub> -N <sub>2</sub> -Water System	98
15. Surface Area of Detached Bubbles for NH <sub>3</sub> -N <sub>2</sub> -Water System	99
16. Volume of Detached Bubbles for NH <sub>3</sub> -N <sub>2</sub> -Water System	100
17. Liquid Flow Rotameters Calibration Data	A-2
18. Bubble Area and Volume vs. Time for Run M6	A-10
19. Bubble Area and Volume vs. Time for Run M7	A-11
20. Bubble Area and Volume vs. Time for Run M8	A-12
21. Bubble Area and Volume vs. Time for Run M9	A-13





22. Bubble Area and Volume vs. Time for Run M10	A-14
23. Bubble Area and Volume vs. Time for Run M11	A-15
24. Bubble Area and Volume vs. Time for Run M12	A-16
25. Mass Transfer Coefficients for the $\text{NH}_3\text{-N}_2\text{-Water}$ System	A-17



## CHAPTER 1

### INTRODUCTION

Many industrial applications involve the use of gas-liquid contactors, such as distillation columns, absorption columns, and sparged reactors. A rational design of these units requires a knowledge of the rate of the transfer processes occurring, and to improve our ability to predict the transfer rate it is useful to have an understanding of the fundamental phenomena involved.

Gas-liquid contactors often involve dispersing a gas into a liquid in the form of bubbles. Transfer to or from the bubbles takes place in at least three recognized regions, namely bubble formation, bubble rise, and bubble breakup at the liquid surface.

Although considerable experimental data and theoretical analyses are available for mass transfer during bubble rise, the analysis of transfer during formation has been rather limited. The only reported experimental results for mass transfer during bubble formation are those of Kalra [49] who studied the transfer from carbon dioxide bubbles growing in a moving water phase. His results indicate a higher rate of mass transfer ( $k_L = 100$  to  $225$  cm/hr) occurring in this regime as compared to that obtained during bubble rise ( $k_L \approx 125$  cm/hr). In contrast, Calderbank and Patra [15] have reported no such enhanced rate based on a direct study of mass transfer for carbon dioxide, sulphur dioxide, and acetylene bubbles formed in a stagnant water phase. But they have not given any experimental results. Some other quantitative information has been obtained indirectly by Calderbank [9], Haselden et. al.





[37], Licht et. al. [57, 58], and Dixon et. al. [27] by treating mass transfer during bubble formation as an end effect and has been interpreted to indicate a significant amount (25 - 50%) of the total mass transfer occurring during bubble formation. These authors had extrapolated the bubble rise data to zero liquid height and had assumed it to be applicable to bubble formation.

The above mentioned studies, although limited, were for mass transfer during bubble formation under liquid phase controlling transfer conditions. No investigation is believed to have been undertaken to date for mass transfer from a bubble during its growth when the resistance to transfer lies in the gas phase. However, Calderbank [9], Thorogood [77], and Haselden et. al. [37] have attempted to estimate the mass transfer into a growing bubble from a liquid phase under gas-phase controlled conditions and conclude that a considerable amount (20 - 50%) of the possible transfer may occur during formation of the bubble.

The lack of published data and the presence of uncertainty as to the amount of mass transfer occurring in the bubble formation region justified the study undertaken here. Two systems, namely the carbon dioxide-water system and the ammonia-nitrogen-water system were investigated in a gas-liquid column by using an experimental technique similar in approach to the one described by Kalra [49]. The effect of varying the gas and the liquid flow rate on the transfer coefficient was studied. It is expected that the main resistance to mass transfer is, in the continuous phase for the  $\text{CO}_2$  - water system, and in the dispersed phase for the ammonia-nitrogen-water system.

A review of the theoretical approaches to predicting mass



transfer during formation is given and in some cases modifications are proposed.





## CHAPTER 2

### LITERATURE REVIEW

To analyze mass transfer from gas bubbles during formation it is helpful to have information on the mechanics of bubble formation, and any experimental data available for mass transfer rates, and a theoretical understanding of the transfer process. Comprehensive reviews on bubble phenomenon have been undertaken by Jackson [46], Valentin [80], Calderbank [11], and Kalra [49].

In this literature review an attempt is made to summarize the conclusions of previous workers under the following categories:

- (1) Effect of variables on bubble behaviour
- (2) The bubble shape during growth
- (3) Mass transfer in the continuous phase
- (4) Mass transfer in the dispersed phase.

#### 2.1 Effect of Variables on Bubble Behaviour

The principal factors which might be expected to affect the diameter of a bubble formed at an orifice are:

- (1) the volumetric flow-rate of gas through the orifice
- (2) the orifice diameter
- (3) the gas density and viscosity
- (4) the liquid density and viscosity
- (5) the surface tension
- (6) the wetting properties of the orifice material
- (7) the pressure drop across the orifice



- (8) the chamber volume below the orifice
- (9) the submergence of the orifice
- (10) the shape of the orifice
- (11) the angle of inclination of the orifice; and
- (12) the hydrodynamics of the continuous phase.

Some of these factors are clearly interdependent, for example, the orifice pressure drop is related to the gas flow, the orifice diameter, and the submergence. The effect of some of the above variables is discussed below.

#### 2.1.1 Effect of Gas Flow Rate

As the gas flow rate is increased, four different bubble formation regimes are encountered, namely

- (a) constant volume region
- (b) slowly increasing volume region
- (c) constant frequency (laminar) region; and
- (d) turbulent region.

The change from one region to the other has been characterized in terms of the orifice Reynolds number which is defined as,

$$Re_o = \frac{\rho_d U_o D_o}{\mu_c} \text{-----} (2.1)$$

##### (a) Constant Volume Region

At low gas flow rates ( $Re_o$  upto 100 or 150), the gas bubble forms discretely and slowly at the orifice and is substantially constant in volume. Thus, the frequency of bubble formation is propor-





tional to the gas flow rate. The diameter of the bubble at detachment from the orifice can be calculated by a force balance between the surface tension and the buoyant forces as follows:

Buoyancy force,

$$F_b = (\pi/6) d_f^3 \Delta \rho g \quad \text{-----} \quad (2.2)$$

Surface tension force,

$$F_s = \pi D_o \gamma (\cos \theta_c) \quad \text{-----} \quad (2.3)$$

If the orifice is perfectly wetted by the liquid, then,

$$d_f = (6 D_o \gamma / \Delta \rho g)^{1/3} \quad \text{-----} \quad (2.4)$$

Van Krevelin et. al. [81], Quigley et. al. [69], Hughes et. al. [43], Coppock and Meikeljohn [19], Leibson et. al. [52] and Datta et. al. [22] are in agreement with the above observations.

#### (b) Slowly Increasing Volume Region

This is a transition region for the changeover from the constant volume to the constant frequency (laminar) region. A range of  $Re_o$  of 100 - 300 has been suggested for this region by Valentin [80]. Neither the bubble volume nor the bubble frequency are constant in this region of bubble behaviour. Davidson and Shuler [25] have carried out experiments in this region and report an increasing predominance of the inertial effects. The following equation for bubble diameter is suggested,

$$d_f = \text{const.} (D_o \gamma / \Delta \rho)^{1/3} (\omega \mu_L)^{1/4} \quad \text{-----} \quad (2.5)$$



(c) Constant Frequency (Laminar) Region

With a further increase in gas flow rate ( $Re_o$  about 1,000 to 2,100) the bubble frequency becomes independent of the gas flow rate and approaches a constant maximum value, which is a function of the orifice diameter. The bubble volume, however, increases with increasing gas rate.

Davidson and Amick [24] have reported the value of this constant frequency as 15/sec. for an orifice diameter of 0.32 cm. and Eversole et. al. [28] found the value to be 45/sec. for a 0.02 cm. diameter orifice. The former authors found the following empirical relation to hold for the bubble diameter,

$$d_f = 0.445 (\omega D_o^{0.5})^{0.29} \text{-----} (2.6)$$

where,  $d_f$  = bubble diameter, cm.

$\omega$  = gas flow rate to orifice,  $\text{cm}^3/\text{sec}$ .

$D_o$  = orifice diameter, cm.

(d) Turbulent Region

As the gas flow rate is increased further to a value of  $Re_o$  greater than 2,100 a range of bubble sizes is formed, i.e. bubble break-up or coalescence starts occurring very near the orifice. Very small satellite bubbles of about 5 - 50 micron diameter are produced around the primary bubbles and cause considerable disturbance to the surface of the latter thus enhancing mass transfer. Leibson et. al. [52] and Calderbank [10] worked in the Reynold's number range of



2,100 - 10,000 and are in agreement with this behaviour.

### 2.1.2 Effect of Orifice Characteristics

#### (a) Orifice Diameter

During the constant volume region the bubble size is proportional to the cube root of the orifice diameter as can be visualised from equation (2.4). The size of the bubble will eventually become smaller than the orifice diameter as the orifice size is increased. This causes unstable bubble formation and can result in liquid weeping through the orifice. Davidson and Amick [24] have found that orifices of radius larger than 0.7 cms. could not produce stable bubbles in the constant volume region.

In the constant frequency region Van Krevelin et. al. [81] have reported that the bubble volume is independent of orifice diameter. Davidson and Amick [24], however, found it to vary as 0.43 power of the orifice radius.

#### (b) The Angle of Inclination of the Orifice

Datta, Napier and Newitt [22] from their extensive experimental data found that the bubble size from an inclined orifice was smaller than from a vertical one. This could be explained by the tendency of the buoyancy forces to drag the bubble across the orifice, thus allowing the surface forces to operate over only a portion of it.

#### (c) The Orifice Surface Wettability

This factor is important for preventing liquid leakage through





the orifice. Stable bubble formation requires that the orifice surface be non-wettable by the liquid. Bowman et. al. [8] have used teflon covers on the orifice to improve the non-wettability for cases where liquid leakage occurred due to the orifice diameter being too large.

### 2.1.3 Effect of Chamber Volume

The importance of the chamber volume on bubble behaviour has been emphasized by Hughes et. al. [43], Davidson and Amick [24], Bowman and Johnson [8], Hayes et. al. [38], Leibson et. al. [52] and Mahoney et. al. [62]. The chamber volume is defined as the volume below the orifice to the nearest restriction in the gas line. The bubble stability can be controlled effectively by varying the chamber volume which also affects the volume of bubble. A capacitance number has been defined by Hughes et. al. as,

$$N_c = \frac{4g\Delta\rho V_c}{\pi D_o^2 \rho_d c^2} \text{-----} (2.7)$$

The formation of stable discrete bubbles occurs when  $N_c$  is below a certain critical value. For chamber volumes where  $N_c$  is greater than the critical value the bubble formation becomes unstable and a phenomena referred to as chain bubbling occurs. Davidson et. al. [24] and Hughes et. al. [43] found the bubble behaviour to be independent of  $N_c$  for  $N_c < 0.8$  at low gas flow rates and for  $N_c < 0.2$  at higher flow rates. It also becomes independent of  $N_c$  if very large chamber volumes are used (constant pressure condition).

A different approach to the influence of chamber volume has



been taken by Davidson and Shuler [25, 26], and more recently by Kumar and co-workers [50, 70, 72]. Two limiting cases of bubble formation are defined wherein the chamber volume does not have any significant influence on the stability of bubble formation. They are; a) formation under constant flow conditions, and b) formation under constant pressure conditions. In the former case the flow rate of the gas into the bubble is maintained constant by causing a large pressure drop across the orifice, and in the latter the pressure of the gas below the orifice is maintained constant by using a chamber volume very much greater than the critical value defined in eqn. (2.7). However, it has been shown [25, 26, 50, 70, 72] that the dependence of bubble volume on other variables is different for the two cases. This may account for some of the discrepancies between the results of different workers on the effect of variables on bubble phenomena.

#### 2.1.4 Effect of Liquid Seal Height

Khurana and Kumar [50] have recently investigated the effect of liquid seal height on bubble behaviour both theoretically and experimentally for such chamber volumes that both the pressure inside the chamber and flow rate into the bubble are time dependent. The experiments were conducted for air bubbles in a water-alcohol mixture and air flow rates were varied from 3 cc/sec. to 20 cc/sec. through an orifice of diameter 0.3 cm. Orifice submergence was varied from 15.6 cm. to 128 cm. and two chamber volumes of 65 and 600 cc were studied. They report that the bubble volume reduces exponentially with increase in orifice submergence. Bowman et. al. [8] and Leonard et. al. [54]





have also shown a similar effect.

However, Quigley et. al. [69], Davidson et. al. [24], Coppock and Meikeljohn [19], Hayes et. al. [38], and Towell et. al. [79] have all reported a negligible effect of seal height on bubble formation.

#### 2.1.5 Effect of Physical Properties of the Liquid

Some workers have varied liquid properties considerably in their investigations, but their conclusions are largely contradictory.

Datta et. al. [22] found that the bubble size decreased slowly with increasing liquid viscosity. On the other hand Quigley et. al. [69] observed a slow increase and Davidson et. al. [24] a marked increase. Coppock and Meikeljohn [19] found no effect of viscosity on bubble volume.

An increase in liquid density was found to decrease the bubble size by Coppock et. al. [19], Benzing and Myers [4] and Davidson and Shuler [25]. Contrary to this Quigley et. al. [69] state that it has no effect.

The bubble size was reported to increase with an increase in surface tension by Datta et. al. [22], Coppock and Meikeljohn [19] and Benzing and Myers [4]. However, Quigley et. al. [69] and Siemes et. al. [74] claim that it has no effect. This can perhaps be explained from Davidson and Shuler's results [26] who found that surface tension has a negligible effect when the experiments are carried out under constant flow conditions and high pressure drop, but for constant pressure conditions the effect is appreciable. In other words, surface tension is important only when inertial forces are relatively unimportant.



### 2.1.6 Effect of Liquid Velocity

The experimental data of Sullivan et. al. [76] indicates that the liquid velocity past an orifice does not have any significant effect on the diameter of bubbles. Air bubbles at air-flow rates of 0.5 - 100 cc/sec. through orifice diameters of 0.16 to 0.32 cm. were formed in water flowing at velocities of 0.34 to 2.5 cm./sec. horizontally to the orifice.

### 2.2 The Bubble Shape During Growth

Kalra [49] employed high speed photography to determine the shape of the bubble during its growth from a horizontal orifice and his findings are depicted in Figure 1 which shows a typical bubble during its various stages of formation. The gas bubble oscillates in the axial direction during the initial stages of growth which is due to the break-off of the previous bubble. However, these oscillations cease fairly quickly and the bubble grows steadily and uniformly thereafter in an almost spherical pattern until the volume of the bubble approaches a limiting value. A neck then develops and the bubble begins oscillating in its axial direction, finally breaking off from the orifice. Leibson et. al. [52] have suggested this necking to be due to inward liquid circulation at the level of the orifice. Cine pictures of a bubble growing from an orifice of 0.25 inch diameter as obtained by McCann and Price [60] follow the same general pattern as described above.

The area of the growing bubble as a function of time is required in order to determine the average mass transfer coefficient





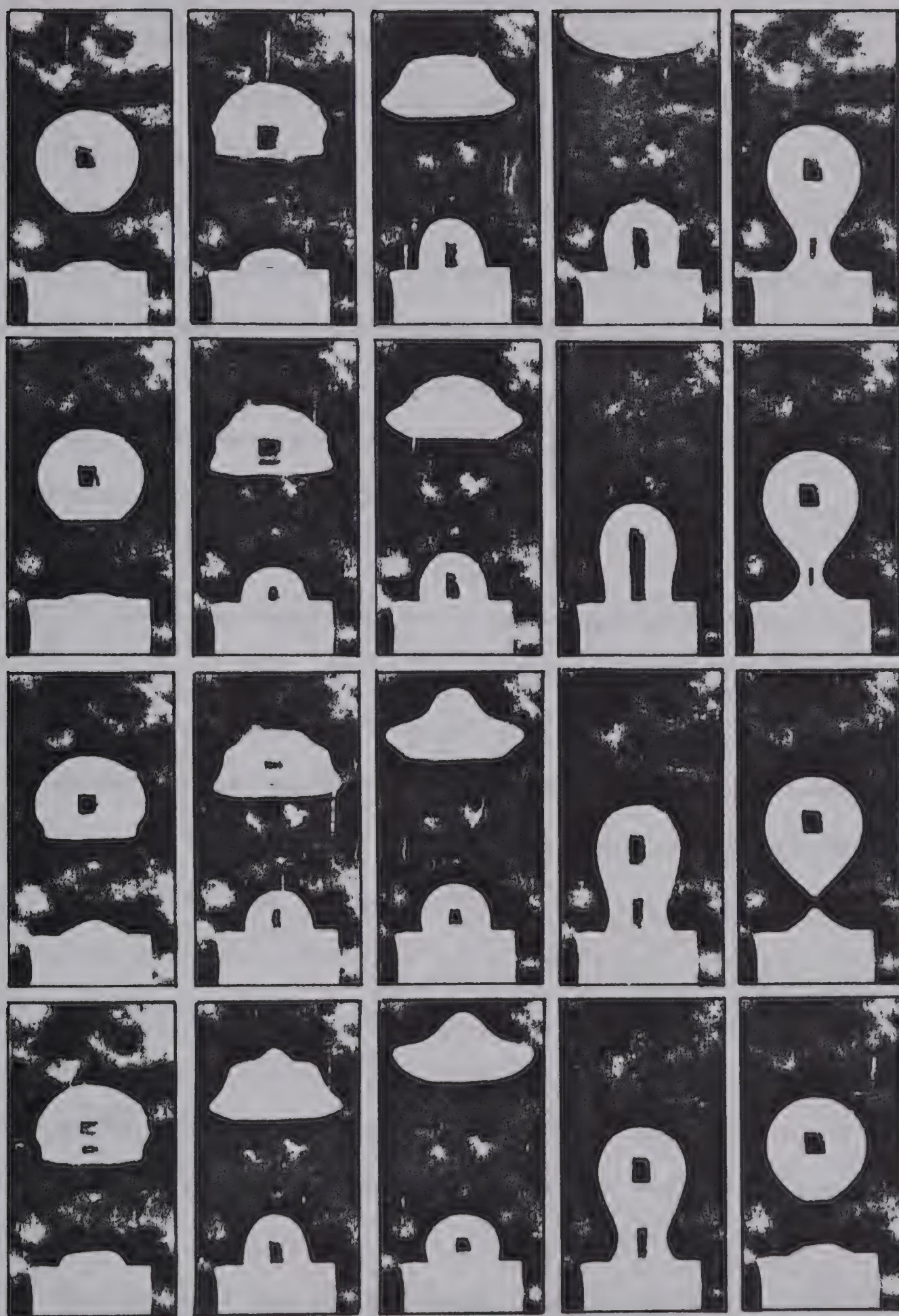


FIG. 1. PHOTOGRAPHS OF BUBBLE  
BEHAVIOUR





during the entire formation regime and has been investigated by Kalra [49], and Calderbank and Patra [15]. Poutanen et. al. [68] and Halligan et. al. [34] have developed equations to describe the bubble profile but these do not predict the variation with time.

From the photographs of bubbles forming at an orifice Kalra [49] evaluated the surface area and volume at various stages of growth by reading the coordinates of various points on the bubble periphery and subsequently using a computer oriented numerical integration approach. His experimental results indicated the area of bubble upto neck formation to follow the relationship

$$A = k_1 t^{0.85} \text{-----} (2.8)$$

where  $k_1$  is a constant.

Calderbank et. al. [15] through a similar frame-by-frame analysis of the cine film records using an analytical projector report an empirical correlation of the type

$$\frac{A}{A_m} = 1 - \left(\frac{t_f - t}{t_f}\right)^{1.86} \text{-----} (2.9)$$

where  $t$  is the time from commencement of bubble formation,  $t_f$  is the total formation time, and  $A_m$  is the maximum area obtained during the bubble growth.

The volume of the bubble varies linearly with time provided the gas flow rate to the orifice is held constant [49].



## 2.3 Mass Transfer in Continuous Phase

### 2.3.1 Transfer During Bubble Rise

#### 2.3.1.1 Experimental Data:

Mass transfer from a bubble rising singly in a liquid has been studied quite extensively and a considerable amount of experimental data are available which are summarized in Table 1 for the carbon dioxide-water system. Considerable scatter in the values of transfer coefficient exists and can be attributed partly to different experimental techniques used by various authors. The bubble rise velocity lies in the range of 20 - 40 cm./sec. depending on the bubble size.

The value of the continuous phase coefficient reaches a maximum as the bubble diameter increases but subsequently decreases with any further increase in bubble diameter. Valentin [80], Zieminski and Raymond [85], and Calderbank et. al. [16] report such a peak for equivalent bubble diameters in the range of 0.1 - 0.4 cm. which may be due to a progressive transition from rigid bubble behaviour to circulating bubble behaviour as the bubble diameter increases. The subsequent fall in the value of transfer coefficient with increase in diameter of the circulating bubble is due to an increase in the value of the contact time.

#### 2.3.1.2 Theoretical Analyses:

Calderbank [11], Redfield and Houghton [71], and Valentin [80] have categorized the analysis of mass transfer during bubble rise as





Reference	Range of Variables			
	Equivalent Bubble Diameter cm.	Temper- ature °C	Bubble Rise Velocity cm./sec.	Continuous Phase Transfer Coefficient cm./hr.
Davenport et. al. [23]	0.4 - 2.2	16	24 - 40	79.0 - 93.5
Baird & Davidson [1]	0.8 - 4.2	20	20 - 40	90.0 - 108.0
Calderbank et. al. [14]	0.5 - 3.0	17 - 23	20 - 30	57.5 - 108.0
Calderbank et. al. [13]	0.2 - 0.8	25	-	25.2 - 288.0
Zieminski et. al. [85]	0.26 - 0.38	25	-	162.0 - 216.0
Bowman & Johnson [8]	0.1 - 0.35	25	23 - 29	119.0
Hammerton & Garner [35]	0.3 - 0.5	16	21 - 24	115.0 - 151.0
Bogandy et. al. [6]	0.26 - 0.48	20	-	108.0 - 205.0
Leonard [53]	0.5 - 1.5	25	20 - 25	64.8 - 79.0
Guyer & Pfitser [33]	0.2 - 0.5	25	-	108.0 - 126.0
Calderbank et. al. [16]	0.2 - 4.0	25	20 - 35	54.0 - 108.0
Himmelblau et. al. [42]	0.5 - 0.8	32	-	101.0 - 147.5

Table 1: Summary of Available Data on the CO<sub>2</sub> - Water System During Bubble Rise



follows:

- (a) transfer from rigid spheres
- (b) transfer from circulating spheres.

Small bubbles below about 0.1 cm. are considered to have no internal circulation and consequently do not have any velocities at the interface. On the other hand large bubbles have a mobile interface because of the fluid inside them being under constant circulation. This internal circulation is caused by viscous forces between the two fluid phases.

Mass transfer from each of the above mentioned categories is generally analyzed for different magnitudes of the Reynolds number which is defined as,

$$Re = \frac{d_f U \rho_L}{\mu_L} \text{-----} (2.10)$$

where  $d_f$  = equivalent diameter of bubble

$U$  = terminal velocity of rise of bubble

$\rho_L$  = continuous phase density

$\mu_L$  = continuous phase viscosity.

### Solid Spheres:

Levich [55] obtained the following equation for creeping flow around a solid sphere ( $Re < 1$ ) by assuming a thin concentration boundary layer ( $100 < Pe < 1000$ ) in the continuous phase.

$$Sh = 1.01 Pe^{1/3} \text{-----} (2.11)$$



Friedlander [29] and Baird et. al. [2] have also obtained similar results with proportionality constants of 0.89 and 0.99 respectively instead of 1.01.

The Stokes equation can be used for the bubble rise velocity in equation (2.11) and is,

$$U = \frac{184}{\nu} V^{2/3} \text{ ----- (2.12)}$$

where  $\nu$  is the kinematic viscosity of the liquid in centipoise,  $V$  is the bubble volume in c.c., and  $U$  is in cm./sec.

Under conditions where inertial effects can no longer be neglected ( $Re \gg 1$ ) a semi-theoretical approach is usually used. Griffith [31] proposed the following relationship,

$$Sh = 2 + 0.57 Re^{0.5} Sc^{0.35} \text{ ----- (2.13)}$$

As  $Re$  approaches zero, the above equation reduces to Frosseling's equation for steady diffusion from a stagnant sphere which is,

$$Sh = 2 \text{ ----- (2.14)}$$

#### Circulating Spheres:

For creeping flow ( $Re < 1$ ) around a circulating sphere when the assumption of a thin concentration boundary layer ( $Pe \gg 1$ ) holds, Levich [55] obtained





$$Sh = 0.65 Pe^{0.5} \text{ ----- (2.15)}$$

A similar equation has been reported by Ward et. al. [84] for the case when the interface moves quickly with respect to the main stream velocity. However, when the interfacial velocity is a fraction of the main stream velocity, Ward et. al. find that

$$Sh = 1.08 Pe^{1/3} \text{ ----- (2.16)}$$

The dividing line between equations (2.15) and (2.16) is at about  $Pe$  equal to 1,000.

The Hadamard - Rybczynski equation for the terminal velocity in this regime is:

$$U = \frac{126}{v} v^{2/3} \text{ ----- (2.17)}$$

For cases where  $Re \gg 1$  Lochiel and Calderbank [59] assumed the thickness of the velocity boundary layer to be far less than the equivalent spherical radius of the dissolving bubble and the concentration boundary layer to be far thinner than the velocity boundary layer ( $Sc \gg 1$ ). On this basis they derived:

$$Sh = 1.13 (1 - 2.96 Re^{-0.5})^{0.5} Pe^{0.5} \text{ ----- (2.18)}$$

The indicated range of  $Re$  for this equation is 100 to 400.

When  $Re$  is very large equation (2.18) reduces to the Boussinesq



[7] equation for circulating spheres in potential flow,

$$Sh = 1.13 Pe^{0.5} \text{ ----- (2.19)}$$

or,

$$k_L = 1.13 \left( \frac{D_L U}{d_f} \right)^{0.5} \text{ ----- (2.20)}$$

The bubble rise velocity to be used in equations (2.19) and (2.20) is derived by Levich [55] and is,

$$U = \frac{42}{v} v^{2/3} \text{ ----- (2.21)}$$

For gas bubbles in liquids Higbie [41] suggested that the mean exposure time of the elements of interface can be taken as the time for the bubbles to rise through a distance equal to their vertical diameter. With this assumption equation (2.20) becomes the familiar Higbie equation,

$$k_L = 2 \sqrt{\left( \frac{D_L}{\pi t_e} \right)} \text{ ----- (2.22)}$$

### 2.3.2 Transfer During Bubble Formation

The study of mass transfer during bubble formation has been rather limited. The only reported experimental results are those of Kalra [49] for carbon dioxide bubbles in water which indicate an enhanced rate of mass transfer ( $k_L = 100$  to  $225$  cm./hr.) in comparison to that during bubble rise ( $k_L = 125$  cm./hr.) for the same equivalent bubble diameter. Calderbank and Patra [15] have reported that the





average liquid-phase mass transfer coefficient during the formation of a bubble at a submerged orifice is less than the value observed during its subsequent ascent but have not given any experimental results. Some other quantitative information has been obtained indirectly by Calderbank [9], Haselden et. al. [37], Licht et. al. [57, 58] and Dixon et. al. [27] by treating mass transfer during bubble formation as an end effect and has been interpreted to indicate a significant amount (25 - 50%) of the total mass transfer occurring during bubble formation. These authors had extrapolated the bubble rise data to zero liquid height and had assumed it to be applicable to bubble formation. The only other experimental studies have been on mass transfer during drop formation.

Popovich et. al. [67] have shown that the models proposed for mass transfer into the continuous phase from a growing drop by Licht and Pansing [58], Heertjes et. al. [40], Groothuis and Kramers [32], Ilkovic [44, 45] and Michels [64] can all be expressed by the general equation

$$N' = \beta k_1 t_f^{[(2k_2+1)/2]} \sqrt{(D/\pi)} (C_1 - C_o) \text{ ----- (2.23)}$$

where the variation of drop area with time is given by

$$A = k_1 t^{k_2} \text{ ----- (2.24)}$$

and the variables are defined as:

$N'$  = mass transferred during bubble formation per unit area



$k_1$  = empirical constant

$k_2$  = empirical constant

$t_f$  = formation time

$\beta$  = empirical constant

The value of  $\beta$  in equation (2.23) takes different values depending on the mechanism assumed. Popovich et. al. found their experimental data on liquid drops to correspond to Ilkovic's model. The value of  $\beta$  is 1.31 for this model provided spherical drop growth is assumed. In other words when  $k_1 = \pi d_f^2 t_f^{-2/3}$ , and  $k_2 = 2/3$ , where  $d_f$  is the drop diameter at the end of formation period.

However, the shape of bubbles forming at an orifice is generally less nearly spherical than liquid drops and hence the applicability of the analogy with liquid drops is uncertain.

Calderbank and Patra [15] studied the mass transfer during bubble formation for carbon dioxide, acetylene and sulphur dioxide bubbles in water. They proposed an empirical correlation for the variation of bubble surface area with time which was given as equation (2.9). It was assumed that each freshly formed element of surface is segregated from older elements. Using the theory for diffusion into a semi-infinite body Calderbank et. al. derived the following equation for the quantity of material dissolved during bubble formation:

$$N''(t_f) = 1.56 (C_i - C_o) A_m t_f^{0.5} \sqrt{\left(\frac{D_L}{\pi}\right)} \quad \text{-----} \quad (2.25)$$

The average mass transfer coefficient was calculated by assuming that the quantity of material transferred as given by equation (2.25) is



the same as would be dissolved if the bubble was formed instantaneously and remained at its maximum size for a time  $t_f$ . This implies

$$N''(t_f) = k_L A_m t_f (C_1 - C_o) \quad \text{-----} \quad (2.26)$$

From equations (2.25) and (2.26),

$$k_L = 1.56 \sqrt{\left(\frac{D_L}{\pi t_f}\right)} \quad \text{-----} \quad (2.27)$$

All of the experimental results of Calderbank and Patra [15] with carbon dioxide and acetylene bubbles in distilled water agreed well with equation (2.27).

Mass transfer coefficients during bubble formation and bubble rise can be compared from equations (2.20) and (2.27). One obtains

$$\frac{k_L \text{ (formation)}}{k_L \text{ (rise)}} = 0.78 \sqrt{\left(\frac{d_f}{U t_f}\right)} \quad \text{-----} \quad (2.28)$$

If ' $\ell$ ' is assumed to be the vertical distance between rising bubble centres, then for discrete bubble formation from the orifice,

$$\ell = U t_f \quad \text{-----} \quad (2.29)$$

and equation (2.28) becomes,

$$\frac{k_L \text{ (formation)}}{k_L \text{ (rise)}} = 0.78 \sqrt{\left(\frac{d_f}{\ell}\right)} \quad \text{-----} \quad (2.30)$$





Hence the mass transfer coefficient during bubble formation as defined by equation (2.26) is always lower than that during bubble rise as  $(d_f/\ell)$  is less than one if there is no bubble coalescence at the orifice.

Beek and Kramers [3] have analyzed the mechanism of mass transfer from an expanding spherical surface when the resistance to mass transfer lies in the continuous phase. They assumed that circulation existed inside the growing surface and that the increase in surface occurred by stretching of the surface. For the case where the depth of penetration could be considered small compared to the radius of the cavity, they derived the following expression for the amount transferred during formation:

$$m_f = 4 \sqrt{(\pi)} 3^{1/6} \frac{6}{(7+4p)^{1/2}} C_i D^{1/2} a_p^{2/3} t_f^{(7+4p)/6} \quad (2.31)$$

when  $\frac{a_p^2 t^{2p-1}}{D^3} \gg 1$ , and the radius of the bubble at any time is expressed as,

$$R(t) = (3 a_p t^{p+1})^{1/3} \quad (2.32)$$

## 2.4 Mass Transfer in Dispersed Phase

### 2.4.1 General Models

The mechanism of internal mass transfer has been discussed by Newman [66], Kronig and Brink [51], Crank [20], Harriott [36], Skelland and Wellek [75], Miller [65], Johns et. al. [47], Thorogood



[77], and Calderbank [11].

The simplest model is Newman's [66] who studied the drying of porous solids, spherical in shape, during that portion of the drying time in which the surfaces are substantially dry and evaporation takes place as rapidly as liquid can diffuse from the interior of the surfaces. He expressed the differential equation for unsteady state diffusion across a shell of thickness,  $\partial r$ , within the sphere at radial position,  $r$ , as

$$\frac{\partial c}{\partial t} = D_G \left( \frac{\partial^2 c}{\partial r^2} + \frac{2}{r} \frac{\partial c}{\partial r} \right) \text{-----} (2.33)$$

where  $D_G$  is the diffusivity in the dispersed phase, and  $c$  is the concentration at radial position,  $r$ , at time,  $t$ .

The following boundary conditions were specified:

- (a) the initial liquid concentration is uniform throughout the solid, i.e.  $C = C_0$  at  $t = 0$  and  $0 < r < R$ .
- (b) the liquid concentration on the surface falls to the equilibrium value immediately at the start of the drying, i.e.  
 $C = C_1$  at  $t > 0$  and  $r = R$ .

With these conditions Newman expressed the solution of equation (2.33) as,

$$\frac{C - C_1}{C_0 - C_1} = \frac{2R}{\pi r} \sum_{n=1}^{\infty} \frac{(-1)^n}{n} \sin \frac{n\pi r}{R} \exp (-D_G n^2 \pi^2 t / R^2) \text{-----} (2.34)$$

If the average concentration at a time,  $t$ , in the sphere is  $C_t$ ,





then the expression for the fractional approach to equilibrium,  $E$ , could be deduced and is,

$$E = \frac{C_o - C_t}{C_o - C_1} = 1 - \frac{6}{\pi^2} \sum_{n=1}^{\infty} \frac{1}{n^2} \exp(-n^2 D_G \pi^2 t / R^2) \quad (2.35)$$

Crank [20] has also derived a similar equation for diffusion into or from a sphere.

Calderbank [11] assumed the first term of the series in equation (2.35) only to be significant for values of  $E$  greater than 0.4 (long contact times) and obtained,

$$E = 1 - \frac{6}{\pi^2} \exp(-\pi^2 D_G t / R^2) \quad (2.36)$$

By defining  $k_G$  as

$$k_G a' t = -\ln(1-E) = k_G \left(\frac{3}{R}\right) t \quad (2.37)$$

where  $a'$  is the interfacial area per unit volume of dispersed phase, Calderbank derived an approximate equation for  $k_G$ , which is

$$k_G = (1/3) \frac{\pi^2 D_G}{R} \quad (2.38)$$

For values of  $E$  less than 0.4 (short contact times) Calderbank showed that

$$E = \frac{6}{R} \sqrt{\left(\frac{D_G t}{\pi}\right)} \quad (2.39)$$



and approximated equation (2.37) as,

$$-\ln(1-E) = E = k_G \left(\frac{3}{R}\right)t \quad \text{-----} \quad (2.40)$$

From equations (2.39) and (2.40) he obtained

$$k_G = 2 \sqrt{\left(\frac{D_G}{\pi t}\right)} \quad \text{-----} \quad (2.41)$$

where  $t$  is the total residence time of the dispersed phase in the phase contacting equipment.

Geddes [30] also defined  $k_G$  as in equation (2.37) and assumed only the first term of the series expansion in equation (2.35) to be significant. Thus he obtained,

$$k_G = -\frac{R}{3t} \ln \left( \frac{6}{\pi^2} \exp \frac{-D_G \pi^2 t}{R^2} \right) \quad \text{-----} \quad (2.42)$$

where  $t$  is the gas contact time.

Kronig and Brink [51] have considered the effect of internal circulation on the extraction of a substance from a spherical drop falling in a stagnant fluid, and have derived the following equation for the efficiency of mass transfer, by assuming the concentration of the diffusing substance, and the resistance to mass transfer in the continuous phase to be negligible.

$$E = \frac{C_o - C_t}{C_o - C_i} = 1 - \frac{3}{8} \sum_{n=1}^{\infty} A_n^2 \exp - \left( \frac{16 \lambda_n D_G t}{R^2} \right)$$



where  $A_1 = 1.32$ ,  $A_2 = 0.73$

$$\lambda_1 = 1.678, \lambda_2 = 9.83$$

This equation has been accurately represented empirically by Calderbank and Korchinski [12] as,

$$E = [1 - \exp(-2.25 D_G \pi^2 t / R^2)]^{1/2} \quad \text{-----} \quad (2.43)$$

Vermeulen [82] presented an accurate representation of equation (2.35) by

$$E = 1 - \exp(-\pi^2 D_G t / R^2)^{1/2} \quad \text{-----} \quad (2.44)$$

By comparing equations (2.43) and (2.44) it becomes apparent that the Kronig and Brink model of internal circulation results in an effective diffusion coefficient of 2.25 times the molecular value. Calderbank [11] and Miller [65] report a similar observation.

Experimental internal drop transfer rates have been found to vary from the rigid sphere characteristic for highly viscous liquids up to three or four times the Kronig and Brink rate for fluids of low viscosity by Calderbank and Korchinski [12], McDowell and Meyers [61], Skelland and Wellek [75], Heertjes et. al. [40], and Johnson and Hamielec [48].

Mehta and Sharma [63] studied the gas phase mass transfer resistance of a chain of bubbles and found  $k_G a$  to be proportional to  $D_G^{0.5} \omega^{0.75} H^{0.33}$ , where  $\omega$  is the gas flow rate and  $H$  is the height of the liquid seal.





### 2.4.2 Studies During Bubble Formation

Calderbank [9], Thorogood [77], and Haselden et. al. [37] are believed to be the only ones who have tried to isolate the mass transfer into a growing bubble from a continuous phase under gas-phase controlled conditions.

Calderbank [9] assumed that as the bubble is formed from the orifice, concentration gradients which may be set up at the interface never extend to the centre of the bubble, since this is continuously being fed with fresh gas. Thus it was permissible to use the Higbie's penetration theory for diffusion into a semi-infinite body, i.e.

$$k_G = 2 \sqrt{\left(\frac{D_G}{\pi t'}\right)} \text{ ----- (2.45)}$$

where  $t'$  is the mean age of the interface.

Since there is a high degree of circulation within the bubble  $t'$  is some small fraction of the total time  $t$  from the commencement of bubble formation. Calderbank [9] assumed this fraction to be  $\left(\frac{1}{x} \cdot t\right)$  and thus expressed the variation of the gas phase transfer coefficient during the life span of the forming bubble as

$$k_G = 2 \sqrt{\left(\frac{x D_G}{\pi t}\right)} \text{ ----- (2.46)}$$

where  $x$  is a constant characteristic of the system, e.g.,  $x = 1$  for transfer from a rising gas bubble under continuous phase controlled diffusion.

On this basis Calderbank [9] derived an expression for the



maximum efficiency attainable during bubble formation when the bubble could be assumed spherical and when bubble volume increased regularly with time. The latter condition implied that flow rate of gas to the centre of the bubble was constant. The equation is

$$E = \frac{C_o - C_f}{C_o - C_i} = \frac{P t_f^{1/6}}{(1+P t_f^{1/6})} \quad \text{-----} \quad (2.47)$$

where  $P = \frac{6(x D_G/\pi)^2}{[\frac{3}{4}\pi\omega]^{1/3}}$ ,  $t_f$  is the

formation time of bubble, and  $\omega$  is the flow rate of fresh gas to the bubble.

Thorogood [77] has modified Calderbank's above mentioned approach for the case when the flow rate of the gas into the bubble increases as the bubble grows in size. He assumed the level of turbulence inside the bubble to remain constant during the bubble growth and consequently represented  $k_G$  during formation as,

$$k_G = 2 \sqrt{\left(\frac{D_{EG}}{\pi t_f}\right)} \quad \text{-----} \quad (2.48)$$

where  $D_{EG}$  is effective gas phase diffusivity and  $t_f$  is the time of formation.

He also assumed the height of the top of the bubble above the surface of the orifice to be proportional to the time elapsed from the commencement of bubble growth and derived the expression for efficiency as:

$$E = \frac{2 k_G}{2 k_G + (dh/dt)} \quad \text{-----} \quad (2.49)$$





where  $h$  is the height of bubble at any time.

Thorogood's [77] assumption of the height of the bubble increasing at a constant rate has been supported experimentally by Haselden and Thorogood [37] who studied the distillation of the oxygen-nitrogen-argon system on a perforated plate.

There are indications that a significant amount of mass transfer may be occurring in the bubble formation regime. Calderbank [9] carried out experiments on evaporation rates of water and some organic liquids into air wherein air was present as the dispersed phase and obtained the mass transfer at zero submergence by extrapolation. The amount of transfer was considerable and was interpreted as occurring during bubble formation. Haselden and Thorogood [37] calculated the mass transfer during bubble formation as the difference in vapour feed rate and the computed vapour throughput from the observed bubble sizes at detachment and the bubble frequency, and concluded that 20 - 50% of the possible transfer may occur during formation of the bubble.

#### 2.4.3 Mechanisms for Mass Transfer During Drop Formation

Heertjes and de Nie [39] have proposed two models for the mechanism of mass transfer to drops during formation when the resistance in the continuous phase is negligible. Both of these are based on no internal circulation in the drop and are applicable when the relationship between area and volume of a drop at any time follows the equation:

$$A(t) = B \cdot V(t) + A_0 \quad \text{-----} \quad (2.50)$$



where  $A(t)$  and  $V(t)$  are the surface area and volume respectively for the drop at any time  $t$ ,  $A_o$  is surface of the restdrop, and  $B$  is a proportionality factor independent of the flow rate and time but dependent on the orifice diameter.

Also, mass transfer is assumed to take place by unsteady state diffusion into a semi-infinite medium.

The first model assumes mass transfer through a stretching surface and results in

$$E = \left(\frac{7}{3}\right)^{1/2} \left[ \frac{2A_o}{V(t_f)} + \frac{2}{3} B \right] \left( \frac{Dt_f}{\pi} \right)^{1/2} \text{-----} (2.51)$$

where  $E$  is defined as the efficiency of mass transfer and is equal to actual mass transferred divided by the total possible mass transfer.

The second model assumes mass transfer through a surface expanding by the formation of fresh elements such that there is no mixing between elements of different age and predicts the efficiency of transfer as:

$$E = \left[ 2 \frac{A_o}{V(t_f)} + \frac{4}{3} B \right] \left( \frac{Dt_f}{\pi} \right)^{1/2} \text{-----} (2.52)$$

Groothius and Kramers [32] have also derived a result analogous to (2.52) but have not considered the effect of the restdrop.

The experimental results of Heertjes et. al. [39] and Groothius et. al. [32], on transfer to isobutanol drops in water and sulphur dioxide absorption by water drops respectively, are in fair agreement with the values predicted from equation (2.52).



## CHAPTER 3

### THEORY

#### 3.1 General Theories of Interphase Mass Transfer

The various mass transfer mechanisms which have been postulated are based on Fick's laws for diffusion processes. Fick's first law is applicable for steady state conditions and is,

$$N_A = - D \left( \frac{\partial c_A}{\partial Z} \right) \text{-----} (3.1)$$

Fick's second law for unidirectional diffusion applies to unsteady state mass transfer and can be written as,

$$\frac{\partial c}{\partial t} = D \left( \frac{\partial^2 c}{\partial Z^2} \right) \text{-----} (3.2)$$

Both of these laws are applicable when there is no fluid motion.

##### 3.1.1 The Film Theory

The film theory was first proposed by Lewis and Whitman [56] in 1924 and the basic concept involves occurrence of mass transfer into or out of a moving fluid phase by molecular diffusion through a thin film of stagnant fluid at the phase boundary. Mass transfer through the stagnant film is presumed to be considerably slower than in the bulk phase and controls the overall transfer rate. Steady state mass transfer is assumed to take place and the diffusion is assumed to





occur only in a direction perpendicular to the interface.

With these assumptions Fick's first law holds and equation (3.1) on integration yields,

$$\bar{N}_A = \frac{D}{\delta} (C_1 - C) \quad \text{-----} \quad (3.3)$$

Defining the mass transfer coefficient as,

$$\bar{N}_A = k (C_1 - C) \quad \text{-----} \quad (3.4)$$

one obtains from a comparison of equations (3.3) and (3.4),

$$k = \frac{D}{\delta} \quad \text{-----} \quad (3.5)$$

where,  $D$  and  $\delta$  are molecular diffusivity and stagnant film thickness respectively.

### 3.1.2 The Penetration Theory

The penetration or surface renewal theory was introduced by Higbie [41] in 1935. The key difference between the film theory and this theory is the applicability of the latter for unsteady state transfer processes. The main assumptions are:

- (a) discontinuous contact between phases
- (b) fresh fluid is brought to the phase boundary for each new contact and the length of time each new element of fluid remains at the interface is constant.



- (c) the fluid, during the period of contact, remains quiescent, and mass transfer occurs by molecular diffusion in a direction perpendicular to the interface.
- (d) the fluid field is semi-infinite in depth
- (e) the transfer is entirely by molecular diffusion.

Fick's second law (equation 3.2) applies and the conditions required for solving are:

- (i) the initial concentration of the absorbing material is uniform throughout the fluid;

$$C(Z,0) = C_o$$

- (ii) the concentration of dissolved material deep in the fluid remains constant at the initial concentration;

$$C(\infty, t) = C_o$$

$$\left(\frac{\partial C}{\partial Z}\right)_{Z \rightarrow \infty} = 0$$

- (iii) the concentration of solute is constant at the interface;

$$C(0, t) = C_i$$

The solution of equation (3.2) is,

$$\frac{C - C_o}{C_i - C_o} = \operatorname{erfc} \frac{Z}{2 \sqrt{Dt}} \quad \text{-----} \quad (3.6)$$





If concentration in equation (3.6) is differentiated with respect to  $Z$ , and the differential is evaluated at  $Z = 0$ , the result, when multiplied by molecular diffusivity,  $D$ , yields for the instantaneous mass flux for solute crossing the phase boundary,

$$N_A(t) = \sqrt{\left(\frac{D}{\pi t}\right)} (C_i - C_o) \quad \text{-----} \quad (3.7)$$

When this expression is averaged over time of exposure, which Higbie assumed to be a constant for all the fluid elements contacting a phase boundary, the result is

$$\bar{N}_A = 2 \sqrt{\left(\frac{D}{\pi t}\right)} (C_i - C_o) \quad \text{-----} \quad (3.8)$$

The total amount of solute absorbed in time  $t$  can be expressed as

$$I = \bar{N}_A t a = \bar{k} a (C_i - C_o) t \quad \text{-----} \quad (3.9)$$

Equations (3.8) and (3.9) give,

$$\bar{k} = 2 \sqrt{\left(\frac{D}{\pi t}\right)} \quad \text{-----} \quad (3.10)$$

where,  $t$  is the exposure time of fluid elements. For a bubble, of diameter  $d_f$  rising in a liquid with a velocity  $U$ , this exposure time is often taken as,

$$t = \frac{d_f}{U} \quad \text{-----} \quad (3.11)$$



### 3.2 Continuous Phase Controlled Mass Transfer

To analyse the mass transfer in the continuous phase around a growing bubble two models are proposed based on different mechanisms for the expansion of interface. In the first model the surface is assumed to stretch, that is all elements of surface have the same life history, and in the second model the surface is assumed to be composed of elements of different ages but no transfer between these elements is assumed.

#### 3.2.1 Mass Transfer Through the Stretching Surface

This model was initially proposed by Beek and Kramers [3] and an attempt is made to clarify their derivation.

The expanding surface is assumed to grow spherically due to a time dependent source at the origin. The origin of the spherical cavity remains fixed in space throughout the formation period. The only motion of the continuous phase is assumed to be in the radial direction which is a consequence of the surface growth. Further, the concentration of the solute at the interface is presumed to remain constant and far away from the interface the concentration of the same component is zero. Any increase in surface is assumed to occur by stretching and hence all elements of surface are exposed to the continuous phase for the total formation time. The fluid underneath the surface is assumed to move with the velocity of the interface. They assumed that the normal gradient of the tangential velocity is zero at depths where diffusion takes place.

Let the radius of the growing surface at any time be,



$$R(t) = (3 a_p t^{p+1})^{1/3} \quad \text{-----} \quad (2.32)$$

where  $a_p$  is a point source defined as  $(\omega/4\pi)$  in which  $\omega$  is the flow rate into the bubble.

Volume of bubble at time  $t$  is,

$$V = \frac{4}{3} \pi R^3 = 4 \pi a_p t^{p+1} \quad \text{-----} \quad (3.12)$$

The strength of the source is given by,

$$\frac{dv}{dt} = 4 \pi a_p (p+1) t^p \quad \text{-----} \quad (3.13)$$

The equation for the non-steady diffusion taking place outside the surface of the growing cavity is,

$$\frac{\partial c}{\partial t} = \frac{D}{r^2} \frac{\partial}{\partial r} \left( r^2 \frac{\partial c}{\partial r} \right) - v_r \frac{\partial c}{\partial r} \quad \text{-----} \quad (3.14)$$

This equation applies in the region  $r > R$  and for  $p > -1$ . The first term on the right hand side represents the transfer due to molecular diffusion and the second term represents the convective transfer in the radial direction due to the bubble growth.

$v_r$  is the radial velocity at  $r$  from the centre of bubble and can be expressed as,

$$v_r = \frac{dv}{dt} / 4\pi r^2 = \frac{a_p (p+1) t^p}{r^2} \quad \text{-----} \quad (3.15)$$





The boundary conditions are,

$$(i) \quad C = C_1 \text{ at } r = (3 a_p t^{p+1})^{1/3} \text{ for } t \geq 0$$

i.e. the concentration at the interface remains constant.

$$(ii) \quad C = 0 \text{ at } r = \infty \text{ for } t > 0$$

i.e. the concentration of material being absorbed remains zero in the bulk liquid.

$$(iii) \quad C = 0 \text{ at } r > 0 \text{ for } t = 0$$

i.e. the initial concentration of material to be absorbed is zero throughout the liquid.

Introduce the transformation,

$$\rho^3 = r^3 - R^3 \quad \text{-----} \quad (3.16)$$

$r$  is time independent as it refers to the distance of a point outside the bubble surface from the centre of bubble, which does not change with time.  $R$  is the bubble radius and is constantly changing with time. Hence  $\rho$  becomes time dependent.

The radial velocity as expressed in equation (3.15) is measured from a fixed point, namely the centre of bubble. Once the transformation (3.16) is introduced the radial velocity becomes zero as it is now referred to a time dependent variable.

$$\frac{\partial c}{\partial r} = \frac{\partial c}{\partial \rho} \frac{\partial \rho}{\partial r}$$



or,

$$\frac{\partial c}{\partial r} = \frac{\partial c}{\partial \rho} \cdot (\rho^3 + 3a_p t^{p+1})^{2/3} \cdot \frac{1}{\rho^2} \quad \text{-----} \quad (3.17)$$

$$\frac{\partial^2 c}{\partial r^2} = \frac{\partial c}{\partial \rho} \cdot \frac{\partial^2 \rho}{\partial r^2} + \frac{\partial \rho}{\partial r} \cdot \frac{\partial^2 c}{\partial \rho^2} \cdot \frac{\partial \rho}{\partial r}$$

$$\frac{\partial^2 \rho}{\partial r^2} = 2r (r^3 - 3a_p t^{p+1})^{-2/3} - 2r^4 (r^3 - 3a_p t^{p+1})^{-5/3}$$

$$= \frac{2(\rho^3 + 3a_p t^{p+1})^{1/3}}{\rho^2} - \frac{2(\rho^3 + 3a_p t^{p+1})^{4/3}}{\rho^5}$$

$$\begin{aligned} \frac{\partial^2 c}{\partial r^2} &= \frac{\partial c}{\partial \rho} \left[ \frac{2(\rho^3 + 3a_p t^{p+1})^{1/3}}{\rho^2} - \frac{2(\rho^3 + 3a_p t^{p+1})^{4/3}}{\rho^5} \right] \\ &+ \frac{\partial^2 c}{\partial \rho^2} \cdot \frac{1}{\rho^4} (\rho^3 + 3a_p t^{p+1})^{4/3} \quad \text{-----} \quad (3.18) \end{aligned}$$

Equation (3.14) now reduces to:

$$\begin{aligned} \frac{\partial c}{\partial t} &= D \left[ 2 \frac{\partial c}{\partial \rho} \cdot \frac{1}{\rho^2} (\rho^3 + 3a_p t^{p+1})^{1/3} \right] + \frac{\partial c}{\partial \rho} D \left[ \frac{2(\rho^3 + 3a_p t^{p+1})^{1/3}}{\rho^2} \right. \\ &\quad \left. - \frac{2(\rho^3 + 3a_p t^{p+1})^{4/3}}{\rho^5} \right] + \frac{\partial^2 c}{\partial \rho^2} \cdot \frac{D}{\rho^4} (\rho^3 + 3a_p t^{p+1})^{4/3} \\ &= \frac{D(\rho^3 + 3a_p t^{p+1})^{4/3}}{\rho^5} \left[ \rho \frac{\partial^2 c}{\partial \rho^2} + \frac{\partial c}{\partial \rho} \left( \frac{4\rho^3}{\rho^3 + 3a_p t^{p+1}} - 2 \right) \right] \end{aligned}$$

or,

$$\frac{\partial c}{\partial t} = \frac{D(\rho^3 + 3a_p t^{p+1})^{4/3}}{\rho^5} \left[ \rho \frac{\partial^2 c}{\partial \rho^2} + 2 \frac{\rho^3 - 3a_p t^{p+1}}{\rho^3 + 3a_p t^{p+1}} \frac{\partial c}{\partial \rho} \right] \quad \text{-----} \quad (3.19)$$

The new boundary conditions for equation (3.19) are:

$$C = C_i \quad \text{at} \quad \rho = 0 \quad \text{for} \quad t > 0$$

$$C = 0 \quad \text{at} \quad \rho = \infty \quad \text{for} \quad t > 0 \quad \text{-----} \quad (3.20)$$

$$C = 0 \quad \text{at} \quad \rho > 0 \quad \text{for} \quad t = 0$$





The solution is greatly simplified by restricting it to a region,

$$\rho^3 \ll 3a_p t^{p+1} \quad \text{-----} \quad (3.21)$$

which may not be correct at a very early stage as  $3a_p t^{p+1}$  itself is very small. But this is relatively unimportant as the surface is small and the mass transfer at this stage may not be significant in comparison to the rest of the time.

With this condition equation (3.19) reduces to,

$$\frac{\partial c}{\partial t} = \frac{D(3a_p t^{p+1})^{4/3}}{\rho^5} \left[ \rho \frac{\partial^2 c}{\partial \rho^2} - 2 \frac{\partial c}{\partial \rho} \right] \quad \text{-----} \quad (3.22)$$

Let,

$$\eta = \frac{\rho^3}{A t^{(7+4p)/6}} \quad \text{-----} \quad (3.23)$$

where,  $A = 6 \left( \frac{3D}{7+4p} \right)^{1/2} (3a_p)^{2/3}$

$$\frac{\partial c}{\partial t} = \frac{\partial c}{\partial \eta} \cdot \frac{\partial \eta}{\partial t}$$

$$= \frac{\partial c}{\partial \eta} \left[ - \frac{(7+4p)}{6} \frac{\rho^3}{A t^{(13+4p)/6}} \right]$$

$$= \frac{\partial c}{\partial \eta} \left[ - \frac{(7+4p)}{6} \frac{\eta A t^{(7+4p)/6}}{A t^{(13+4p)/6}} \right]$$

$$\frac{\partial c}{\partial t} = - \frac{(7+4p)}{6} \cdot \frac{\eta}{t} \cdot \frac{\partial c}{\partial \eta} \quad \text{-----} \quad (3.24)$$



$$\frac{\partial c}{\partial \rho} = \frac{\partial c}{\partial \eta} \cdot \frac{\partial \eta}{\partial \rho}$$

or,

$$\frac{\partial c}{\partial \rho} = \frac{\partial c}{\partial \eta} \cdot \frac{3 \rho^2}{A t (7 + 4p)/6} \quad \text{-----} \quad (3.25)$$

$$\frac{\partial^2 c}{\partial \rho^2} = \frac{\partial^2 c}{\partial \eta^2} \left( \frac{\partial \eta}{\partial \rho} \right)^2 + \frac{\partial c}{\partial \eta} \cdot \frac{\partial^2 \eta}{\partial \rho^2}$$

or,

$$\frac{\partial^2 c}{\partial \rho^2} = \frac{\partial^2 c}{\partial \eta^2} \cdot \frac{9 \rho^4}{A^2 t (7 + 4p)/3} + \frac{\partial c}{\partial \eta} \cdot \frac{6 \rho}{A t (7 + 4p)/6} \quad \text{-----} \quad (3.26)$$

Substituting from equations (3.24, 3.25, 3.26) into (3.22)

$$\begin{aligned} - \frac{(7 + 4p)}{6} \frac{\eta}{t} \frac{\partial c}{\partial \eta} &= \frac{D(3a_p t^{p+1})^{4/3}}{\rho^5} \left[ \frac{\partial^2 c}{\partial \eta^2} \cdot \frac{9 \rho^5}{A^2 t (7 + 4p)/3} + \frac{\partial c}{\partial \eta} \cdot \right. \\ &\quad \left. \frac{6 \rho^2}{A t (7 + 4p)/6} - \frac{6 \rho^2}{A t (7 + 4p)/6} \cdot \frac{\partial c}{\partial \eta} \right] \end{aligned}$$

Simplifying,

$$\frac{\partial^2 c}{\partial \eta^2} + 2\eta \frac{\partial c}{\partial \eta} = 0 \quad \text{-----} \quad (3.27)$$

Solving this ordinary differential equation with boundary conditions (3.20), we get

$$\frac{C}{C_i} = 1 - \frac{2}{\sqrt{\pi}} \int_0^{\frac{\rho^3}{A t (7 + 4p)/6}} e^{-\eta^2} d\eta \quad \text{-----} \quad (3.28)$$

The rate of mass transfer at time  $t$  is given by Fick's law and is,



$$\phi(t) = - (4 \pi r^2) D \left( \frac{\partial c}{\partial r} \right)_{r = (3a_p t^{p+1})^{1/3}} \quad (3.29)$$

The total amount of mass transfer during formation can be calculated by integrating equation (3.29) over the entire life of the bubble

$$m_f = \int_0^{t_f} \phi(t) dt \quad (3.30)$$

or,

$$m_f = \int_0^{t_f} (-4\pi r^2 D \left( \frac{\partial c}{\partial r} \right)_{r=R}) dt \quad (3.31)$$

and,

$$\frac{\partial c}{\partial r} = \frac{\partial c}{\partial \eta} \cdot \frac{\partial \eta}{\partial \rho} \cdot \frac{\partial \rho}{\partial r} \quad (3.32)$$

The concentration gradient at the interface can be found from equations (3.28), (3.23), (3.16) and (3.32) and is

$$\left( \frac{\partial c}{\partial r} \right)_{r=R} = - \sqrt{\left( \frac{7+4p}{3\pi Dt} \right)} C_i \quad (3.33)$$

Equation (3.31) on substitution for R from equation (2.32)

and  $\left( \frac{dc}{dr} \right)_{r=R}$  from equation (3.33) gives,

$$m_f = \int_0^{t_f} 4\pi (3a_p t^{p+1})^{2/3} D \sqrt{\left( \frac{7+4p}{3\pi Dt} \right)} C_i dt \quad (3.34)$$

$$= 4\pi^{1/2} 3^{1/6} \frac{6}{(7+4p)^{1/2}} C_i D^{1/2} a_p^{2/3} t_f^{(7+4p)/6} \quad (3.35)$$

For a time independent source at the centre,





$$p = 0 \quad \text{-----} \quad (3.36)$$

and from equation (2.32) the radius is,

$$R(t) = (3a_p t)^{1/3} \quad \text{-----} \quad (3.37)$$

The bubble radius at the end of the formation period is given by

$$R_f = (3a_p t_f)^{1/3}$$

$$\text{or, } a_p = \frac{R_f^3}{3t_f} \quad \text{-----} \quad (3.38)$$

Substitution from equations (3.36) and (3.38) into (3.35) yields for the mass transfer during the entire bubble formation period,

$$m_f = 24 \pi^{1/2} 3^{1/6} 7^{-1/2} C_1 D^{1/2} \frac{R_f^2}{(3t_f)^{2/3}} t_f^{7/6}$$

$$= 5.24 C_1 D^{1/2} R_f^2 t_f^{1/2} \pi^{1/2}$$

$$\text{or, } m_f = 1.31 C_1 \sqrt{(\pi D)} d_f^2 t_f^{1/2} \quad \text{-----} \quad (3.39)$$

Popovich et. al. [67] have summarised the various models available for mass transfer during single drop formation and report that Ilkovic's model results in the same equation as (3.39).

The average mass transfer coefficient can be defined as,



$$m_f = k_L C_i \int_0^{t_f} S dt \quad \text{-----} \quad (3.40)$$

For spherical growth of the bubble,

$$S = 4\pi R(t)^2 \quad \text{-----} \quad (3.41)$$

From equations (3.37) and (3.41),

$$S = 4\pi (3a_p t)^{2/3} \quad \text{-----} \quad (3.42)$$

Substitution for  $a_p$  from (3.38) into above gives

$$S = 4\pi R_f^2 \left(\frac{t}{t_f}\right)^{2/3} = \pi d_f^2 \left(\frac{t}{t_f}\right)^{2/3} \quad \text{-----} \quad (3.43)$$

Hence,

$$\int_0^{t_f} S dt = 0.6 \pi d_f^2 t_f \quad \text{-----} \quad (3.44)$$

Equations (3.39), (3.40) and (3.44) can be simplified to give,

$$k_L = 2 \sqrt{\left(\frac{D}{\pi t_f}\right)} \quad \text{-----} \quad (3.45)$$

This close resemblance with the general solution of the penetration theory is not surprising as the mean exposure time of the elements was assumed to be  $t_f$  in this derivation.

Equation (3.39) is valid only when the depth of penetration is small compared to the radius of the bubble as it was one of the assumptions (3.21) in the derivation. Quantitatively when,



$$\rho^3 \ll 3 a_p t \quad \text{-----} \quad (3.46)$$

From (3.38) and (3.46),

$$\rho^3 \ll R_f^3 \frac{t}{t_f} \quad \text{-----} \quad (3.47)$$

Comparing the film theory and the penetration theory,

$$\rho \approx 2 \sqrt{Dt} \quad \text{-----} \quad (3.48)$$

where,  $(\rho/2)$  is assumed to be the effective film thickness.

Equations (3.47) and (3.48) can be combined to give the final condition for the application of equation (3.39) as,

$$8 \frac{D^{3/2} t^{1/2} t_f}{R_f^3} \ll 1 \quad \text{-----} \quad (3.49)$$

The mass transfer coefficients during bubble formation and bubble rise can be compared from equations (2.22), (3.11), (3.45), and (2.29). The result obtained is,

$$\frac{k_L \text{ (formation)}}{k_L \text{ (rise)}} = \sqrt{\left(\frac{d_f}{\ell}\right)} \quad \text{-----} \quad (3.50)$$

which implies that the mass transfer coefficient during bubble formation is always lower than its value during bubble rise as  $(d_f/\ell)$  is always less than one if there is no bubble coalescence at the orifice.

The limitations of this model are as follows:





- (a) the effect of continuous phase velocity is not considered
- (b) spherical bubble growth is assumed which is the case of minimum transfer as any deviation from sphericity would increase the area and hence the transfer.

### 3.2.2 Mass Transfer Through An Interface Expanding by the Formation of Fresh Elements

In the previous model each element of the interface was assumed to have a life span equivalent to the total formation time.

Calderbank and Patra [15] have represented the growth phenomenon by assuming that the additional interface formed in the course of the time is entirely fresh and that there is no exchange of matter between elements of different age. This shall be used as the basis for our model. All the other basic conditions of Higbie's penetration theory are assumed to apply.

The general solution of the penetration theory gives the instantaneous rate of mass transfer per unit area as,

$$N(t) = \sqrt{\frac{D_L}{\pi t}} (C_i - C_o) \text{ ----- (3.7)}$$

By integrating, the amount transferred in time  $t$  per unit area is

$$N' = 2\sqrt{\frac{D_L t}{\pi}} \cdot (C_i - C_o) \text{ ----- (3.51)}$$

The total amount of mass transfer from the growing bubble



starting from an initial area  $S(0)$  consists of:

- (a) transfer from the surface elements having a life at the interface equal to the total bubble formation time,  $t_f$ .
- (b) transfer from the surface elements having a life span of  $(t_f - \theta)$ ; where  $\theta > 0$ .

Since no surface element is assumed to leave the interface once it reaches there, it is imperative that area  $S(0)$  will have a total age of  $t_f$  and the amount transferred from these elements is obtained from equation (3.51) as,

$$N'' = 2(C_i - C_o) \sqrt{\left(\frac{D_L t_f}{\pi}\right)} S(0) \quad \text{-----} \quad (3.52)$$

Any subsequent surface element added to the interface during bubble growth has a unique life span uncommon to other elements. If one such element is added at time  $\theta > 0$ , the amount transferred from it per unit area from equation (3.51) will be,

$$N'(t_f - \theta) = 2(C_i - C_o) \sqrt{\left(\frac{D_L (t_f - \theta)}{\pi}\right)} \quad \text{-----} \quad (3.53)$$

The contribution to the total mass transfer from all these unique elements can be expressed as,

$$N'' = \int_0^{t_f} N'(t_f - \theta) \frac{ds(\theta)}{d\theta} d\theta \quad \text{-----} \quad (3.54)$$

The total mass transfer during bubble growth is found by adding equations (3.52) and (3.54) and is,

$$N''(t_f) = \int_0^{t_f} N'(t_f - \theta) \frac{ds(\theta)}{d\theta} d\theta + 2(C_i - C_o) \sqrt{\left(\frac{D_L t_f}{\pi}\right)} S(0) \quad \text{---} \quad (3.55)$$



Substituting from equation (3.53), we get

$$\begin{aligned}
 N''(t_f) &= 2(C_i - C_o) \sqrt{\left(\frac{D_L}{\pi}\right)} \left[ \int_0^{t_f} (t_f - \theta)^{1/2} \frac{ds(\theta)}{d\theta} d\theta + t_f^{1/2} S(0) \right. \\
 &= 2(C_i - C_o) \sqrt{\left(\frac{D_L}{\pi}\right)} \left[ (t_f - \theta)^{1/2} S(\theta) \Big|_{\theta=0}^{t_f} + \frac{1}{2} \int_0^{t_f} \frac{S(\theta)}{(t_f - \theta)^{1/2}} d\theta + t_f^{1/2} S(0) \right]
 \end{aligned}$$

or,

$$N''(t_f) = (C_i - C_o) \sqrt{\left(\frac{D_L}{\pi}\right)} \int_0^{t_f} \frac{S(\theta)}{(t_f - \theta)^{1/2}} d\theta \quad \text{-----} \quad (3.56)$$

Assume the area of the growing bubble to vary as,

$$S(\theta) = S_o + K' \theta \quad \text{-----} \quad (3.57)$$

where,  $S(\theta)$  = Surface area of bubble at any time,  $\text{cm}^2$ .

$S_o$  = Surface area of rest bubble remaining at the orifice  
after bubble detachment,  $\text{cm}^2$ .

$K'$  = Slope of area - time curve,  $\text{cm}^2/\text{sec}$ .

With this substitution equation (3.56) gives,

$$\begin{aligned}
 N''(t_f) &= (C_i - C_o) \sqrt{\left(\frac{D_L}{\pi}\right)} \int_0^{t_f} \frac{S_o + K' \theta}{(t_f - \theta)^{1/2}} d\theta \\
 &= (C_i - C_o) \sqrt{\left(\frac{D_L}{\pi}\right)} \left[ \int_0^{t_f} \frac{S_o}{(t_f - \theta)^{1/2}} d\theta - K' \int_0^{t_f} \frac{(t_f - \theta) - t_f}{(t_f - \theta)^{1/2}} d\theta \right]
 \end{aligned}$$





$$\begin{aligned}
 N''(t_f) &= (C_i - C_o) \sqrt{\left(\frac{D_L}{\pi}\right)} \left[ \int_0^{t_f} \frac{S_o + K' t_f}{(t_f - \Theta)^{1/2}} d\Theta - K' \int_0^{t_f} (t_f - \Theta)^{1/2} d\Theta \right] \\
 &= (C_i - C_o) \sqrt{\left(\frac{D_L}{\pi}\right)} \left[ 2(S_o + K' t_f) t_f^{1/2} - \frac{2}{3} K' t_f^{3/2} \right]
 \end{aligned}$$

or,

$$N''(t_f) = 2 (C_i - C_o) \sqrt{\left(\frac{D_L t_f}{\pi}\right)} \left[ S_o + \frac{2}{3} K' t_f \right] \text{-----} (3.58)$$

where,  $N''(t_f)$  = Total mass transfer during bubble formation, gm-moles

$C_i$  = Concentration of material being absorbed at the interface, gm-moles/cm<sup>3</sup>.

$C_o$  = Concentration of material being absorbed in the bulk liquid, gm-moles/cm<sup>3</sup>.

$D_L$  = Liquid phase diffusivity, cm<sup>2</sup>/sec.

$t_f$  = Time of bubble formation, sec.

$S_o$  = Surface area of rest bubble, cm<sup>2</sup>.

$K'$  = Slope of area-time curve, cm<sup>2</sup>.

The main limitations of this model are that the effect of liquid velocity on mass transfer is not considered and the penetration theory is assumed to apply.

Also, if  $k_L$  is defined by

$$N''(t_f) = k_L \left( \int_0^{t_f} S(\Theta) d\Theta \right) (C_i - C_o) \text{-----} (3.59)$$

then substitution from equations (3.57) and (3.58) gives the average mass transfer coefficient during bubble formation as,

$$k_L = 2 \sqrt{\left(\frac{D_L}{\pi t_f}\right)} \left[ \frac{S_o + 0.67 K' t_f}{S_o + 0.5 K' t_f} \right] \text{-----} (3.60)$$



where,  $k_L$  = average continuous phase mass transfer coefficient during bubble formation, cm./sec.

Calderbank and Patra [15] had also assumed a similar model and had derived an expression for  $k_L$  by defining it as,

$$m_f = k_L A_m t_f (C_i - C_o) \quad \text{-----} \quad (2.26)$$

which gave,

$$k_L = 1.56 \sqrt{\left(\frac{D_L}{\pi t_f}\right)} \quad \text{-----} \quad (2.27)$$

They had proposed an empirical correlation for the variation of bubble surface area with time as

$$\frac{A}{A_m} = 1 - \left(\frac{t_f - t}{t_f}\right)^{1.86} \quad \text{-----} \quad (2.9)$$

which implies that the area at time zero is equal to zero. If one neglects  $S_o$  in equation (3.60), the solution obtained is,

$$k_L = 2.68 \sqrt{\left(\frac{D_L}{\pi t_f}\right)} \quad \text{-----} \quad (3.61)$$

Equations (2.27) and (3.61) are identical except for the value of the constant. In Calderbank's equation (2.27), the value of  $k_L$  is low because of the way he defined  $k_L$  in equation (2.26).

To have a true comparison it is imperative to define  $k_L$  in the same fashion. Thus, by changing equation (2.26) to



$$m_f = k_L (C_i - C_o) \int_0^{t_f} A dt \quad \text{-----} \quad (3.62)$$

equations (3.59) and (3.62) become compatible.

Substituting for A in equation (3.62) from equation (2.9), integrating and comparing the resulting equation for  $m_f$  with equation (2.25) one finds that Calderbank's solution is expressed by the following equation instead of equation (2.27)

$$k_L = 2.4 \sqrt{\left(\frac{D_L}{\pi t_f}\right)} \quad \text{-----} \quad (3.63)$$

It can readily be seen that equation (3.63) is very close to the solution derived here, equation (3.61). This difference in the values of constant can be due to different area-time relationships used in the two solutions, equations (2.9) and (3.57).

From equations (2.22), (3.11), (3.60), and (2.29) it can be shown that,

$$\frac{k_L(\text{formation})}{k_L(\text{rise})} = \sqrt{\left(\frac{d_f}{\ell}\right)} \left[ \frac{S_o + 0.67 K' t_f}{S_o + 0.5 K' t_f} \right] \quad \text{-----} \quad (3.64)$$

and for very small  $S_o$ ,

$$\frac{k_L(\text{formation})}{k_L(\text{rise})} = 1.34 \sqrt{\left(\frac{d_f}{\ell}\right)} \quad \text{-----} \quad (3.65)$$

which for very low frequencies of bubble formation predicts the mass transfer coefficient during formation to be smaller than its value during bubble rise.





## CHAPTER 4

### EXPERIMENTAL

#### 4.1 Choice of Systems

The carbon dioxide-distilled and dimineralized water system was selected to determine the liquid phase mass transfer coefficient during bubble formation. The choice was justified as,

- (i) the solubility of carbon dioxide in water under atmospheric conditions is small and so the resistance to mass transfer can be assumed to be in the liquid phase;
- (ii) the diffusivity of carbon dioxide in water can be assumed constant at a particular temperature;
- (iii) the heat effects are negligible as the heat of solution of carbon dioxide is small.

The ammonia-nitrogen-distilled dimineralized water system was chosen for a study of mass transfer in the dispersed phase for the following two reasons:

- (i) the major mass transfer resistance can be assumed to be in the dispersed phase as the solubility of ammonia in water is very high;
- (ii) the nitrogen provides transfer resistance in the dispersed phase and its transfer to air saturated water can be neglected.

#### 4.2 Basis of the Experimental Method

In general, the mass transferred during the formation of a bubble was determined as a difference between the gas flow rate to the orifice and the product of the frequency of bubble formation and the



mean volume of the detached bubbles. Mathematically

$$\text{Mass transfer} = \omega - n V_f \text{ ----- (4.1)}$$

where,  $\omega$  is the gas flow rate in cc/sec

$n$  is the bubble frequency in sec

$V_f$  is the mean volume of the detached bubbles in c.c.

The validity of the experimental method employed was checked by using the air-water system wherein no mass transfer should occur if water saturated air and air saturated water are used.

### 4.3 Experimental Set-up

#### 4.3.1 Carbon Dioxide-Water System

A schematic flowsheet of the experimental set up is shown in Figure 2. Bone dry carbon dioxide gas (minimum purity 99.8%) from a high pressure cylinder (1) was saturated with distilled water in a 3 inch diameter lucite absorber (2) having a 3 feet packed height of glass beads (1/4 inch o.d.) and was then metered through a soap film meter (3). The gas pressure at the soap film meter was regulated by a pressure regulating valve on the gas cylinder and fine control was subsequently achieved by a diaphragm valve just before the soap film meter. The pressure reading was taken on a mercury manometer (5). The gas flow rate was accurately controlled by a micrometer needle valve (4). The gas then passed through an adjustable chamber volume (6) to the



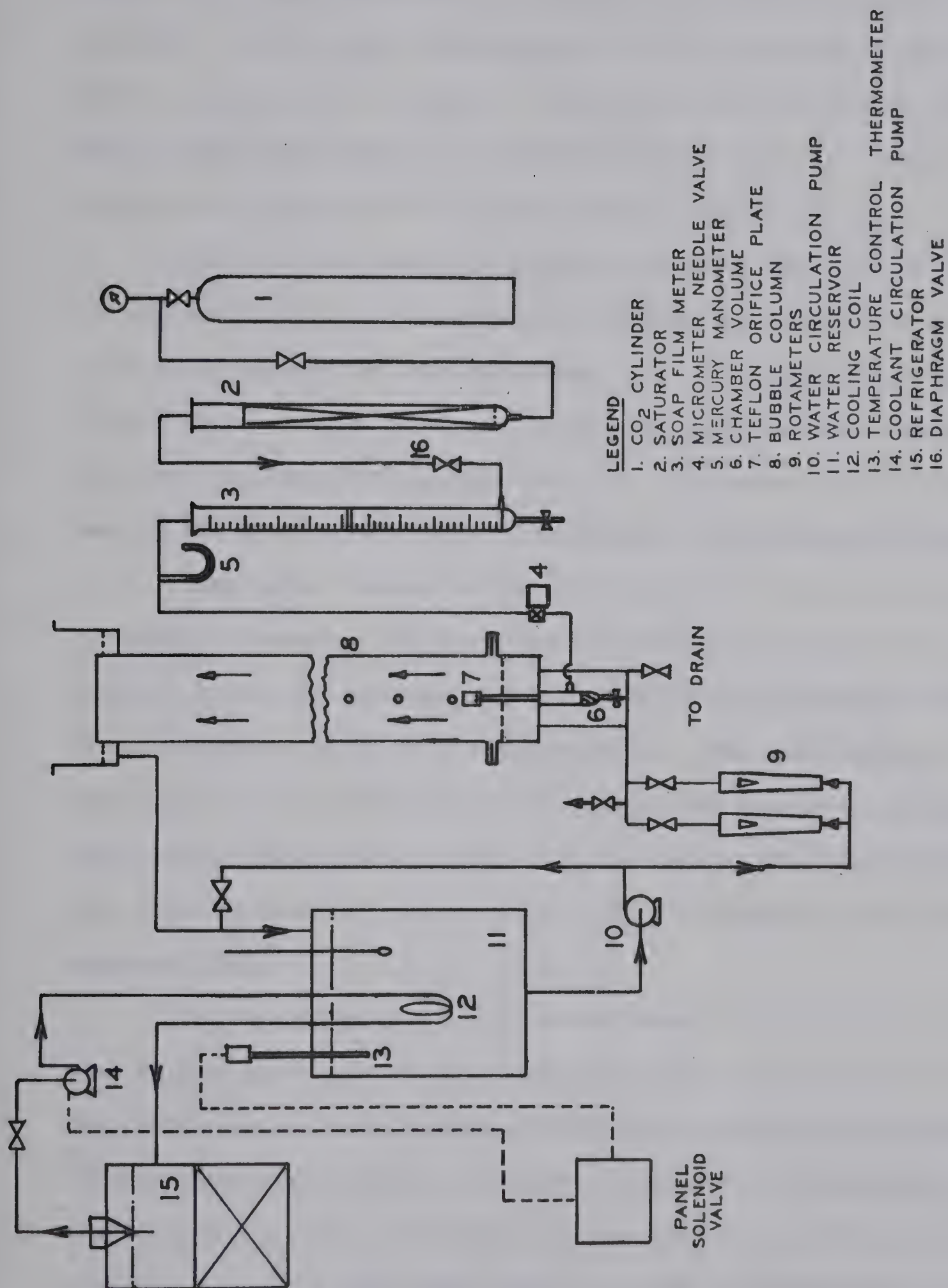


FIG. 2. FLOWSHEET FOR CARBON DIOXIDE WATER SYSTEM.





orifice (7), made of 316 stainless steel tubing 0.408 cm. inside diameter. A teflon cover was provided at the top of the orifice to make it non-wettable with water. The orifice was installed in a lucite bubble column (8) having an internal diameter of 20.2 cm., a wall thickness of 0.635 cm., and a total height of 100 cms.

The water was stored in a lucite reservoir tank (11) of about 100 gallons capacity and was pumped by a centrifugal pump (10) through a set of rotameters (9) into the column (8). The flow of water and gas through the column was co-current. The water overflow from the column (8) went back into the reservoir tank (11). Polyvinyl Chloride was used as the material of construction for all the liquid pipe lines.

Temperature control to  $\pm 0.05^{\circ}\text{C}$  was achieved with the use of a Beckman thermometer (13) installed in the water reservoir (11). A control circuit was automatically activated by the thermometer when the water temperature exceeded the desired value. When this happened a small capacity centrifugal pump (14) started and circulated cooling water from a refrigerated storage (15) (the temperature in which was maintained at about  $4^{\circ}\text{C}$ ) to a cooling coil (12) immersed in the water reservoir (11).

The experimental set-up described above is essentially the same as that used by Kalra and described in detail in his thesis [49]. Some modifications were, however, made towards perfecting the experimental technique. The most effective change was the introduction of a diaphragm valve, for controlling the gas flow rate, just before the soap film meter. A very steady gas flow could be obtained even at extremely low frequencies of bubble formation (one bubble per two sec-



onds). Also, since the gas pressure reading is very important in subsequent calculations it was read on a mercury manometer.

#### 4.3.2 Ammonia-Nitrogen-Water System

The flow sheet of the equipment used for studying the ammonia-nitrogen-water system is shown schematically in Figure 3.

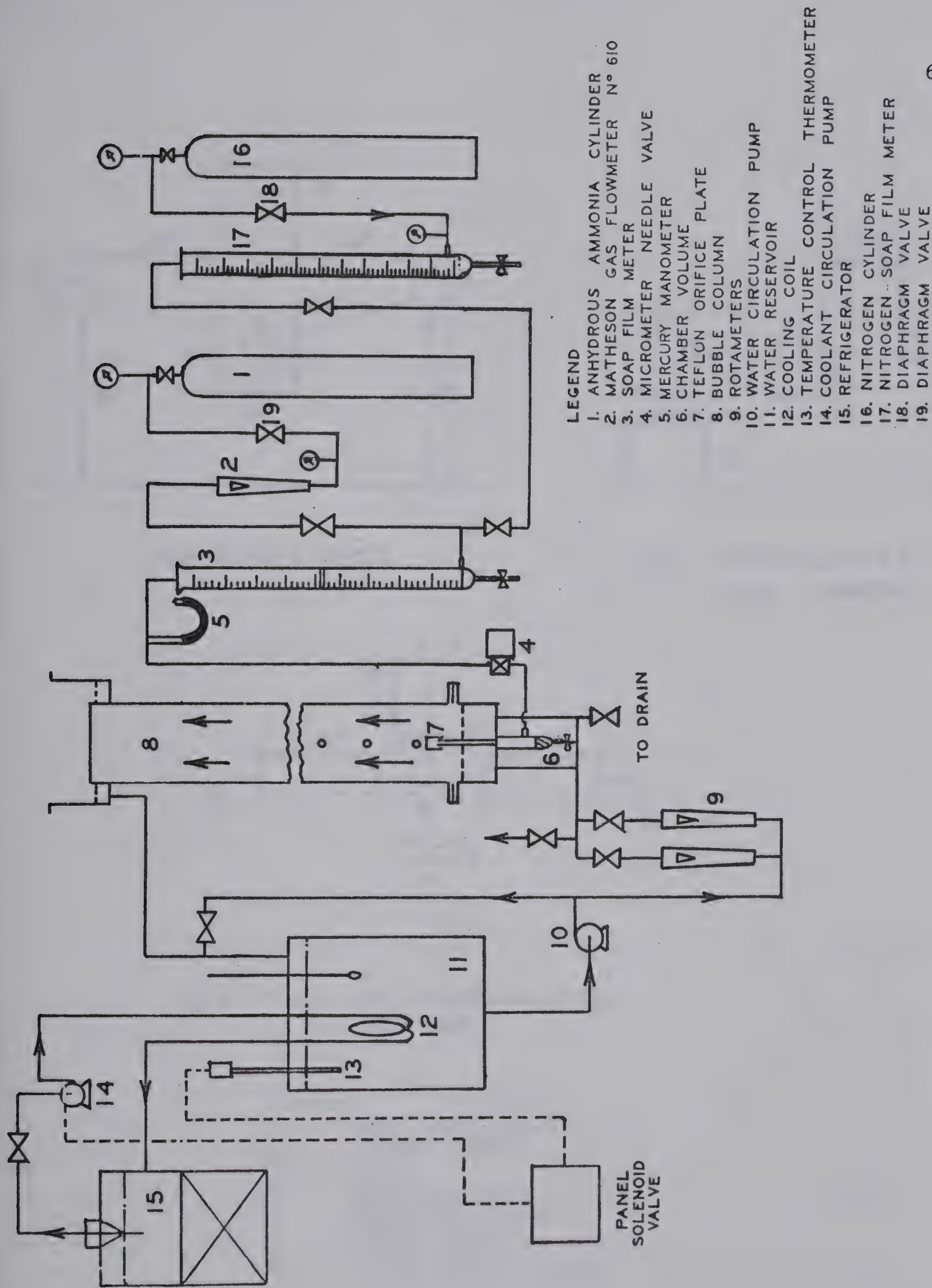
Ammonia gas from an anhydrous ammonia cylinder (1) was metered through a previously calibrated Matheson gas flow rotameter (2). A soap film meter was tried to measure the ammonia gas flow but was abandoned as the soap film kept breaking due to the high solubility of ammonia in soap-water solution. Nitrogen gas from a high pressure nitrogen cylinder (16) was mixed with ammonia gas in a T-mixer after metering through a soap film meter (17). A fine flow control for both the ammonia and the nitrogen was achieved individually by installing a diaphragm valve in each gas line before the gases enter their respective flowmeters. The flow of ammonia-nitrogen gas mixture was then measured in another soap film meter (3) to allow a check on the material balance. The remaining flow scheme is the same as described above for the carbon dioxide-water system.

#### 4.4 The Photographic Technique

A high speed camera was used to take motion pictures of the bubble during its growth from the orifice. A key factor in obtaining well defined periphery of the bubble on the pictures was the technique used for lighting. The photographic set-up used is shown schematically in figure 4 in which sketches a, b and c show the layout of the side







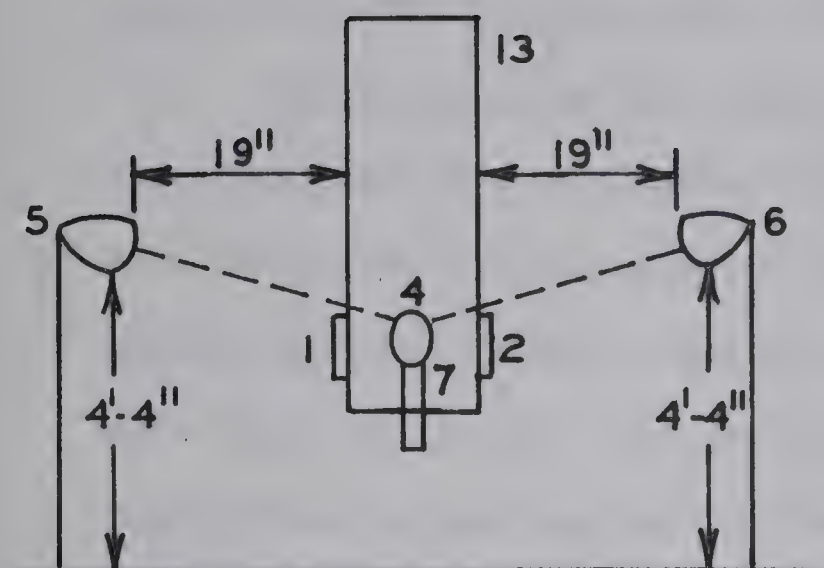
# LEGEND

1. ANHYDROUS AMMONIA CYLINDER
2. MATHESON GAS FLOWMETER N° 610
3. SOAP FILM METER
4. MICROMETER NEEDLE VALVE
5. MERCURY MANOMETER
6. CHAMBER VOLUME
7. TEFLON ORIFICE PLATE
8. BUBBLE COLUMN
9. ROTAMETERS
10. WATER CIRCULATION PUMP
11. WATER RESERVOIR
12. COOLING COIL
13. TEMPERATURE CONTROL THERMOMETER
14. COOLANT CIRCULATION PUMP
15. REFRIGERATOR
16. NITROGEN CYLINDER
17. NITROGEN SOAP FILM METER
18. DIAPHRAGM VALVE
19. DIAPHRAGM VALVE

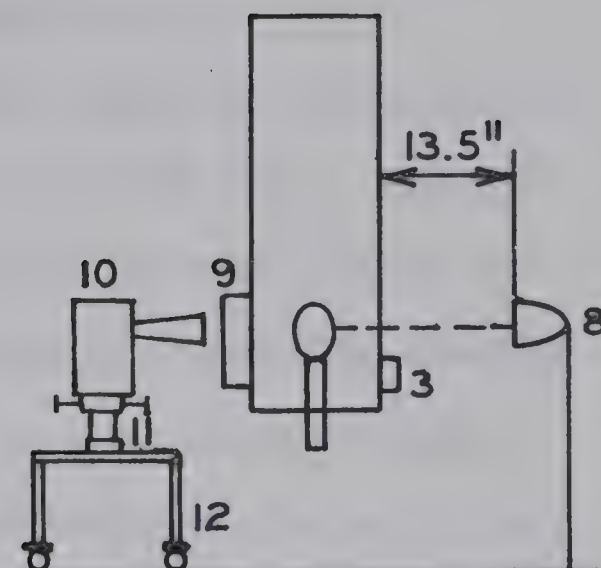
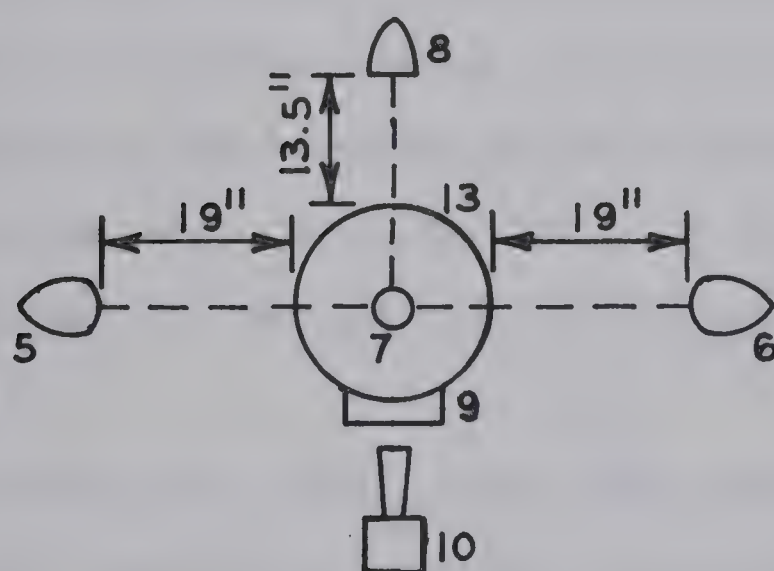
FIG. 3. FLOWSHEET FOR AMMONIA - NITROGEN WATER SYSTEM







(A) SIDE-LIGHTS

(B) BACK-LIGHTS  
AND CAMERA(C) PLAN OF PHOTOGRAPHIC  
SET-UP.

## LEGEND

1,2,3	PAPER LIGHT SHIELDS
4	GROWING BUBBLE
5,6,8	LAMPS
7	ORIFICE
9	CORRECTION LENS
10	HIGH SPEED CAMERA
11	CAMERA STAND
12	CAMERA TABLE
13	LUCITE BUBBLE COLUMN

FIG. 4. PHOTOGRAPHIC ARRANGEMENT.



lights, the arrangement of the back-light and the camera, and a plan view of the entire photographic set-up, respectively.

The lighting was provided by two side lights (5, 6) and a back-light (8) each with an illuminating intensity of 300 watts. The light from the former came at an angle to the orifice, whereas it came horizontally from the latter. Surplus light was reflected back by aluminum foil sheets (1, 2, 3). The inside surface of these foils was black which helped in cutting out the light reflections from the lucite surface of the column to the bubble.

A correction lens (9) was used in front of the bubble column to avoid distortion of the bubble due to curvature of the column. This lens consisted essentially of a hollow lucite casing filled with water and had the same curvature as that of the bubble column on one side and a plane edge towards the camera. A detailed description of this correction lens together with the ray diagram is given in Kalra's thesis [49].

A Hycam, model K2004E, 16 mm. high speed motion picture camera was used for taking the pictures and it had a maximum film capacity of 400 feet and a speed range of zero to 11,000 frames per second. The camera (10) was supported on a camera stand (11) which had provisions, for horizontal movement on a camera table (12), for horizontal rotation of the camera, and for adjustment of the inclination of the camera lens axis to the horizontal plane. The camera table (12) was fitted with wheels to enable the movement of the camera unit as a whole.

The Eastman Tri-X Reversal film type 7278 was used in the camera and was developed as a reversal film meaning thereby that the



dark and bright spots of the object appeared as dark and bright spots respectively on the film.

A Milli-Mite timing light generator model TLG-3 was connected to the camera and could be used to determine the exact speed of the film as the light generator left a mark on the edge of the film at adjustable frequencies of 10, 100 and 1,000 per second.

During the development stages of the above mentioned photographic set-up some problems were encountered. Since a circular column was used, light reflections on the periphery of the bubble image on the film were noticed. However, these reflections were eliminated by using the balanced lighting approach illustrated in figure 4. Also, some difficulty was encountered in obtaining a good colour contrast between the object and background as both gas bubble and water were colourless. The solution was found after trial and error and it involved finding the right combination of the intensity of lighting, the speed of the camera in terms of frames of film advanced per second, the focal length of the camera lens, and the aperture of the lens. Very good pictures were obtained when, the orifice was illuminated by three 300 watt lamps, the camera speed was 600 frames per second, the camera lens had a 100 mm. extension, and the lens opening was f/11.0.

#### 4.5 The Experimental Procedure

Since the experiments involve the measurement of very small quantities, a very careful experimental technique is needed to obtain reliable results. The experimental procedure which was followed closely during the course of this investigation is described below.







#### 4.5.1 The Preparation for Runs

The equipment was carefully cleaned prior to making any experimental measurements and several checks were made before each experimental run to ensure a proper working of the set-up.

##### (a) The Cleaning of Equipment

The cleaning of equipment is essential as any contamination in the system could conceivably affect the reliability of results.

After the initial assembly of the equipment, the system was left running with air bubbles being formed in circulating water for a few hours. The water was then drained completely and the procedure repeated with a fresh batch of distilled water. After repeating this for three days it was assumed that all the suspended impurities like PVC chips etc., were completely removed. At this point distilled water, containing detergent, was introduced in the water reservoir and recirculated through the water pump, rotameters and column for a day. This was done to remove any traces of oil entrapped in the system. The equipment was rinsed free of detergent by recirculating fresh batches of distilled water about fifteen times.

The column was then opened and glass beads, previously cleaned by immersing in concentrated chromic acid for a couple of days and rinsed thoroughly with distilled water and dried, were introduced into the bottom section of the column. The purpose of these glass beads is to obtain a flat velocity profile for the liquid in the column. The teflon orifice cover was also cleaned inside and outside by detergent, washed with distilled water and dried. It was then attached to the



orifice tip and the column was completely sealed. One fresh batch of dimineralized distilled water was circulated through the system and drained out.

The equipment was then considered ready for a calibration run.

After every run the water was drained to below the level of teflon orifice cover in the column. Before any subsequent run the water reservoir was completely drained and the system flushed with a fresh batch of dimineralized distilled water. The flush water was discarded completely and the system was refilled with dimineralized water.

(b) Checks Before Any Run

Before proceeding with any experimental run the following checks were made:

1. The system was checked for leaks in the gas lines by closing the needle valve (4) in Figures 2 and 3 and bringing the gas lines to a pressure of about 5 PSIG by introducing air and then leaving the isolated system under pressure overnight.
2. The quality of dimineralized distilled water being fed to the water reservoir was continually checked. The satisfactory limit was set at a maximum salt concentration of 0.05 ppm. The cartridges in the Bantam Dimineralizer were replaced if this limit was exceeded.
3. The camera was checked to make sure that it was, in working order, and running at the indicated speed on the dial.
4. The gas flow rate was checked by taking measurements on the



soap film meter to ensure that a steady flow could be obtained at the desired frequency of bubble formation.

#### 4.5.2 The Calibration Run With Air-Water

The supply air pressure was regulated to the desired value and the diaphragm valve (16), Figure 2, was set to give a steady pressure of about 2 PSIG on the discharge end. The air was fed to the saturator (2) slowly to prevent a surge of water through the gas lines. The micrometer needle valve (4) was left wide open during the initial stages.

The column (8) was then filled with water at a very slow rate and then the rate was adjusted to the desired value. The set point of the Beckman thermometer (13) was fixed at 25°C and the temperature control circuit was turned on. The flow of cooling water through the cooling coil (12) was adjusted manually till the temperature could be controlled to within a limit of  $\pm 0.05^{\circ}\text{C}$ .

The equipment for measuring the bubble frequency - namely the laser, photocell, universal counter and the oscilloscope - were turned on. The description of the circuit in detail is given in Kalra's thesis [49]. The principle of operation is that once the laser beam is adjusted such that it intercepts the bubble after detachment, the photocell interprets every interruption of the beam as a discrete signal and transmits it to the universal counter. The universal counter displays the time elapsed between each interruption and this can be taken as the time period of bubble formation. This time period was brought close to the desired value by adjusting the needle valve (4) opening.







Enough time was allowed for to attain steady state. The steady state in this context is defined as the state of the system when the bubble frequency, gas flow rate through the soap film meter (3), water reservoir temperature and water flow rate have attained constant values.

All the variables were recorded and bubbles photographed by using the procedure outlined in (4.5.3). The variables were once again recorded to get an average value of the variables during the time pictures were being taken.

The water pump, cooling circuit, frequency measuring circuit were then turned off. Water was drained from the column to the bottom of the teflon cover on the orifice. The gas supply valve was then shut off.

#### 4.5.3 The Photographic Procedure

The photographic arrangement was previously described in article 4.4 and shown schematically in Figure 4. The 'loaded' camera was adjusted to such a position that the lens axis was exactly horizontal, and perpendicular to the correction lens. This is necessary to avoid any distortion of the bubble image. Focussing was done on the orifice with back light turned on and the lens aperture fully open. The appropriate values were set on the speed control of the camera and frequency output of the Milli-Mite cycle timer. The camera was locked in this set position to avoid any movement during the run and pictures were taken with all the lights turned on after all the variables pertinent to the experiment had achieved stable values.



#### 4.5.4 Mass Transfer Runs With Carbon Dioxide-Water System

The procedure was essentially the same as already described for the air-water system in article 4.5.2. The exception was that much more time was given to flush the gas lines with carbon dioxide gas before filling the column with the liquid. The purpose of doing this was to remove any entrapped air from the lines.

The continuous phase was analysed for carbon dioxide to determine the driving force for mass transfer. The analysis of  $\text{CO}_2$  in water was done by back titrations. A blank titration of  $\text{Ba}(\text{OH})_2$  solution against standard  $\text{HCl}$  solution was done for each experimental run in an atmosphere of nitrogen. To titrate the water sample, a known volume of it was added to a known volume of  $\text{Ba}(\text{OH})_2$  solution and the mixture was titrated with  $\text{HCl}$  to a green end point of Bromo Thymol Blue indicator. A nitrogen atmosphere was used throughout the titration. The concentration of  $\text{CO}_2$  in water could then be determined by calculation as indicated in Appendix C of Kalra's thesis [49]. The water sample was analysed both before and after taking the pictures.

#### 4.5.5 Mass Transfer Run with Ammonia-Nitrogen-Water System

A constant composition gas mixture was obtained by accurately controlling the flow rates of both nitrogen and ammonia gas separately and then mixing them in a T-mixer (see Figure 3). The pressures of nitrogen and ammonia lines were adjusted to the same value by setting the openings of diaphragm valves (18) and (19) respectively. The rest of the experimental procedure followed was the same as that for the air-water system described in 4.5.2. The time needed to achieve the steady-state was much longer in this case as the composition of the gas mixture





varied slightly with any change in the setting of the needle valve (4), needed for adjusting the frequency of bubble formation.

The bulk phase, water, was analysed for dissolved ammonia both before and after taking the pictures by titrating the water sample against a standard solution of HCl.

Nitrogen and ammonia gas flow rates were recorded individually to check the material balance against the recorded gas flow rate of the mixture in the soap film meter (3).

#### 4.5.6 Sample Data Sheets

Since it is necessary to record all the variables precisely, the format in which the data was taken is included for reference. Tables 2, 3 and 4 are for air-water, carbon dioxide-water, and ammonia-nitrogen-water respectively. These tables refer to three actual runs and will be used later to illustrate the procedure for calculations. A number of readings were taken for the time period of bubble formation both before and after taking the pictures as these readings were used to statistically determine the number of bubbles which had to be analysed for volume calculations.

#### 4.6 Analysis of Results

Step 1           The measured gas flow rate at the soap film meter was converted to the orifice conditions of temperature and pressure by assuming the ideal gas law to apply.

Step 2           The arithmetic mean time period of bubble formation was calculated from the recorded readings of time period.





Variable Recorded	Before Taking Pictures	After Taking Pictures
Atmospheric pressure	702.2 mm. Hg.	702.2 mm. Hg.
Air pressure @ diaphragm valve	2.0 psig	2.0 psig
Air pressure @ manometer	(1.9 + 1.6) inches Hg.	(1.9 + 1.6) inches Hg.
Saturator pressure	3.0 psig	3.0 psig
Water flow rate (rotameter reading)	84	82
Room temperature	74°F	74°F
Air temperature	74°F	74°F
Water temperature	24.8°C	24.8°C
Refrigerated reservoir temperature	3.2°C	3.8°C
Gas flow rate	10 cc./130.7 sec.	10 cc./131.5 sec.
	10 cc./130.5 sec.	10 cc./131.4 sec.
	10 cc./130.8 sec.	10 cc./131.6 sec.
Time period of bubble formation	0.9750, 0.9840, 0.9824, 0.9927, 0.9954, 0.9931, 0.9752, 0.9884, 0.9720, 0.9942, 0.9848, 0.9856, 0.9748, 0.9727, 0.9871, 0.9845, 0.9742, 0.9976, 0.9867, 0.9793, 0.9690, 0.9899, 0.9803, 0.9734, 0.9724, 0.9718, 0.9972, 0.9800, 0.9811, 0.9924, 0.9709, 0.9861, 0.9635, 0.9873, 0.9897, 0.9903, 0.9908, 0.9828, 0.9773, 0.9740, 0.9890, 0.9813, 0.9853, 0.9647, 0.9820, 0.9638, 0.9828, 0.9887, 0.9800, 0.9844	0.9687, 0.9663, 0.9849, 0.9603, 0.9821, 0.9680, 0.9890, 0.9747, 0.9905, 0.9780, 0.9754, 0.9905, 0.9867, 0.9767, 0.9848, 0.9718, 0.9775, 0.9919, 0.9789, 0.9944, 0.9793, 0.9860, 0.9982, 0.9667, 0.9876, 0.9663, 0.9668, 0.9828, 0.9888, 0.9630, 0.9856, 0.9576, 0.9814, 0.9851, 0.9940, 0.9705, 0.9974, 0.9833, 0.9848, 0.9930, 0.9747, 0.9672, 0.9631, 0.9530, 0.9698, 0.9919, 0.9920, 0.9585, 0.9914, 0.9852
Film speed	600 frames/sec.	
Lens opening	f/11	
Time of camera run	12 sec.	
Timer frequency	100 pips/sec.	

Table 2: Sample Data Sheet for Air-Water System (Run A-2)



Quantity Recorded	Before Taking Pictures	After Taking Pictures
Atmospheric pressure	707.0 mm. Hg.	707.0 mm. Hg.
Gas pressure @ diaphragm valve	2.0 psig	2.0 psig
Gas pressure @ manometer	3.5 inches Hg.	3.5 inches Hg.
Saturator pressure	3.0 psig	3.0 psig
Gas cylinder discharge pressure	10 psig	10 psig
Water flow rate (Rotameter reading)	40 (Big rotameter)	40 (Big rotameter)
Water quality	< 0.05 ppm	-
Room temperature	72°F	72.5°F
Water temperature	25°C	25°C
Refrigerated reservoir temperature	4°C	4°C
Gas flow rate	10 cc./121.1 sec. 10 cc./121.3 sec. 10 cc./123.2 sec.	10 cc./121.3 sec. 10 cc./122.2 sec. 10 cc./120.6 sec.
Analysis for CO <sub>2</sub> conc. in water:		
- Blank	12.6 cc. HCl/20 cc. Ba(OH) <sub>2</sub>	-
- Actual	12.6 cc. HCl/20 cc. Ba(OH) <sub>2</sub> + 20 cc. water sample	12.6 cc. HCl/20 cc. Ba(OH) <sub>2</sub> + 20 cc. water sample
Time period of bubble formation, sec.	0.9529, 0.9715, 0.9533, 0.9523, 0.9661, 0.9532, 0.9561, 0.9724, 0.9800, 0.9787, 0.9520, 0.9732, 0.9778, 0.9648, 0.9367, 0.9629, 0.9751, 0.9699, 0.9898, 0.9603, 0.9588, 0.9679, 0.9551, 0.9455, 0.9512, 0.9787, 0.9635, 0.9759, 0.9521, 0.9853, 0.9632, 0.9856, 0.9497, 0.9485, 0.9411, 0.9581, 0.9692, 0.9709, 0.9448, 0.9733, 0.9513, 0.9435, 0.9448, 0.9471, 0.9488, 0.9595, 0.9401, 0.9486, 0.9352, 0.9449	0.9537, 0.9459, 0.9497, 0.9718, 0.9320, 0.9520, 0.9831, 0.9525, 0.9552, 0.9646, 0.9642, 0.9337, 0.9618, 0.9730, 0.9667, 0.9643, 0.9769, 0.9490, 0.9787, 0.9562, 0.9456, 0.9637, 0.9563, 0.9577, 0.9619, 0.9529, 0.9455, 0.9605, 0.9525, 0.9568, 0.9671, 0.9502, 0.9790, 0.9753, 0.9802, 0.9897, 0.9577, 0.9399, 0.9712, 0.9443, 0.9740, 0.9608, 0.9786, 0.9791, 0.9568, 0.9583, 0.9660, 0.9785, 0.9532, 0.9413
Film speed	600 frames/sec.	
Lens opening	f/11	
Length of the film run	200 ft.	
Timer frequency	100 pips/sec.	

Table 3: Sample Data Sheet for Carbon Dioxide-Water System (Run M-8)



Quantity Recorded	Before Taking Pictures	After Taking Pictures
Atmospheric pressure	701.3 mm. Hg.	701.3 mm. Hg.
Ammonia pressure @ diaphragm valve	2.3 psig	2.3 psig
Nitrogen pressure @ diaphragm valve	2.3 psig	2.3 psig
Gas pressure @ manometer	4.25 inches Hg.	4.25 inches Hg.
Water flow rate (rotameter reading)	80	80
Water quality	<0.05 ppm	-
Room temperature	76°F	76°F
Water temperature	25°C	25°C
Refrigerated reservoir temperature	1°C	2.5°C
Gas flow rates:		
- Ammonia (rotameter reading)	3.5	3.5
- Nitrogen	15 cc./64.8 sec.	15 cc./64.0 sec.
	15 cc./64.0 sec.	15 cc./63.8 sec.
	15 cc./64.0 sec.	15 cc./63.8 sec.
	15 cc./52.4 sec.	15 cc./52.2 sec.
	15 cc./52.2 sec.	15 cc./52.2 sec.
	15 cc./52.2 sec.	15 cc./52.4 sec.
Analysis for ammonia conc. in water	0.25 cc. HCl/10 cc. sample	0.25 cc. HCl/10 cc. sample
Time period of bubble formation, sec.	0.3306, 0.3129, 0.3143, 0.3227, 0.3221, 0.3157, 0.3178, 0.3144, 0.3195, 0.3181, 0.3327, 0.3198, 0.3212, 0.3297, 0.3269, 0.3092, 0.3167, 0.3120, 0.3303, 0.3300, 0.3347, 0.3347, 0.3276, 0.3171, 0.3326, 0.3271, 0.3185, 0.3197, 0.3181, 0.3424, 0.3371, 0.3113, 0.3214, 0.3338, 0.3215, 0.3136, 0.3218, 0.3321, 0.3101, 0.3266, 0.3118, 0.3280, 0.3161, 0.3194, 0.3362, 0.3116, 0.3361, 0.3309, 0.3175, 0.3210	0.3167, 0.3349, 0.3306, 0.3351, 0.3168, 0.3182, 0.3392, 0.3312, 0.3133, 0.3343, 0.3115, 0.3298, 0.3234, 0.3165, 0.3125, 0.3274, 0.3389, 0.3169, 0.3343, 0.3104, 0.3128, 0.3241, 0.3363, 0.3223, 0.3300, 0.3314, 0.3166, 0.3280, 0.3332, 0.3329, 0.3162, 0.3146, 0.3181, 0.3263, 0.3278, 0.3279, 0.3153, 0.3083, 0.3262, 0.3313, 0.3138, 0.3180, 0.3164, 0.3181, 0.3249, 0.3096, 0.3146, 0.3311, 0.3240, 0.3192
Film speed	600 frames/sec.	
Lens opening	f/11	
Time and length of film	6 sec. ~ 100 ft.	
Timer frequency	100 pips/sec.	

Table 4: Sample Data Sheet for NH<sub>3</sub>-N<sub>2</sub>-Water System (Run N-2)





Step 3            The number of detached bubbles that had to be analysed for volume was determined statistically from the recorded readings of time period by using the formula,

$$N = \frac{6.61 \times 10^4}{(n - 1) (\bar{x})^2} \sum_{i=1}^n (x_i - \bar{x})^2 \text{ ----- (4.2)}$$

where,    N    is the number of bubbles to be analysed

          n    is the number of data points

$\bar{x}$     is the arithmetic mean time period

$x_i$     is the  $i^{\text{th}}$  time period

This formula gives a confidence limit of 99%. The calculations were aided by a computer program written for the purpose by Kalra and documented in his thesis [49].

A minimum of ten bubbles were analysed.

Step 4            The films were screened to see that they complied with the desired specifications of, sharpness of the bubble and orifice edges, and contrast between the bubble and its background.

Step 5            A number of detached bubbles, as determined in step 3, were analysed by using a digitizer set-up available in the Department of Chemical Engineering, University of Alberta. The film was projected on a horizontal screen calibrated in two directions (X and Y) in terms of standard voltages. It meant that any point on the screen could be represented discretely by two voltages corresponding to its X and Y coor-



ordinates respectively. These voltages could be punched automatically on to computer cards by the use of the digitizer. The orifice image on the film served as a reference object thus enabling one to convert any point, read on the projected film and punched on the computer card, to its actual coordinates as follows:

Say, 10 cm. on screen = 2 volts

Voltage recorded by digitizer across

the projected orifice image =  $V$ , volts

Known orifice diameter =  $D$ , cm.

∴ Conversion scale for all digitizer readings =  $\frac{D}{V}$ , cm/volt

Let, voltage corresponding to  $X$  and  $Y$  coordinates of a point on the film be  $V_1$  and  $V_2$  volts respectively.

Then, the  $X$  - coordinate of that point =  $\frac{D}{V} \times V_1$ , cm.

and, the  $Y$  - coordinate of that point =  $\frac{D}{V} \times V_2$ , cm.

A chosen number of points on the projected image of the bubble periphery were read and transferred on to the computer cards. A program previously written by Kalra [49] was then used to obtain the surface area and the volume of the bubble. His program numerically integrates the following two equations for surface area and volume respectively.

$$S = 2\pi \int f(v) \sqrt{1 + (f'(v))^2} dv \quad \text{-----} \quad (4.3)$$

$$V = \pi \int [f(v)]^2 dv \quad \text{-----} \quad (4.4)$$



Where  $f(v)$  is a numerically determined polynomial function describing the periphery of the bubble and  $f'(v)$  is the derivative of  $f(v)$  with respect to  $v$ .

The errors for surface area and volume, calculated from the program, were stated by Kalra to be within 0.1% and 1.0% respectively.

Step 6 The amount of mass transferred during bubble formation was calculated from equation 4.1.

Step 7 For the mass transfer runs the bubble having a detached volume closest to the mean value of all analysed detached bubbles from Step 5, was analysed at various points during its formation by following the same procedure as in Step 5. The areas of the growing bubble as obtained from the computer program were plotted as a function of time and the area under this curve was graphically integrated to give a value for  $\int_0^{t_f} A dt$

Step 8 The average mass transfer coefficient during bubble formation was calculated from the following equations,

$$k_L = \frac{m_f t_f}{(\int_0^{t_f} A dt) C_i} \quad \text{-----} \quad (4.5)$$

$$K_{GC} = \frac{m_f t_f}{(\int_0^{t_f} A dt) y_m} \quad \text{-----} \quad (4.6)$$

Where  $k_L$  and  $K_{GC}$  are the liquid and overall gas phase transfer coefficients respectively.  $m_f$  is average mass transfer rate as calculated from equation 4.1, and  $C_i$  and  $y_m$  are the concentration driving forces for the liquid and gas phase con-





trolled systems respectively since from the experimental analysis during the mass transfer runs it was observed that the concentration of solute in the bulk phase was negligible.

For the CO<sub>2</sub>-water system  $C_i$  was taken as the solubility of CO<sub>2</sub> in water, and for the NH<sub>3</sub>-N<sub>2</sub>-water system  $y_m$  was defined as,

$$y_m = \frac{y_i - y_f}{\ln (y_i / y_f)} \text{-----} (4.7)$$

Where  $y_i$  is the mole fraction of ammonia in the gas feed to the orifice and  $y_f$  is the ammonia concentration in the detached bubble and is calculated from material balance as shown in appendix A.4.

#### 4.7 Precautions

A number of precautions were observed during the course of this investigation and are strongly recommended to obtain reliable results.

- (a) The chamber volume should be held constant for all the experimental runs and the criterion to select this constant value should be to obtain a stable bubble frequency.
- (b) The centrifugal pump for water circulation should always be run at a certain discharge head. Failure to do this could result in air bubbles being entrained and circulated through the column. To ensure that the pump runs properly the valve on the by-pass line to the water reservoir from the pump discharge was



kept partially closed.

- (c) While draining water out of the bubble column, care should be taken to make certain that the level in the column does not fall below the top of the glass beads. This prevents air from getting entrapped between the beads.
- (d) The purity of the water used should be consistent for all the experimental runs.
- (e) During the experimental run the water temperature should be controlled very accurately.
- (f) All titrations should be done under a nitrogen atmosphere.
- (g) About half an hour's warming up time should be allowed for the universal counter. This corresponds to the minimum time recommended by the manufacturer.
- (h) Since the barometer used for recording the atmospheric pressure was in a different laboratory, the exhaust fans in both the laboratories were switched off during the experiment.
- (i) The level of soap solution in the soap film meters should be as high as practicable. This avoids undue pressure fluctuations in the gas lines when the soap film is being formed.
- (j) Before proceeding with the run a quick visual observation should be made of the system to ensure that there are no entrapped air bubbles in liquid lines or rotameters and that the bubble growth is steady.
- (k) Enough time should be allowed for the system to stabilise after any minor change is made. The system response is very slow



because of the low gas flow rates under study.

- (l) It is absolutely necessary to align the camera properly as described in the photographic procedure. Any slight inclination of the lens axis to horizontal could cause a distorted image of the bubble. More so, because no reference source was used in the vertical direction.
- (m) The camera and table should be as free of vibrations as possible.
- (n) There should be no gap between the correction lens and the outer surface of the bubble column and the water in the correction lens should be free of entrapped air bubbles.
- (o) The camera lens should be focussed on the orifice edge.
- (p) The camera lights should be turned on for as little a time as possible in order to reduce heat effects.
- (q) While analysing the films, the digitizer calibration should be checked frequently in order to detect any drift which might have occurred.
- (r) When projecting the film on the screen, the projector should be exactly horizontal to the ground and the projector lens axis should be at  $45^\circ$  to the mirror surface. This is necessary to avoid distortion of the bubble image.





## CHAPTER 5

### EXPERIMENTAL RESULTS

#### 5.1 General

The results of this investigation are subdivided into:

- (i) Calibration runs with air-water
- (ii) Mass transfer runs with carbon dioxide-water
- (iii) Mass transfer runs with ammonia-nitrogen-water

The following parameters were the same for all the experimental runs:

- (i) Orifice inside diameter = 0.408 cm.
- (ii) Orifice outside diameter = 0.738 cm.
- (iii) Water height in the bubble column above the orifice tip = 91.7 cm.

#### 5.2 Calibration Runs with Air-Water

The runs with air-water were necessary to check the validity and accuracy of the experimental technique used and a number of them were made over the entire duration of the test program. The first calibration run was done before starting the mass transfer runs with carbon dioxide-water, the second run was done about half way through CO<sub>2</sub>-water runs, the third run was completed after the technique for ammonia-nitrogen-water runs was perfected, and the last run was done after finishing the experiments.

The results together with the experimental conditions are presented in Table 5. Table 2 is a detailed data sheet for one of



Run No.	Bubble Frequency $f, (\text{sec.}^{-1})$	Water Velocity (cm./sec.)	Water Temperature (°C)	Orifice Pressure (PSIA)	Flow Rate To The Orifice, G (cc./sec.)	Number Of Bubbles Analysed	Mean Detached Bubble Volume, V (cc.)	Calculated Flow Rate At The Orifice $G^* = f.V$ (cc./sec.)	% Error $\frac{G-G^*}{G} \times 100$
A1	2.95	0.95	20.0	14.89	0.3258	10	0.1089	0.3215	+ 1.40
A2	1.02	1.00	24.8	14.87	0.0795	10	0.0772	0.0787	+ 1.06
A3	1.02	1.00	25.0	14.86	0.0777	-	0.0772	0.0788	- 1.40
A4	0.473	0.99	25.1	14.88	0.0400	6	0.0832	0.0393	+ 1.75

Table 5: Results of Calibration Runs



these runs (A2).

These results indicate that the bubble volume can be determined with an accuracy of  $\pm 2\%$ .

### 5.3 Mass Transfer Runs with Carbon Dioxide-Water

Initially experiments were conducted with carbon dioxide as the gas phase and water as the continuous phase for gas bubble frequencies of 3 and 5 bubbles per second. Four different water flow rates varying from 0.34 cm./sec. to 1.09 cm./sec. were studied. These runs indicated the percentage mass transfer occurring during bubble formation to be in the range of 0.5% to 2.5% which fell within the experimental uncertainty of  $\pm 2\%$ . The results are tabulated in Table 6 and are for qualitative use only.

On this basis it was decided to study the mass transfer for bubble frequencies of 1 and 0.5 bubble/sec. and water velocities of 0.3 to 2.5 cm./sec. The choice of lower limit of bubble frequency was dictated by the film capacity of the high speed camera. The camera could not take more than 400 ft. of film which could only record about 12 bubbles at 1/2 bubble per second and 600 frames/sec. camera speed. By statistical analysis it was repeatedly found that approximately 10 bubbles had to be analyzed. The camera speed could not be reduced below about 600 frames/sec. as it could not record the bubble at detachment at speed below this value.

The upper limit of water velocity was set at 2.5 cm./sec. as the bubble column started overflowing above this velocity. The lower limit of 0.3 cm./sec. was chosen as it was thought to be the minimum





Run No.	Bubble Frequency $f, (\text{sec.}^{-1})$	Water Velocity (cm./sec.)	Water Temperature (°C)	Orifice Pressure (PSIA)	Flow Rate To The Orifice, G (cc./sec.)	Number Of Bubbles Analysed	Mean Detached Bubble Volume, V (cc.)	Calculated Flow Rate At The Orifice $G^* = f \cdot V$ (cc./sec.)	% Mass Transfer $\frac{G-G^*}{G} \times 100$
M1	3.03	0.34	21.0	14.70	0.2909	10	0.0936	0.2836	2.5
M2	3.00	0.59	21.5	14.70	0.2879	10	0.0938	0.2815	2.2
M3	2.98	0.85	22.0	14.71	0.2856	10	0.0938	0.2791	2.3
M4	2.96	1.09	22.0	14.71	0.2834	10	0.0943	0.2793	1.4
M5	5.00	0.82	23.0	14.86	0.4815	10	0.0957	0.4792	0.5

Table 6: Initial Mass Transfer Runs With CO<sub>2</sub>-Water



water flow needed to maintain a constant water temperature in the column and reservoir.

Table 7 gives the main variables studied in each run. The data are recorded in Table 8 and the final results are presented in Table 9. Table 3 is a detailed data sheet for run number M8 and sample calculations for this run are presented in the appendix (A.3).

The surface area and volume of the detached bubbles as obtained from the films are listed in Table 10 and Table 11 respectively. They give an indication of the digitizer consistency.

The surface area of the growing bubble is presented in the appendix A.5 (Tables 18 to 24) as a function of time and was found to increase linearly with time during most of the formation period. The main deviation from linearity was observed towards the end of the formation period. This region corresponds to the 'necking' period. The bubble becomes elongated and forms a neck just before detaching from the orifice. A portion of the forming bubble remains at the orifice and the rest moves upward through the column. The former is called the 'rest bubble' and the latter the detached bubble. Two typical area-time curves are plotted in Figure 5 which correspond to runs M8 and M11 for 1 bubble/sec. and half bubble/sec. respectively. The area of the rest bubble was added to the area of the detached bubble since at the instant of bubble detachment both the rest bubble and the detached bubble are contributing to the mass transfer. Quantitatively this relationship can be approximated by a linear function of the form,

$$A = A_0 + k' t \quad \text{-----} \quad (5.1)$$



Run No.	Gas Rate To Orifice (cc./sec.)	Bubble Frequency (sec <sup>-1</sup> )	Water Velocity (cm./sec.)
M1*	0.2909	3.03	0.34
M2*	0.2879	3.00	0.59
M3*	0.2856	2.98	0.85
M4*	0.2834	2.96	1.09
M5*	0.4815	5.00	0.82
M6	0.0859	1.075	1.05
M7	0.0854	1.02	1.02
M8	0.0860	1.04	2.44
M9	0.0860	1.045	1.71
M10	0.0871	1.043	0.33
M11	0.0409	0.474	0.33
M12	0.0399	0.46	1.71

\*These runs were used for deciding the operating range only

Table 7: Range of Variables Studied for CO<sub>2</sub>-Water





Run No.	Bubble Frequency $f, (\text{sec.}^{-1})$	Water Velocity (cm./sec.)	Water Temperature ( $^{\circ}\text{C}$ )	Orifice Pressure (PSIA)	Flow Rate To The Orifice, G (cc./sec.)	Number Of Bubbles Analysed	Mean Detached Bubble Volume, V (cc.)	Calculated Flow Rate At The Orifice $G^* = f \cdot V$ (cc./sec.)	Area Time Integral During Bubble Formation $\int A \, dt$ ( $\text{cm}^2\text{-sec.}$ )	Surface Area Of Rest Bubble ( $\text{cm}^2$ )	Volume Of Rest Bubble (cc.)
M6	1.075	1.05	25.0	14.84	0.0859	8	0.0764	0.0822	0.46	0.147	0.00634
M7	1.02	1.02	25.0	14.79	0.0854	10	0.0789	0.0808	0.45	0.141	0.00600
M8	1.04	2.44	25.0	14.96	0.0860	10	0.0769	0.0801	0.45	0.117	0.00587
M9	1.045	1.71	24.9	14.96	0.0860	10	0.0781	0.0816	0.46	0.146	0.00603
M10	1.043	0.33	25.0	14.95	0.0871	10	0.0777	0.0811	0.49	0.141	0.00579
M11	0.474	0.33	25.0	14.82	0.0409	10	0.0754	0.0356	0.97	0.147	0.00626
M12	0.46	1.71	25.0	14.78	0.0399	10	0.0764	0.0352	0.98	0.147	0.00618

Table 8: Data For  $\text{CO}_2$ -Water Runs



Run No.	Bubble Frequency (sec <sup>-1</sup> )	Water Velocity (cm./sec.)	Gas Flow Rate To The Orifice (cc./sec.)	Mass Transfer (cc./sec.)	% Mass Transfer	Average Liquid Phase Coefficient (cm./hr.)
M6	1.075	1.05	0.0859	0.0037	4.40	34
M7	1.02	1.02	0.0854	0.0046	5.42	45
M8	1.04	2.44	0.0860	0.0059	6.93	58
M9	1.045	1.71	0.0860	0.0044	5.13	41
M10	1.043	0.33	0.0871	0.0061	6.94	53
M11	0.474	0.33	0.0409	0.0053	12.93	52
M12	0.46	1.71	0.0399	0.0047	11.77	47

Table 9: Results of CO<sub>2</sub>-Water System



S. No. Of Bubble Analysed	Surface Area of Detached Bubble, cm <sup>2</sup>									
	Run M6	Run M7	Run M8	Run M9	Run M10	Run M11	Run M12			
1	0.8446	0.8822	0.8173	0.8483	0.8417	0.8273	0.8391			
2	0.8606	0.8786	0.8385	0.8540	0.8569	0.8428	0.8386			
3	0.8920	0.8764	0.8416	0.8533	0.8505	0.8326	0.8329			
4	0.8729	0.8771	0.8287	0.8553	0.8488	0.8374	0.8379			
5	0.8684	0.8793	0.8561	0.8473	0.8386	0.8437	0.8488			
6	0.8435	0.8819	0.8449	0.8376	0.8461	0.8519	0.8318			
7	0.8510	0.8798	0.8569	0.8347	0.8581	0.8442	0.8427			
8	0.8695	0.8920	0.8743	0.8618	0.8605	0.8228	0.8460			
9	-	0.8783	0.8466	0.8590	0.8632	0.8836	0.8298			
10	-	0.8751	0.8297	0.8584	0.8541	0.8356	0.8399			
Mean	0.8628	0.8801	0.8435	0.8510	0.8519	0.8422	0.8388			

Table 10: Surface Area of Detached Bubbles for CO<sub>2</sub>-Water System





S. No. Of Bubble Analysed	Volume of Detached Bubble, cm <sup>3</sup>						
	Run M6	Run M7	Run M8	Run M9	Run M10	Run M11	Run M12
1	0.0738	0.0795	0.0746	0.0781	0.0770	0.0757	0.0756
2	0.0760	0.0785	0.0776	0.0783	0.0767	0.0744	0.0754
3	0.0803	0.0779	0.0768	0.0802	0.0764	0.0754	0.0754
4	0.0774	0.0786	0.0757	0.0775	0.0786	0.0749	0.0763
5	0.0778	0.0790	0.0781	0.0778	0.0770	0.0754	0.0772
6	0.0737	0.0794	0.0772	0.0768	0.0785	0.0753	0.0773
7	0.0745	0.0790	0.0788	0.0769	0.0778	0.0769	0.0777
8	0.0776	0.0799	0.0793	0.0787	0.0789	0.0740	0.0758
9	-	0.0787	0.0765	0.0789	0.0780	0.0759	0.0757
10	-	0.0783	0.0746	0.0779	0.0778	0.0759	0.0773
Mean	0.0764	0.0789	0.0769	0.0781	0.0777	0.0754	0.0764

Table 11: Volume of Detached Bubbles for CO<sub>2</sub>-Water System



LEGEND:  $\triangle$  EXPERIMENTAL POINTS FOR RUN M 8  
 -.- EQUATION 5.4 FOR RUN M 8  
 $\circ$  EXPERIMENTAL POINTS FOR RUN M 11  
 --- EQUATION 5.4 FOR RUN M 11

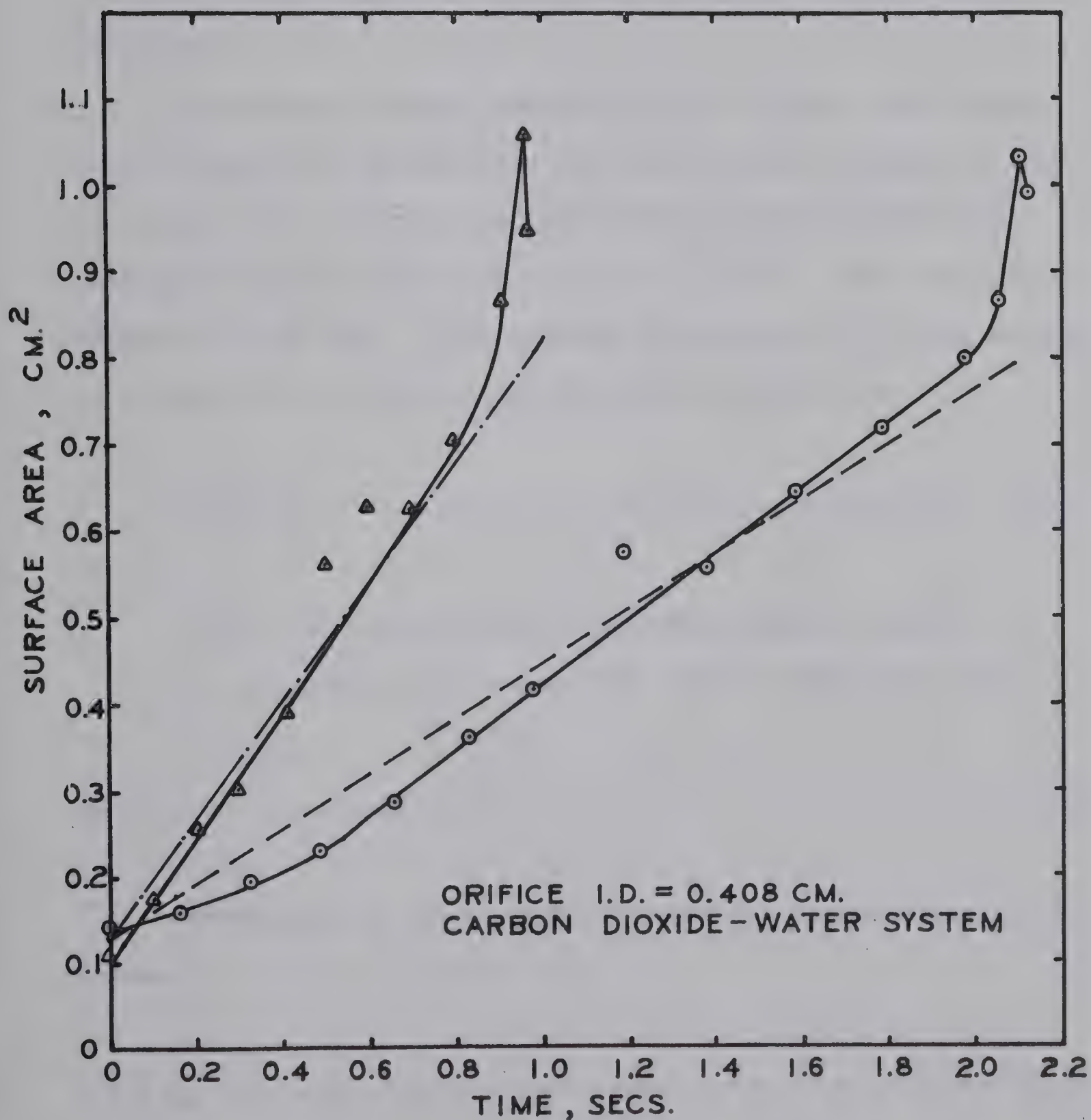


FIG.5. TYPICAL CURVES FOR AREA OF A GROWING BUBBLE.



where,  $A$  = Surface area of the growing bubble at time ' $t$ ',  $\text{cm}^2$

$A_0$  = Surface area of the bubble at time zero,  $\text{cm}^2$

$k'$  = Slope of area-time curve,  $\text{cm}^2/\text{sec}$ .

$t$  = Time at any instant of bubble formation, sec.

The criterion for selecting the value of slope of area-time curve was that  $\int A dt$  should be the same as that determined experimentally.

The slope  $k'$  varied from 0.62 to 0.75  $\text{cm}^2/\text{sec}$ . with a mean value of about 0.66  $\text{cm}^2/\text{sec}$ . for runs with a bubble frequency of one per second. For a frequency of half bubble per second the corresponding values of  $k'$  were from 0.31 to 0.37  $\text{cm}^2/\text{sec}$ . with a mean value of about 0.33  $\text{cm}^2/\text{sec}$ . A new constant in equation (5.1) could be used to account for the effect of gas flow rate and this gave,

$$A = A_0 + 0.66 nt \quad \text{-----} \quad (5.2)$$

where, ' $n$ ' is the frequency of bubble formation ( $\text{sec}^{-1}$ )

$A_0$  in equations (5.1) and (5.2) could be approximated as,

$$A_0 = \frac{\pi}{4} D_o^2 \quad \text{-----} \quad (5.3)$$

where  $D_o$  is the inside orifice diameter. Hence equation (5.2) becomes,

$$A = \frac{\pi}{4} D_o^2 + 0.66 nt \quad \text{-----} \quad (5.4)$$

This equation is plotted in Figure 5 for comparison with the





experimental values. As mentioned before equation (5.4) is not valid for the period just prior to bubble break-up.

The volume of the growing bubble was also found to vary linearly with time. The data are presented in appendix A.5 (Tables 18 through 24) and typical curves are illustrated in Figure 6. The only exception to the linear relationship was in the initial 10% of the life of the bubble. In this period, from visual observation of the film, the bubble was oscillating considerably. The volume of the rest bubble was again added to the volume of the detached bubble.

The quantitative relationship for the volume of the growing bubble can be approximately written as,

$$V = k'' t \quad \text{-----} \quad (5.5)$$

where,  $V$  = Volume of growing bubble at time ' $t$ ',  $\text{cm}^3$

$k''$  = Slope of volume-time curve,  $\text{cm}^3/\text{sec}$ .

$t$  = Time at any instant during bubble formation, sec.

The slope  $k''$  varied from 0.085 to 0.096  $\text{cm}^3/\text{sec}$ . with a mean value of about 0.091  $\text{cm}^3/\text{sec}$ . for a bubble frequency of around one bubble/sec. And the value was 0.0425  $\text{cm}^3/\text{sec}$ . for the bubble frequency of about half bubble/sec.

Equation (5.3) could be generalized to account for the effect of frequency and the resulting form is,

$$V = 0.09 n t \quad \text{-----} \quad (5.6)$$

where, ' $n$ ' is the frequency of bubble formation,  $(\text{sec}^{-1})$



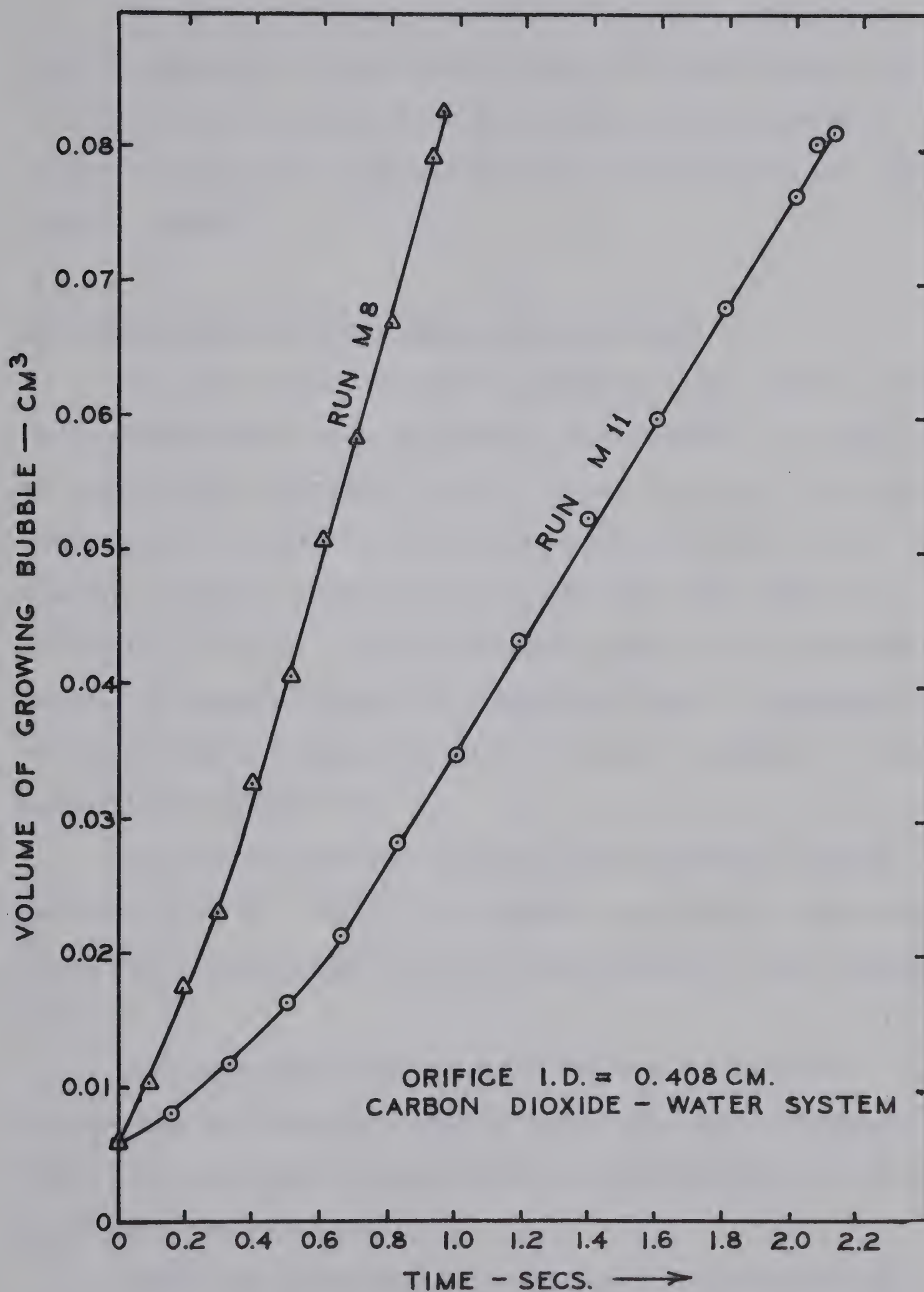


FIG. 6. TYPICAL CURVES FOR VOLUME  
OF A GROWING BUBBLE



The liquid phase mass transfer coefficient was found to be nearly independent of the gas flow rate and the liquid velocity. However, as expected, the percentage mass transfer was observed to be inversely proportional to the gas flow rate. These results are tabulated in Table 9.

#### 5.4 Mass Transfer Runs with Ammonia-Nitrogen-Water

The rate of mass transfer from ammonia-nitrogen bubbles forming in a continuous water phase was measured experimentally. The effect of gas flow rate, or the bubble frequency, on the coefficient was studied while the water velocity in the column was maintained constant at 1 cm./sec. The gas flow rate to the orifice was varied from 0.3 cm<sup>3</sup>/sec to 1.22 cm<sup>3</sup>/sec. giving a frequency range of 3 to 10 bubbles/second. The ammonia-nitrogen feed mixture was kept at a constant composition of about 19% ammonia by volume. The major variables for each run are listed in Table 12.

The data are tabulated in Table 13 and the results are summarized in Table 14. Table 4 is a detailed data sheet for run number N2 and sample calculations for this run are presented in the appendix (A.4).

The surface areas and volumes of the detached bubbles as obtained from the films are listed in Table 15 and Table 16 respectively. The values give a measure of the reproducibility of the experimental technique.

Figure 7 is a graphical representation of the variation of surface area of the bubble with time during the formation period. The variation is linear except in the neck formation zone. For some reason





Run No.	Composition Of The NH <sub>3</sub> -N <sub>2</sub> Mixture (% NH <sub>3</sub> By Volume)	Gas Flow Rate To Orifice (cm <sup>3</sup> /sec.)	Bubble Frequency (sec <sup>-1</sup> )	Water Velocity (cm./sec.)
N1	19.4	0.5160	4.88	0.97
N2	18.4	0.3026	3.10	0.96
N3	18.5	0.6941	6.60	0.96
N4	19.5	1.2207	10.10	0.94

Table 12: Range of Variables Studied for NH<sub>3</sub>-N<sub>2</sub>-Water System



Run No.	Composition Of Gas Mixture (% $\text{NH}_3$ By Vol.)	Bubble Frequency f (sec.)	Water Velocity (cm./sec.)	Water Temperature ( $^{\circ}\text{C}$ )	Orifice Pressure (PSIA)	Flow Rate To The Orifice, G (cc./sec.)	Number Of Bubbles Analysed	Mean Detached Bubble Volume (cc.)	Calculated Flow Rate At The Orifice $G^* = f \cdot V$ (cc./sec.)	Area Time Integral During Bubble Formation $\int A dt$ ( $\text{cm}^2\text{-sec.}$ )	Surface Area Of Rest Bubble ( $\text{cm}^2$ )	Volume Of Rest Bubble ( $\text{cm}^3$ )
N1	19.4	4.88	0.97	25	14.94	0.5160	7	0.0877	0.4286	0.117	0.132	0.00523
N2	18.4	3.10	0.96	25	14.85	0.3026	10	0.0805	0.2492	0.189	0.112	0.00494
N3	18.5	6.60	0.96	25	14.85	0.6941	8	0.0898	0.5909	0.090	0.108	0.00472
N4	19.5	10.10	0.94	25	14.87	1.2207	10	0.1054	1.0656	0.062	0.129	0.00500

Table 13: Data for Ammonia-Nitrogen-Water Runs



Run No.	Composition Of Gas Mixture (% NH <sub>3</sub> By Vol.)	Bubble Frequency (Sec <sup>-1</sup> )	Water Velocity (cm./sec.)	Gas Flow Rate At The Orifice (cc./sec.)	Mass Transfer During Bubble Formation (cc./sec.)	% Mass Transfer During Bubble Formation (cc./sec.)	Average Overall Gas Phase Mass Transfer Coefficient gm-moles/hr-cm <sup>2</sup> -atm.
N1	19.4	4.88	0.97	0.5160	0.0874	16.9	0.259
N2	18.4	3.10	0.96	0.3026	0.0534	17.6	0.229
N3	18.5	6.60	0.96	0.6941	0.1032	14.9	0.263
N4	19.5	10.10	0.94	1.2207	0.1551	12.7	0.287

Table 14: Results of Runs on NH<sub>3</sub>-N<sub>2</sub>-Water System





S. No. Of Bubble Analysed	Surface Area of Detached Bubble, cm <sup>2</sup>			
	Run N1	Run N2	Run N3	Run N4
1.	0.9001	0.8478	0.9245	1.0596
2.	0.9067	0.8551	0.9434	1.0744
3.	0.9252	0.8938	0.9318	1.0470
4.	0.9225	0.8945	0.9286	1.0510
5.	0.9301	0.8485	0.9303	1.0801
6.	0.9184	0.8816	0.9273	1.0655
7.	0.9353	0.8912	0.9616	1.0457
8.	-	0.8794	0.9598	1.0397
9.	-	0.8573	-	1.0404
10.	-	0.8608	-	1.0286
Mean	0.9197	0.8710	0.9384	1.0532

Table 15: Surface Area of Detached Bubbles  
for NH<sub>3</sub>-N<sub>2</sub>-Water System



S. No. Of Bubble Analysed	Volume of Detached Bubble, cm <sup>3</sup>			
	Run N1	Run N2	Run N3	Run N4
1.	0.0884	0.0765	0.0890	0.1064
2.	0.0867	0.0806	0.0896	0.1076
3.	0.0870	0.0826	0.0895	0.1052
4.	0.0871	0.0805	0.0899	0.1061
5.	0.0874	0.0798	0.0892	0.1082
6.	0.0888	0.0814	0.0883	0.1076
7.	0.0884	0.0828	0.0927	0.1053
8.	-	0.0833	0.0900	0.1028
9.	-	0.0774	-	0.1028
10.	-	0.0804	-	0.1018
Mean	0.0877	0.0805	0.0898	0.1054

Table 16: Volume of Detached Bubbles for NH<sub>3</sub>-N<sub>2</sub>-Water System



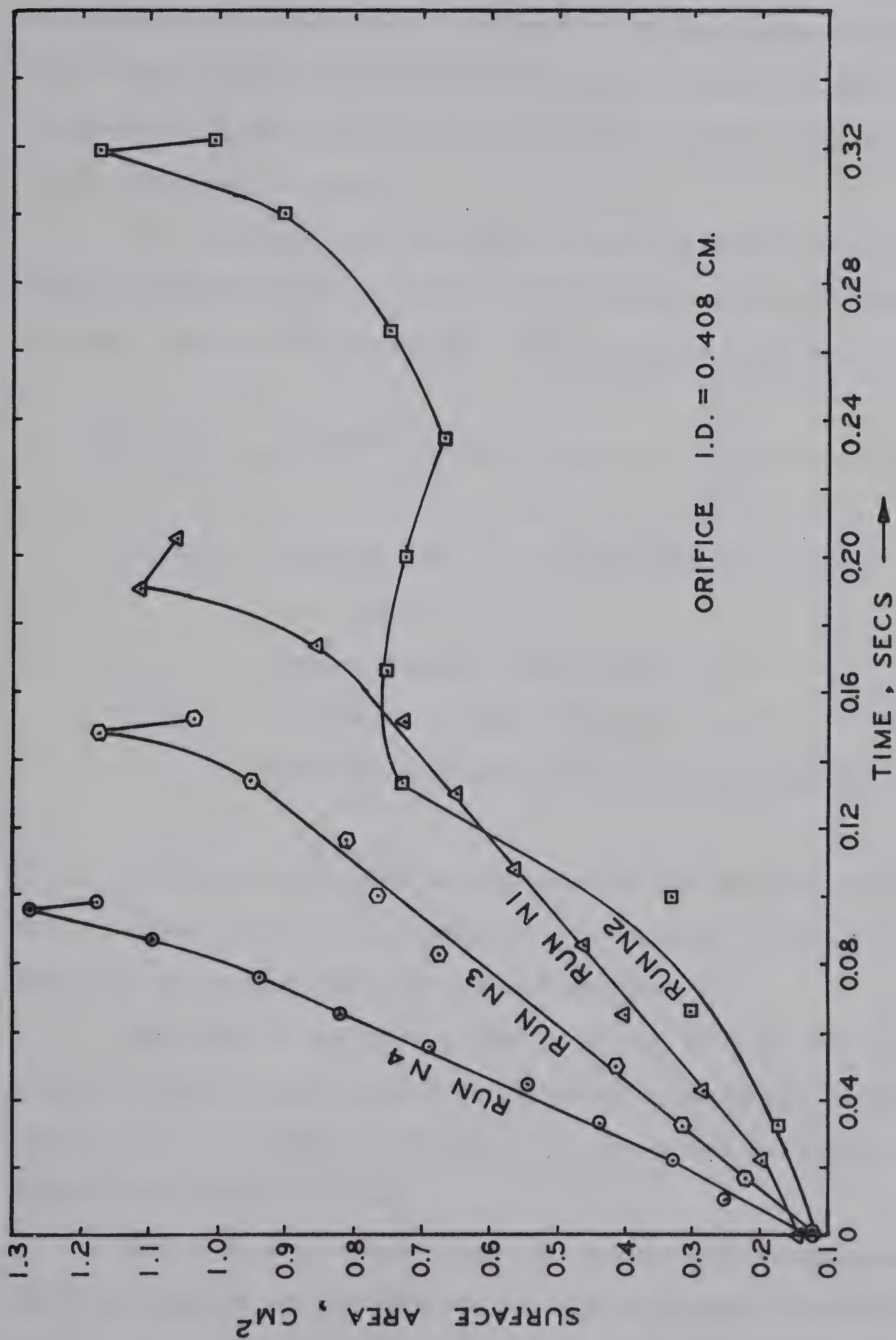


FIG. 7. AREA OF A GROWING BUBBLE  
FOR NH<sub>3</sub> — N<sub>2</sub> — WATER SYSTEM





the growth of the bubble is not well defined for run N2 indicating an unsteady growth of the bubble. The area of the rest bubble was added to the area of the detached bubble since at the instant of bubble detachment both the rest bubble and the detached bubble are contributing to the mass transfer.

The surface area of the bubble at any time during its growth could be approximately correlated to the frequency of bubble formation and time, from the data of Figure 7. The resulting relationship is,

$$A = (\pi/4) D_o^2 + 0.507 n^{1.34} t \text{ ----- (5.7)}$$

where, A = Surface area of the growing bubble at time  
't', (cm<sup>2</sup>)

D<sub>o</sub> = Inside diameter of the orifice, (cm)

n = Frequency of bubble formation, (sec<sup>-1</sup>)

t = Time at any instant of bubble formation, (sec.)

The basis for arriving at this equation was the same as that for the carbon dioxide-water system but this equation is not strictly valid for the necking region of bubble formation.

The volume of the growing bubble was also found to vary linearly with time during the entire growth period. The results are shown in Figure 8. Once again the volume of the rest bubble was added to the volume of the detached bubble.

All the data of Figure 8 could be approximately represented in the following form and the equation quantitatively shows the effect of frequency on the bubble volume at any instant of its growth.



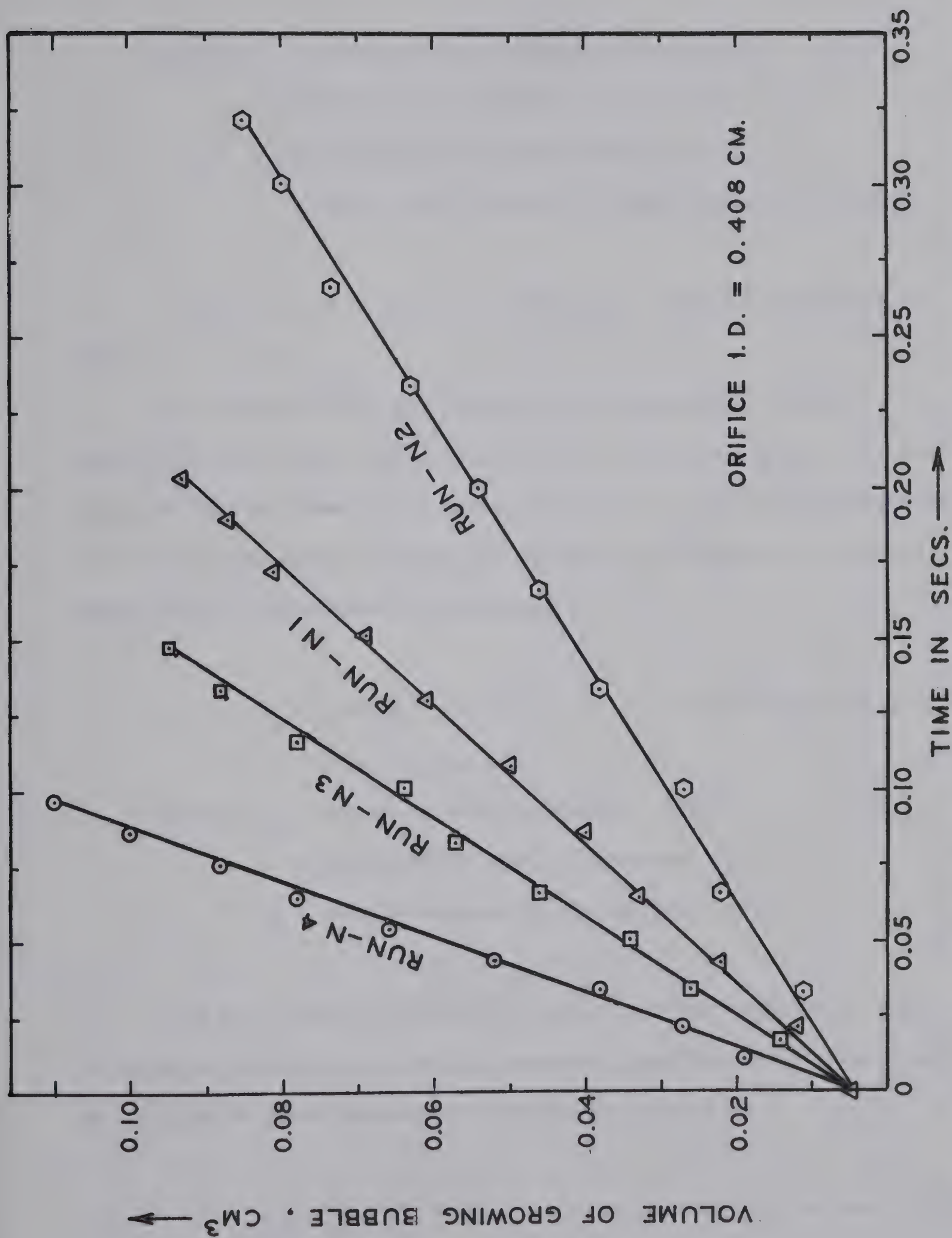


FIG. 8. VOLUME OF A GROWING BUBBLE FOR  $\text{NH}_3 - \text{N}_2$  - WATER SYSTEM



$$V = V_o + 0.056 n^{1.29} t \text{ ----- (5.8)}$$

where,  $V$  = Volume of the growing bubble at time 't', ( $\text{cm}^3$ )

$V_o$  = Volume of the bubble at time zero, ( $\text{cm}^3$ )

$n$  = Frequency of bubble formation, ( $\text{sec}^{-1}$ )

$t$  = Time at any instant of bubble formation, (sec.)

This equation is valid for the entire formation period of the bubble.

The volume of the gas bubbles after detachment for the ammonia-nitrogen-water system was found to vary linearly with the frequency of bubble formation as shown in Figure 9. The range of frequencies studied was from 3 bubbles per second to 10 bubbles per second. Quantitatively, this could be expressed as,

$$V_f = 1.04 D_o^3 + 0.00351 n \text{ ----- (5.9)}$$

(for  $3 \leq n \leq 10$ )

where,  $V_f$  = Volume of detached bubble, ( $\text{cm}^3$ )

$n$  = Frequency of bubble formation, ( $\text{sec}^{-1}$ )

$D_o$  = Inside diameter of the orifice, (cm)

The gas phase mass transfer coefficient was calculated from the measured values of the overall transfer coefficient by correcting for the liquid phase resistance. The equation used is,

$$\frac{1}{K_G} = \frac{1}{k_G} + \frac{m}{k_L} \text{ ----- (5.10)}$$





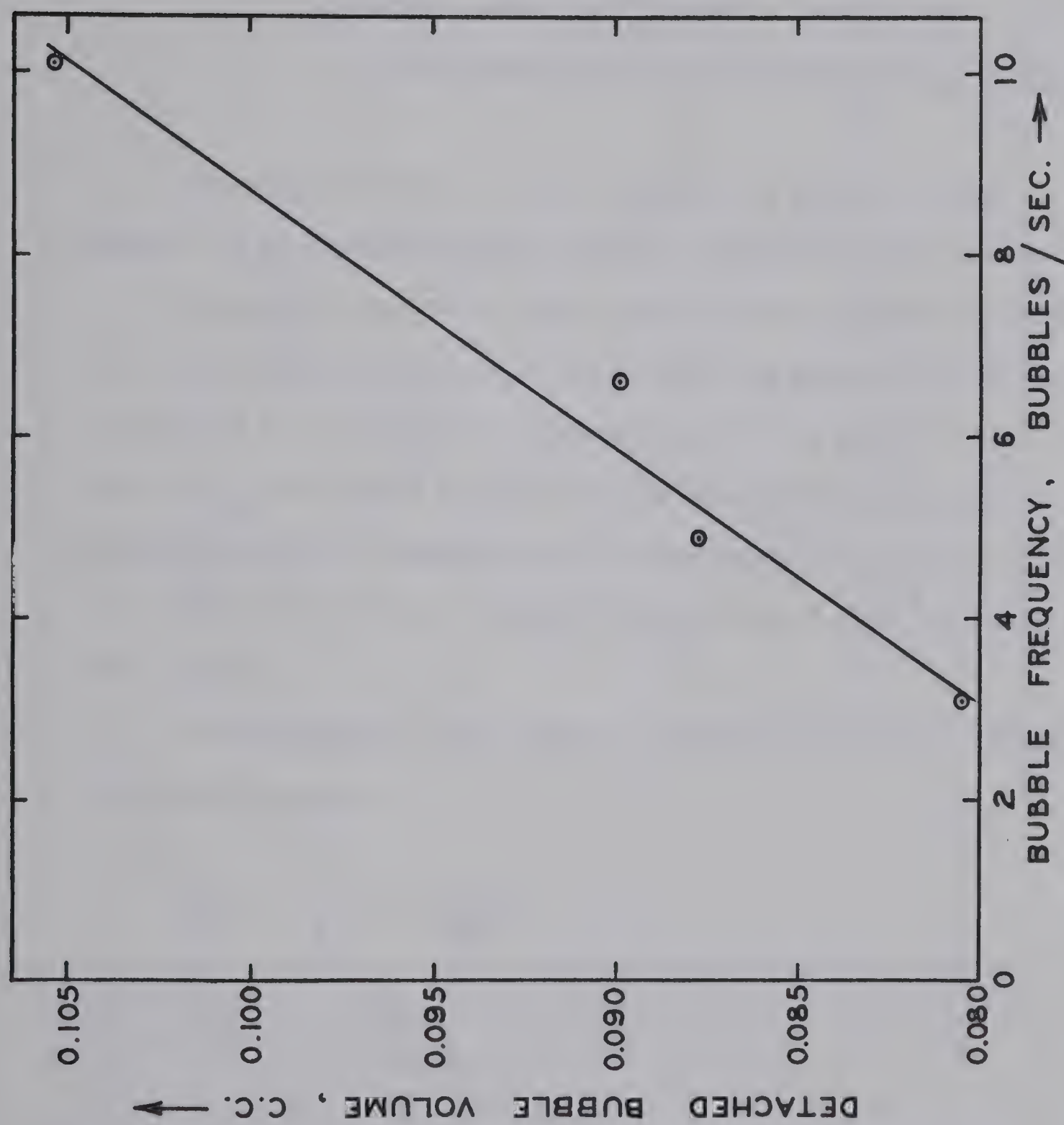


FIG. 9 VARIATION OF DETACHED BUBBLE VOLUME WITH  
FREQUENCY FOR  $\text{NH}_3 - \text{N}_2$  - WATER SYSTEM



where,  $K_G$  is the overall transfer coefficient,

gm-moles/hr-cm<sup>2</sup>-atm.

$k_G$  is the gas phase transfer coefficient,

gm-moles/hr-cm<sup>2</sup>-atm.

$k_L$  is the liquid phase transfer coefficient, cm./hr.

$m$  is the slope of the equilibrium curve,  $\frac{\text{atm.}}{\text{gm-moles/cm}^3}$

The value of 'm' at 1 atm. and 25°C is given in Perry's Handbook as 17.89 atm./gm-moles/cm<sup>3</sup> for the ammonia-water system.

From the experiments done on the CO<sub>2</sub>-water system the value of the liquid phase mass transfer coefficient was measured to be about 50 cm./hr. and it was found to be independent of the gas flow rate. This value of  $k_L$  was assumed to apply to the NH<sub>3</sub>-N<sub>2</sub>-water system also since the diffusivities of ammonia and carbon dioxide in water are about the same ( $1.96 \times 10^{-5}$  cm<sup>2</sup>/sec. for CO<sub>2</sub> in water and  $2 \times 10^{-5}$  cm<sup>2</sup>/sec. for NH<sub>3</sub> in water).

Thus equation (5.10) reduces to the following form for the NH<sub>3</sub>-N<sub>2</sub>-water system,

$$\frac{1}{K_G} = \frac{1}{k_G} + \frac{17.89}{50} \quad \text{-----} \quad (5.11)$$

$$\text{or, } k_G = \frac{K_G}{(1 - 0.3578 K_G)}$$

The values of  $k_G$  as calculated from equation (5.11) are plotted in Figure 10 and are tabulated in the appendix (Table 25). It can be observed that the gas phase mass transfer coefficient during bubble formation increases with the bubble frequency, or the gas flow rate.



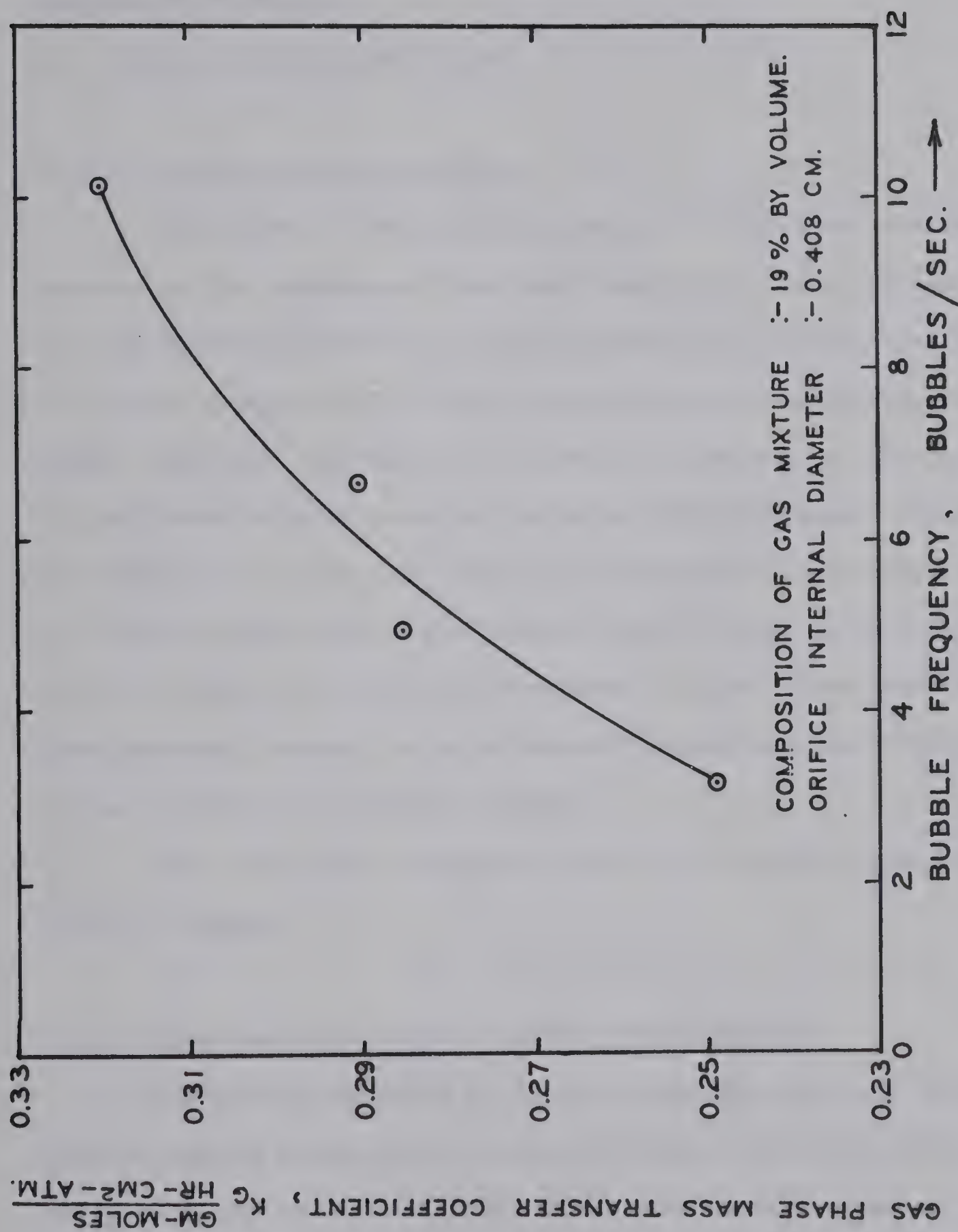


FIG. 10.  $K_G$  VS. BUBBLE FREQUENCY FOR  $\text{NH}_3 - \text{N}_2$  - WATER SYSTEM.





## CHAPTER 6

### DISCUSSION OF RESULTS

#### 6.1 Carbon Dioxide-Water System

##### 6.1.1 Volume of Detached Bubbles

The volume of the detached bubbles for the carbon dioxide-water system, in the experimental runs where negligible amount of mass transfer was observed (Table 6), remained essentially constant at 0.094 c.c. for bubble frequencies of 3 and 5 bubbles/second showing that the bubble formation occurred in the constant volume region. Equation (2.4) is applicable in this formation regime as Reynold's number from definition (Equation 2.1) is less than one in the range of flow rates studied, and predicts the value of the detached bubble volume to be 0.0945 c.c. when the appropriate values of variables are used. Thus there is a good agreement between the experimentally determined and the predicted values of the detached bubble volume.

The final bubble volume was found to increase slightly with the bubble frequency.

##### 6.1.2 Area-Time Relationship For The Growing Bubble

Calderbank and Patra [15] did an experimental study of carbon dioxide bubbles during their formation in water and found an empirical correlation for the area of the bubbles, which was given as,

$$\frac{A}{A_m} = 1 - \left( \frac{t_f - t}{t_f} \right)^{1.86} \text{-----} (2.9)$$



This equation was valid for bubble frequencies of 0.2 to 2.0 bubbles/sec. and equivalent spherical bubble diameters of 0.5 to 1.0 cm. In this equation  $A$  and  $A_m$  are the area at any time  $t$  and the maximum area of the bubble during its formation respectively.

In Figures 11 and 12 a comparison has been made of the values of area predicted by equation (2.9) with the ones found from this experimental investigation. The findings of Kalra [49] are also superimposed on the graphs. In Figure 11 Kalra's results were obtained from a study of mass transfer during bubble formation using the carbon dioxide-water system. The bubble frequency was 1 bubble/sec. and the water velocity in the column was constant at 1 cm./sec. His results in Figure 12 correspond to a frequency of 1/2 bubble/sec. and a water velocity of 1 cm./sec. The results of this investigation compare very well with Kalra's findings. However, the growth of the bubble was observed to be more steady in terms of its surface area in this study. In all the experimental runs the area of the bubble dropped after break-off from the orifice. This may be due to the stretching encountered by the bubble prior to its breaking which results in an elongated neck and hence a larger surface area.

The equation proposed by Calderbank et.al. [15] does not agree with the findings of this study. They have not included the effect of the rest-bubble in their equation. Besides the equation predicts a very uniform increase of area with time till the bubble detaches. This is contrary to the results reported here and by Kalra [49]. In both of the latter studies a very sharp increase of area was noticed in the neck-formation zone of bubble growth. It can also be observed that



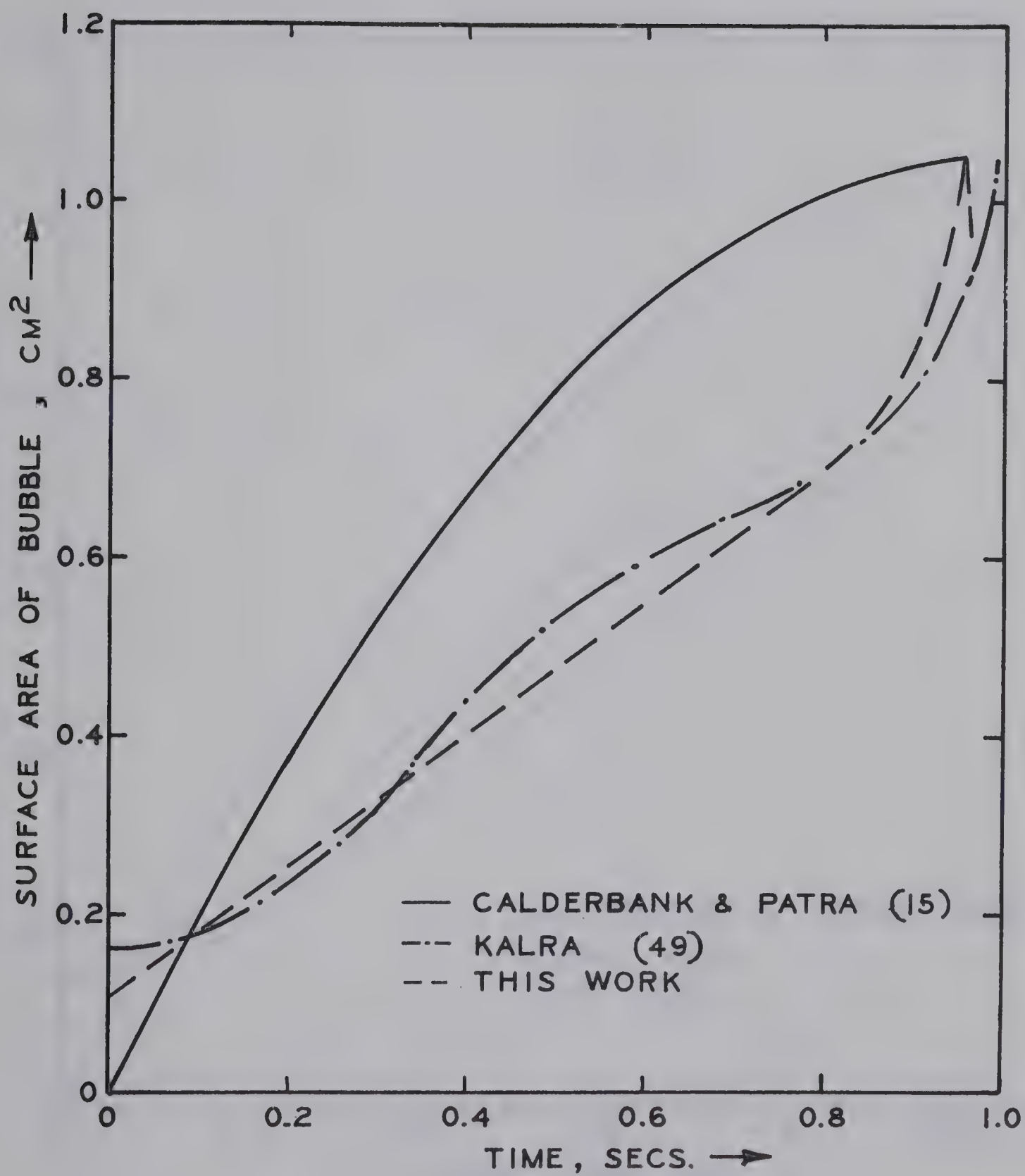


FIG. II. COMPARISON OF AREAS DURING FORMATION FOR RUN 8





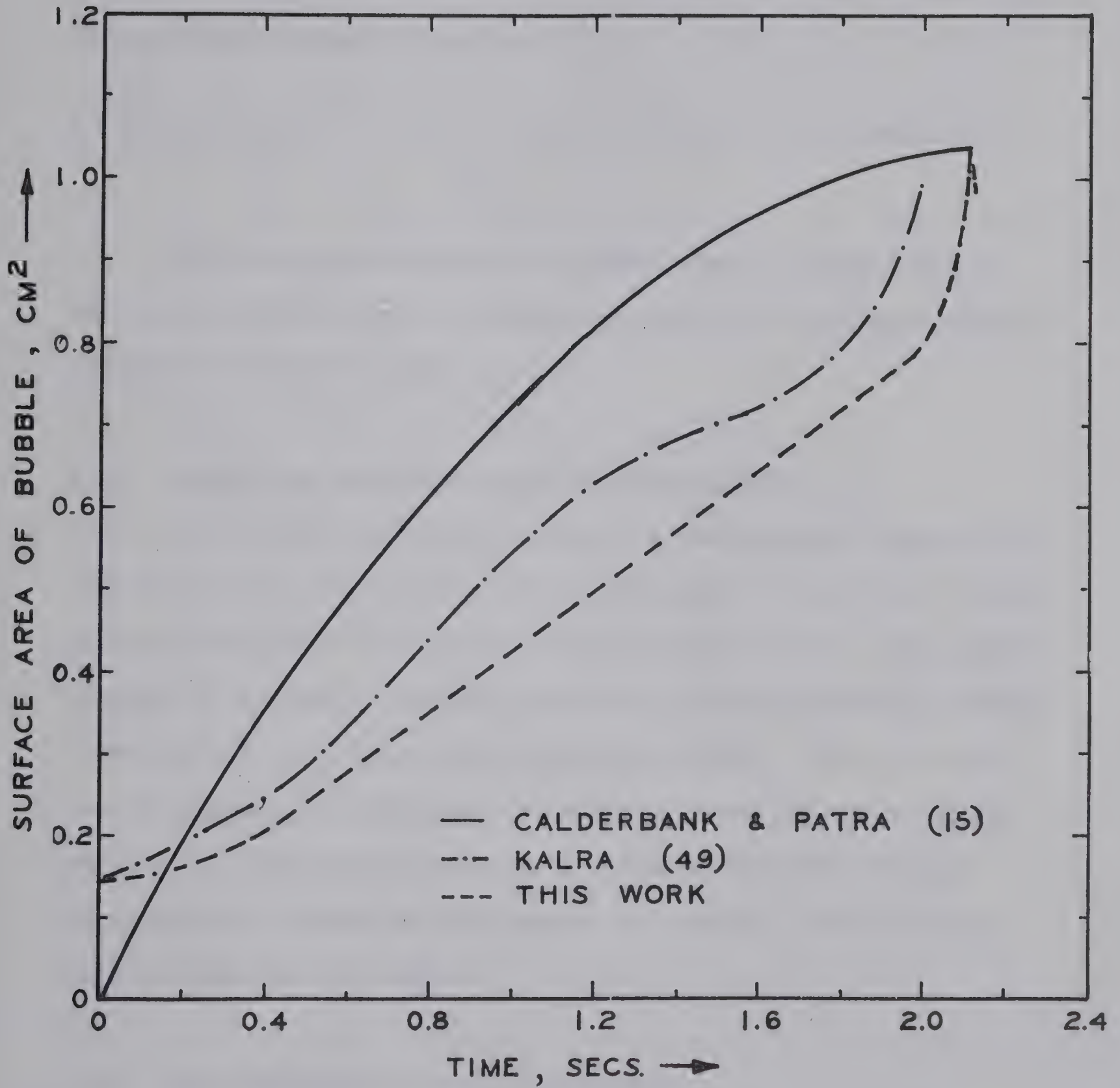


FIG.12. COMPARISON OF AREAS DURING FORMATION OF BUBBLE



Calderbank's equation overestimates the value of the area under the area-time curve.

A new relationship for carbon-dioxide bubbles forming in water from a submerged horizontal orifice of 0.408 cm. is found to exist and is expressed in equation (5.4) as,

$$A = \frac{\pi}{4} D_o^2 + 0.66 nt \quad (\text{for 'n' in the range of 0.5 to 1 bubble/sec.})$$

This equation is plotted in Figure 5 and it can be observed that the agreement with the experimental values is fairly good except in the neck formation region.

### 6.1.3 Volume-Time Relationship For The Growing Bubble

It was found that the volume of the bubble varied linearly with time in most of the formation region. The exception was in the initial period of the growth cycle where it grew a little slowly. This could probably be because of a sudden reduction in pressure inside the bubble after the bulk of it gets detached from the orifice. Since the water head is constant it would have a tendency to force the bubble inside the orifice. The linear variation of volume of the bubble subsequently implies a steady gas flow rate to the orifice. Kalra [49] has also reported similar findings.

### 6.1.4 Liquid Phase Mass Transfer Coefficient

The value of the liquid phase mass transfer coefficient during bubble formation for the carbon dioxide-water system did not vary



appreciably with a superimposed co-current flow of the continuous phase. It held constant at about 45 cm./hr. at 1 bubble per second over a water velocity range of 0.3 cm./sec. to 2.5 cm./sec. A slight increase in the value of  $k_L$  was observed at 0.5 bubble per second bubble frequency and the value remained constant at 49.5 cm./hr. over the same range of water velocity. Though the effect of water velocity was not isolated by Kalra [49] he found the values for a similar system to be 160 cm./hr. at 1 bubble per second and 100 cm./hr. at 0.5 bubble/second. His study was done at a water velocity of 1 cm./sec. Kalra's values of the transfer coefficient during formation are higher than those observed by other workers for bubble rise period.

Calderbank and Patra [15] have indicated that their data on a study of mass transfer during bubble formation using the CO<sub>2</sub>-water system agreed well with the equation,

$$k_L = 1.56 \sqrt{\left(\frac{D_L}{\pi t_f}\right)} \text{ ----- (2.27)}$$

where  $k_L$  was defined as in equation (2.26).

For the carbon dioxide-water system at 25°C the value of the diffusivity is  $1.96 \times 10^{-5}$  cm<sup>2</sup>/sec. which gives the mass transfer coefficient at bubble formation as 14 cm./hr. for a bubble frequency of one bubble per second and 9.5 cm./hr. for half a bubble per second. These values are lower than the ones observed in this investigation.

When Calderbank et. al.'s definition of  $k_L$  is changed to equation (3.62) in order to make it consistent with the definition which is used to calculate  $k_L$  in this study. the following equation is obtained,





$$k_L = 2.4 \sqrt{\left(\frac{D_L}{\pi t_f}\right)} \text{ ----- (3.63)}$$

which predicts the value of  $k_L$  to be 21.6 cm./hr. and 14.6 cm./hr. for bubble frequencies of 1 per second and 0.5 per second respectively. The values are still lower than the ones obtained experimentally by us.

By modifying Calderbank and Patra's model to incorporate the area-time relationship of the form defined by equation (3.57), it was derived that,

$$k_L = 2 \sqrt{\left(\frac{D_L}{\pi t_f}\right)} \left[ \frac{A_o + 0.67 k' t_f}{A_o + 0.5 k' t_f} \right] \text{ ----- (3.60)}$$

From the experimental results  $k'$  could be expressed as a function of the bubble frequency as in equation (5.2),

$$k' = 0.66 n = \frac{0.66}{t_f} \text{ ----- (6.1)}$$

which on substitution in equation (3.60) gives,

$$k_L = 2 \sqrt{\left(\frac{D_L}{\pi t_f}\right)} \left[ \frac{A_o + 0.442}{A_o + 0.33} \right] \text{ ----- (6.2)}$$

Further, the surface area of the rest bubble was found to remain essentially constant and could be approximated by equation (5.3). In this study the internal diameter of the orifice used was 0.408 cm. and thus equation (6.2) reduces to,



$$k_L = 2.48 \sqrt{\left(\frac{D_L}{\pi t_f}\right)} \text{ ----- (6.3)}$$

and it predicts the values of the mass transfer coefficient during formation to be 22.2 and 15.1 cm./hr. for bubble frequencies of one and one half per second respectively. Although these values are low as compared to the experimentally observed values of 45 and 49.5 cm./hr., they agree very well with the predictions of Calderbank's modified equation (3.63).

Beek and Kramer's [3] solution was shown in equation (3.45) for a spherical bubble growth to be,

$$k_L = 2 \sqrt{\left(\frac{D_L}{\pi t_f}\right)} \text{ ----- (3.45)}$$

The values of  $k_L$  calculated from this equation for the carbon dioxide-water system are 17.9 cm./hr. at one bubble per second, and 12.2 cm./hr. at half bubble per second. The values are again lower than the experimental measurements but are of the same order of magnitude as those predicted from equations (3.63) and (6.3).

Popovich et. al. [67] have proposed an equation of the form (2.23) for mass transfer during drop formation and found the following equation to be valid from their experimental findings on the sodium iodide drops formed in isobutyl alcohol.

$$N''(t_f) = 1.32 (C_i - C_o) (\pi D_L)^{1/2} d_f^2 t_f^{0.5} \text{ ----- (6.4)}$$



Defining,

$$N''(t_f) = k_L (C_i - C_o) \int_0^{t_f} A dt \quad \text{-----} \quad (6.5)$$

where, A for spherical drop growth is given from equation (2.24) as,

$$A = \pi d_f^2 t_f^{-2/3} t^{2/3} \quad \text{-----} \quad (6.6)$$

From equations (6.4), (6.5) and (6.6) it can be shown that,

$$k_L = 2.2 \sqrt{\left(\frac{D_L}{\pi t_f}\right)} \quad \text{-----} \quad (6.7)$$

This equation, once again, predicts the value of  $k_L$  in the same range as obtained from equations (3.63), (3.45) and (6.3).

The mass transfer during the rise period from a circulating bubble can be predicted from equations (2.20) and (2.21) when the Reynold's number is greater than 400. The detached volume, V, for this study was found to remain constant at about 0.077 c.c. from Table 11. Hence, from equation (2.21) the terminal velocity of carbon dioxide bubbles in water is calculated as 7.6 cm./sec. which is very low when compared to the corresponding experimental values listed in Table 1. The volume of 0.077 c.c. gives an equivalent bubble diameter of 0.528 cm. for which the velocity of bubble rise is about 20 cm./sec.

With this value of velocity the Reynold's number from equation (2.10) is 1055 and hence equation (2.20) can be used. It predicts  $k_L$





during rise to be 110 cm./hr. which is about the same as that observed experimentally by various investigators listed in Table 1.

A comparison of the above value of transfer coefficient with the values obtained for the mass transfer coefficient during bubble formation in this study shows that at a bubble frequency of 1 bubble/second,

$$\frac{k_L \text{ (formation)}}{k_L \text{ (rise)}} = \frac{45}{110} = 0.41 \text{ ----- (6.8)}$$

and at half bubble per second,

$$\frac{k_L \text{ (formation)}}{k_L \text{ (rise)}} = \frac{49.5}{110} = 0.45 \text{ ----- (6.9)}$$

In article 3.2.1 by using a surface stretching model for the transfer coefficient during formation and Higbie's penetration theory for  $k_L$  during rise it is shown that,

$$\frac{k_L \text{ (formation)}}{k_L \text{ (rise)}} = \sqrt{\left(\frac{d_f}{\ell}\right)} \text{ ----- (3.50)}$$

$$\text{where, } \ell = U t_f \text{ ----- (2.29)}$$

As before,  $d_f$  in this study was approximately 0.528 cm. and from Table 1 the corresponding value for  $U$  is 20 cm./sec. Thus equation (3.50) simplifies to,

$$\frac{k_L \text{ (formation)}}{k_L \text{ (rise)}} = 0.162 t_f^{-0.5} \text{ ----- (6.10)}$$



which gives the ratio as 0.162 at 1 bubble per second and 0.115 at 1/2 bubble per second. These values are much lower than those observed experimentally (equations 6.8 and 6.9).

The model described in article 3.2.2 predicted the ratio of mass transfer coefficients during bubble formation and rise as equation (3.64). This equation on comparison with equations (2.29) and (5.4) simplifies to the following equation when the diameter of the orifice is taken as 0.408 cm.

$$\frac{k_L \text{ (formation)}}{k_L \text{ (rise)}} = 1.24 \sqrt{\left(\frac{d_f}{\ell}\right)} \text{ ----- (6.11)}$$

Thus the ratio predicted by equation (6.11) is 24% higher than those by equation (3.50) or equation (6.10). The values of  $k_L$  (formation)/ $k_L$  (rise) are 0.2 and 0.143 for frequencies of 1 and 1/2 bubble per second respectively. Once again, these values are smaller than the ones in equation (6.8) and (6.9).

Hence the mass transfer coefficient during the bubble formation is lower than its value during the subsequent bubble rise period.

## 6.2 Ammonia-Nitrogen-Water System

### 6.2.1 Volume of Detached Bubbles

The volume of the gas bubbles after detachment for the ammonia-nitrogen-water system increased linearly with the frequency as in equation (5.9) showing thereby that the experiments were done in the slowly increasing volume region of bubble formation.



### 6.2.2 Area-Time Relationship for the Growing Bubble

The area of the bubble increased linearly with time but varied as  $1.34^{\text{th}}$  power of the frequency of bubble formation. The relationship is expressed in equation (5.7) and is different from the one obtained for the carbon dioxide-water system. However, the necking region is not well represented by equation (5.7). The variation in the surface area of the rest-bubble was not much ( $0.11$  to  $0.13 \text{ cm}^2$ ) for the  $0.408$  cm. internal diameter orifice used and in equation (5.7) it is approximated to  $0.13 \text{ cm}^2$ .

### 6.2.3 Volume-Time Relationship for the Growing Bubble

The volume-time relationship was found to be much better for the ammonia-nitrogen-water system than for the carbon dioxide-water system. In the latter system a deviation from the linearity existed in the initial growth period of the bubble. On the contrary, no such effect was observed for the former system. The volume of the bubble varied as  $1.285^{\text{th}}$  power of the bubble frequency whereas for the  $\text{CO}_2$ -water system it varied as a linear function of the bubble frequency. The volume of the rest-bubble in equation (5.8) remained essentially constant and had a value of  $0.0696 \text{ cm}^3$  for the  $0.408$  cm. internal diameter orifice used.

The linear variation of bubble volume with time gives an indication of the steadiness of the gas flow rate to the orifice.

### 6.2.4 Gas Phase Mass Transfer Coefficient

The individual gas phase mass transfer coefficient during bubble formation was found to increase with the gas flow rate to the





orifice and the variation is depicted in Figure 10. The value of the transfer coefficient was in the range of 0.25 to 0.32 gm-moles/hr-cm<sup>2</sup>-atm. over a bubble frequency range of 3 to 10 bubbles/second. The orifice inside diameter was 0.408 cm. and the composition of the ammonia-nitrogen feed was about 19% ammonia by volume. The mass transfer during the formation period was such as to decrease the bubble volume by 13 to 17 percent.

Sharma and Mashelkar [73] have determined the values of gas-side mass transfer coefficients during bubble rise by absorbing sulphur dioxide bubbles diluted with air in aqueous solutions of sodium hydroxide. Their experimental value of  $k_G$  was 0.203 gm-moles/hr-cm<sup>2</sup>-atm. The corresponding value for ammonia is estimated to be 0.281 gm-moles/hr-cm<sup>2</sup>-atm. This correction is based on the assumption that  $k_G$  is directly proportional to the square root of the diffusivity of solute in the gas phase. The diffusivities for SO<sub>2</sub> in air and NH<sub>3</sub> in N<sub>2</sub> are 0.133 cm<sup>2</sup>/sec. and 0.254 cm<sup>2</sup>/sec. respectively. Thus the values observed experimentally by us for  $k_G$  during formation are of the same order of magnitude as those obtained during bubble rise.

Geddes' equation (2.42) predicts the value of  $k_G$  during rise from a stagnant sphere and for a gas contact time of  $t_f$  reduces to,

$$k_G \text{ (rise)} = 0.165 \frac{R}{t_f} + \frac{D_G \pi^2}{3R} \text{ ----- (6.12)}$$

and for the ammonia-nitrogen feed the value of  $D_G$  at 25°C and 1 atm. is 0.254 cm<sup>2</sup>/sec. which gives,



$$k_{G(\text{rise})} = \left( 0.165 \frac{R}{t_f} + \frac{0.831}{R} \right), \text{ cm./sec.} \quad \text{-----} \quad (6.13)$$

$$\text{or, } k_G (\text{rise}) = 0.147 \left( 0.165 \frac{R}{t_f} + \frac{0.831}{R} \right), \frac{\text{gm-moles}}{\text{hr-cm}^2\text{-atm.}} \quad \text{---} \quad (6.14)$$

This equation on substitution for the value of bubble radius,  $R$ , from the experimentally determined volumes of the detached bubbles shows  $k_G$  to be 0.47 gm-moles/hr-cm<sup>2</sup>-atm. at 3 bubbles/second and 0.48 gm-moles/hr-cm<sup>2</sup>-atm. at 10 bubbles/second. These values of  $k_G$  are higher than those observed experimentally (0.25 and 0.32 respectively) during bubble formation.

Calderbank's equation (2.38) also predicts about the same values of  $k_G$  as equation (6.14). But this is expected since the only difference in the two equations is the term  $0.165 R/t_f$ , which is small in comparison to the term  $D_G \pi^2/3R$ .

Vivian and Behrmann [83] have studied the absorption of ammonia into distilled water in a short wetted-wall column for various compositions of an ammonia-nitrogen gas mixture. They found the value of the gas phase mass transfer coefficient to be about 0.2 gm-mole/hr-cm<sup>2</sup>-atm. for an ammonia concentration of 19% by volume. This value is of the same order of magnitude as those found experimentally in this investigation for the bubble formation period.

The gas phase mass transfer coefficient during bubble formation can be predicted by Thorogood's equation (2.48). This equation for the ammonia-nitrogen feed at 25°C and 1 atm. simplifies to,



$$k_G = 0.0834 \sqrt{n} \frac{\text{gm.-moles}}{\text{hr.-cm.}^2\text{-atm.}} \text{-----} (6.15)$$

where  $n$  is the frequency of bubble formation,  $\text{sec}^{-1}$ .

A comparison of the values obtained from equation (6.15) with the experimentally measured values shows the latter values to be higher than the predicted values. At 10 bubbles/second the experimental value of  $k_G$  is 0.32 gm-moles/hr-cm<sup>2</sup>-atm. whereas the calculated value from equation (6.15) is 0.26 gm-moles/hr-cm<sup>2</sup>-atm. and at 3 bubbles per second these two values are 0.25 and 0.15 respectively.





## CHAPTER 7

### CONCLUSION

#### 7.1 General

The experimental method used in this investigation is suitable for studying the mass transfer phenomenon during bubble formation provided the amount of mass transfer occurring is such that the bubble volume decreases by 5 percent or more. This limitation is due to the experimental uncertainty involved which was  $\pm 2\%$ .

#### 7.2 Carbon Dioxide-Water System

The value of the liquid phase mass transfer coefficient during bubble formation for the carbon dioxide-water system is lower than its value during bubble rise and the ratio of the two coefficients is about 0.43. The theory predicts a ratio of about 0.2 which is even lower than that observed experimentally.

$k_L$  during bubble formation is independent of the liquid velocity and the bubble frequency over the range studied. The value of  $k_L$  measured is about 47 cm./hr. over a water velocity range of 0.3 to 2.5 cm./second and a bubble frequency range of 0.5 to 1.0 bubble/second.

The experimental value of the transfer coefficient can be used along with the equation,

$$N''(t_f) = k_L (C_i - C_o) \int_0^{t_f} A dt \quad \text{-----} \quad (6.5)$$

to estimate the amount of mass transfer occurring during the formation of



a bubble under the liquid phase controlling conditions. The area of the bubble is given by,

$$A = \frac{\pi}{4} D_o^2 + 0.66 n t \quad \text{-----} \quad (5.4)$$

For example, by using this method the amount of mass transfer occurring at 3 bubbles/second is estimated to be 0.0052 cc/sec. which is in fair agreement with the experimental values.

In additon, a rough approximation of the transfer coefficient is given by the modified penetration theory as,

$$k_L = 2 \sqrt{\left(\frac{D_L}{\pi t_f}\right) \left[\frac{0.786 D_o^2 + 0.442}{0.786 D_o^2 + 0.33}\right]} \quad \text{-----} \quad (6.2)$$

### 7.3 Ammonia-Nitrogen-Water System

The individual gas phase mass transfer coefficient during bubble formation was found to increase with the gas flow rate to the orifice. The value of the transfer coefficient was in the range of 0.25 to 0.32 gm-moles/hr-cm<sup>2</sup>-atm over a bubble frequency range of 3 to 10 bubbles/second. The water velocity in the bubble column was kept constant at 1 cm./sec. and the composition of the ammonia-nitrogen feed was maintained at about 19 percent ammonia by volume.

The gas-side transfer coefficient during bubble formation is of the same order of magnitude as that during bubble rise.

When the gas phase resistance is controlling the mass transfer occurring for a growing bubble can be estimated by using the experimental value of the coefficient into the equation,



$$N''(t_f) = k_G (p_a - p_i)_{\ell m} \int_0^{t_f} A dt \quad \text{-----} \quad (7.1)$$

Where  $(p_a - p_i)_{\ell m}$  is the logarithmic mean driving force during the formation period, and A is the area of the bubble at any time and is,

$$A = \frac{\pi}{4} D_o^2 + 0.507 n^{1.34} t \quad \text{-----} \quad (5.7)$$

In addition, the closest approximation for predicting  $k_G$  is,

$$k_G = \frac{2}{RT} \sqrt{\left(\frac{D_G}{\pi t_f}\right)} \quad \text{-----} \quad (7.2)$$





# NOMENCLATURE

- $a$  = Area,  $\text{cm}^2$ .  
 $a'$  = Interfacial area per unit volume of the dispersed phase.  
 $a_p$  = Point source ( $= \omega/4\pi$ ),  $\text{cm}^3/\text{sec}$ .  
 $A$  = Surface area of the bubble,  $\text{cm}^2$ .  
 $A_m$  = Maximum area of the bubble during formation,  $\text{cm}^2$ .  
 $A_o$  = Surface area of the rest bubble at zero time,  $\text{cm}^2$ .  
 $A(t)$  = Area at any time  $t$ .  
 $B$  = Proportionality constant in equation (2.50).  
 $c$  = Acoustic velocity in the gas.  
 $C$  = Concentration,  $\text{gm-moles}/\text{cm}^3$ .  
 $C_f$  = Concentration of solute in bubble after time  $t_f$ .  
 $C_t$  = Solute concentration at time  $t$ .  
 $d$  = Bubble diameter.  
 $d_e$  = Equivalent spherical diameter of bubble.  
 $d_f$  = Final equivalent bubble diameter,  $\text{cm}$ .  
 $D_C$  = Column diameter.  
 $D_{EG}$  = Effective dispersed phase diffusivity.  
 $D_G$  = Diffusivity in the gas phase,  $\text{cm}^2/\text{sec}$ .  
 $D_L$  = Diffusivity in the liquid phase,  $\text{cm}^2/\text{sec}$ .  
 $D_o$  = Orifice internal diameter.  
 $E$  = Fractional approach to equilibrium ( $= \frac{C_o - C_t}{C_o - C_i}$ ).  
 $h$  = Height of bubble top from the orifice surface at any time  $t$ .  
 $I$  = Total amount of gas absorbed,  $\text{gm-moles}$ .  
 $k_1$  = A constant.  
 $k_2$  = A constant.



- $k'$  = Slope of area-time curve for growing bubble,  $\text{cm}^2/\text{sec}$ .  
 $k''$  = Slope of volume-time curve for growing bubble,  $\text{cm}^3/\text{sec}$ .  
 $k_G$  = Gas phase mass transfer coefficient.  
 $k_L$  = Liquid phase mass transfer coefficient.  
 $K_G$  = Overall gas phase mass transfer coefficient,  $\text{gm-moles/hr.-cm}^2\text{-atm}$ .  
 $K_{GC}$  = Overall gas phase mass transfer coefficient,  $\text{cm./hr}$ .  
 $\ell$  = Vertical distance between rising bubble centres.  
 $m$  = Mass transfer rate,  $\text{gm-moles/sec}$ .  
 $m_f$  = Mass transfer during bubble formation,  $\text{gm-moles/sec}$ .  
 $m_f'$  = Mass transfer flux during bubble formation,  $\text{gm-moles/cm}^2\text{-sec}$ .  
 $n$  = Frequency of bubble formation,  $\text{sec}^{-1}$ .  
 $N$  = Rate of diffusion,  $\text{gm-moles/cm}^2\text{-sec}$ .  
 $N'$  = Mass transfer per unit area,  $\text{gm-moles/cm}^2$ .  
 $N''(t_f)$  = Total mass transfer during bubble formation,  $\text{gm-moles}$ .  
 $N_c$  = Capacitance number.  
 $p_g$  = Partial pressure in the bulk of the gas.  
 $r$  = Polar radius.  
 $r_o$  = Orifice outside radius,  $\text{cm}$ .  
 $r_e$  = Equivalent spherical radius.  
 $R$  = Bubble equivalent radius,  $\text{cm}$ .  
 $R_f$  = Final equivalent bubble radius,  $\text{cm}$ .  
 $S$  = Surface area of the growing bubble,  $\text{cm}^2$ .  
 $S_o$  = Surface area of the rest-bubble,  $\text{cm}^2$ .  
 $t$  = Time.  
 $t_e$  = Exposure time.  
 $t_f$  = Time of formation of bubble,  $\text{sec}$ .



- $u$  = Tangential velocity component.  
 $U$  = Velocity of rise of bubble, cm./sec.  
 $U_o$  = Velocity of gas at the orifice.  
 $U_\infty$  = Bulk liquid velocity, cm./sec.  
 $v$  = Radial velocity component.  
 $V$  = Volume of bubble,  $\text{cm}^3$ .  
 $V_c$  = Chamber volume.  
 $V_o$  = Volume of the bubble at zero time,  $\text{cm}^3$ .  
 $V_f$  = Volume of detached bubble,  $\text{cm}^3$ .  
 $V(t)$  = Volume at any time  $t$ .  
 $x$  = Constant characteristic of the system.  
 $y$  = Distance into the bulk phase normal to the interface.  
 $z$  = Distance measured in the direction of diffusion.

### Greek Symbols

- $\beta$  = Constant in equation (2.23).  
 $\delta$  = Film thickness.  
 $\theta$  = Polar angle.  
 $\mu$  = Viscosity  
 $\nu$  = Kinematic viscosity, centipoise.  
 $\rho$  = Density.  
 $\sigma$  = Surface tension, dyne/cm.  
 $\phi(t)$  = Rate of mass transfer at time  $t$ , gm-moles/sec.  
 $\omega$  = Gas feed rate to the orifice,  $\text{cm}^3/\text{sec}$ .





### Dimensionless Numbers

Pe = Peclet number,  $d_f U / D_L$ .

Re = Reynold number,  $d_f U_c / \mu_c$ .

Re<sub>o</sub> = Orifice Reynold's number,  $\rho_d U_o D_o / \mu_c$ .

Sc = Schmidt number,  $\mu_c / \rho_c D_L$ .

Sh = Sherwood number,  $k_L d_f / D_L$ .

### Subscripts

A = Component A.

c = Continuous phase.

d = Dispersed phase.

e = Equilibrium values.

g = Gas phase.

i = Conditions at interphase.

L = Liquid phase.

O = Initial condition.



BIBLIOGRAPHY

- (1) Baird, M.H.I., and Davidson, J.F., Chem. Eng. Sci., 17, 87, (1962).
- (2) Baird, M.H.I., and Hamielec, A.E., Can. J. Chem. Eng., 40, 119, (1962).
- (3) Beek, W.J., and Kramers, H., Chem. Eng. Sci., 16, 909, (1962).
- (4) Benzing, R.L., and Myers, J.E., Ind. Eng. Chem., 47, 2087, (1955).
- (5) Blokker, P.C., "Proc. 2nd Int. Cong. Surface Activity", Vol. 1, Academic Press, New York, 1957.
- (6) Bogandy, L.V., Rutsch, W., and Stranski, I.N., Chemie-Ingr-Tech., 31, 580, (1959).
- (7) Boussinesq, J., J. Math., 6, 285, (1905).
- (8) Bowman, C.W., and Johnson, A.I., Can. J. Chem. Eng., 40, 139, (1962).
- (9) Calderbank, P.H., Trans. Instn. Chem. Engrs., 34, 79, (1956).
- (10) Calderbank, P.H., Brit. Chem. Eng., 1, 206 and 267, (1956).
- (11) Calderbank, P.H., The Chemical Engineer, CE 209 October, (1967).
- (12) Calderbank, P.H., and Korchinski, I.J.O., Chem. Eng. Sci., 6, 65, (1956).
- (13) Calderbank, P.H., and Moo-Young, M.B., Chem. Eng. Sci., 16, 39, (1961).
- (14) Calderbank, P.H., and Lochiel, A.C., Chem. Eng. Sci., 19, 485, (1964).
- (15) Calderbank, P.H., and Patra, R.P., Chem. Eng. Sci., 21, 719, (1966).



- (16) Calderbank, P.H., Johnson, D.S.L., and Loudon, J., Chem. Eng. Sci., 25, 235, (1970).
- (17) Cheh, H.Y., and Tobias, C.W., I & EC Fundamentals, 7, 48, (1968).
- (18) Chu, J.C., J. Appl. Chem., 1, 529 (1951).
- (19) Coppock, P.D., and Meikeljohn, G.T., Trans. Instn. Chem. Engrs., 29, 75, (1951).
- (20) Crank, J., "The Mathematics of Diffusion", Chapter 6, 2nd Ed., Oxford, 1957.
- (21) Danckwerts, P.V., Ind. Eng. Chem., 43, 1460, (1951).
- (22) Datta, R.L., Napier, D.H., and Newitt, D.M., Trans. Instn. Chem. Engrs., 28, 14, (1950).
- (23) Davenport, W.G., Richardson, F.D., and Bradshaw, A.V., Chem. Eng. Sci., 22, 1221, (1967).
- (24) Davidson, L., and Amick, E.H., A.I.Ch.E. Journal, 2, 337, (1956).
- (25) Davidson, J.F., and Shuler, B.O.G., Trans. Instn. Chem. Engrs., 38, 144, (1960).
- (26) Davidson, J.F., and Shuler, B.O.G., Trans. Instn. Chem. Engrs., 38, 335, (1960).
- (27) Dixon, B.W., and Swallow, J.E.L., J. Appl. Chem., 4, 86, (1954).
- (28) Eversole, W.G., Wagner, G.H., and Stackhouse, E., Ind. Eng. Chem., 33, 1459, (1941).
- (29) Friedlander, S.K., A.I.Ch.E. Journal, 3, 43, (1957).
- (30) Geddes, R.L., Trans. A.I.Ch.E., 42, 79, (1946).
- (31) Griffith, R.M., Chem. Eng. Sci., 12, 198, (1960).





- (32) Groothius, H., and Kramers, H., Chem. Eng. Sci., 4, 17, (1955).
- (33) Guyer, A., and Pfitser, X., Helv. Chim. Acta, 29, 1173, (1946).
- (34) Halligan, J.E., and Burkhart, L.E., A.I.Ch.E. Journal, 14, 411, (1968).
- (35) Hammerton, D., and Garner, F.H., Trans. Instn. Chem. Engrs. Supplement, 32, 18, (1954).
- (36) Harriott, P., Can. J. Chem. Eng., 40, 60, (1962).
- (37) Haselden, G.G., and Thorogood, R.M., Trans. Instn. Chem. Engrs., 42, 81, (1964).
- (38) Hayes, W.B., Hardy, B.W., and Holland, C.D., A.I.Ch.E. Journal, 5, 319, (1959).
- (39) Heertjes, P.M., and de Nie, L.H., Chem. Eng. Sci., 21, 755, (1966).
- (40) Heertjes, P.M., Holve, W.A., and Talsma, H., Chem. Eng. Sci., 3, 122, (1954).
- (41) Higbie, R.W., Trans. A.I.Ch.E., 31, 365, (1935).
- (42) Himmelblau, D.M., and Takayuki, N., A.I.Ch.E. Journal, 13, 697, (1967).
- (43) Hughes, R.R., Handlos, A.E., Evans, H.D., and Maycock, R.L., Chem. Eng. Progr., 51, 557, (1955).
- (44) Ilkovic, D., Coll. Czech. Chem. Commun., 6, 498, (1934).
- (45) Ilkovic, D., J. Chim. Phys., 35, 129, (1938).
- (46) Jackson, R., The Chemical Engineer, CE 107, May 1964.
- (47) Johns, L.E., Beckmann, R.B., and Ellis, W.B., Brit. Chem. Eng., 10, 86, (1965).



- (48) Johnson, A.I., and Hamielec, A.E., A.I.Ch.E. Journal, 6, 145, (1960).
- (49) Kalra, H., M.Sc. Thesis, Department of Chemical and Petroleum Engineering, University of Alberta, Edmonton, Alberta, 1969.
- (50) Khurana, A.K., and Kumar, R., Chem. Eng. Sci., 24, 1711, (1969).
- (51) Kronig, R., and Brink, J.C., Appl. Scient. Res., A-2, 142, (1950).
- (52) Leibson, I., Holcomb, E.G., Cacosso, A.G., and Jacmic, J.J., A.I.Ch.E. Journal, 2, 296, (1956).
- (53) Leonard, J.H., Ph.D. Thesis, Department of Chemical Engineering, University of Pittsburgh, 1961.
- (54) Leonard, J.H., and Houghton, G., Chem. Eng. Sci., 18, 133, (1963).
- (55) Levich, V.G., "Physicochemical Hydrodynamics", Prentice-Hall, New Jersey, 1962.
- (56) Lewis, W.K., and Whitman, W.G., Ind. Eng. Chem., 16, 1215, (1924).
- (57) Licht, W., and Conway, J.B., Ind. Eng. Chem., 42, 1151, (1950).
- (58) Licht, W., and Pansing, W.F., Ind. Eng. Chem., 45, 1885, (1953).
- (59) Lochiel, A.C., and Calderbank, P.H., Chem. Eng. Sci., 19, 471, (1964).
- (60) McCann, D.J., and Prince, R.G., Chem. Eng. Sci., 24, 801, (1969).
- (61) McDowell, R.V., and Meyers, J.E., A.I.Ch.E. Journal, 2, 384, (1956).
- (62) Mahoney, J.F., Jr., and Wenzel, L.A., A.I.Ch.E. Journal, 9, 641, (1963).
- (63) Mehta, V.D., and Sharma, M.M., Chem. Eng. Sci., 21, 361, (1966).
- (64) Michels, H.H., Ph.D. Thesis, Department of Chemical Engineering, University of Delaware, 1960.



- (65) Miller, D.N., Ind. & Eng. Chem., 56, 10 (1964).
- (66) Newman, A.B., Trans. A.I.Ch.E., 27, 203 (1931).
- (67) Popovich, A.T., Jervis, R.E., and Trass O., Chem Eng. Sci., 19, 357, (1964).
- (68) Poutanen, A.A., and Johnson, A.I., Can. J. Chem. Eng., 38, 93, (1960).
- (69) Quigley, C.J., Johnson, A.I., and Harris, B.L., Chem. Eng. Symp. Ser., 16, 31, (1955).
- (70) Ramakrishnan, S., Kumar, R., and Kuloor, N.R., Chem. Eng. Sci., 24, 731, (1969).
- (71) Redfield, J.A., and Houghton, G., Chem. Eng. Sci., 20, 131, (1965).
- (72) Satyanarayan, A., Kumar, R., and Kuloor, N.R., Chem. Eng. Sci., 24, 749, (1969).
- (73) Sharma, M.M., and Mashelkar, R.A., "Absorption with Reaction in Bubble Columns", Paper presented at Tripartite Chemical Engineering Conference, Symposium on Mass Transfer with Chemical Reaction, Montreal, September, 1968.
- (74) Siemes, W., and Kaufman, J.F., Chem. Eng. Sci., 5, 127, (1956).
- (75) Skelland, A.H.P., and Wellek, R.M., A.I.Ch.E. Journal, 10, 491, (1964).
- (76) Sullivan, S.L., Jr., Hardy, B.W., and Holland, C.D., A.I.Ch.E. Journal, 10, 848, (1964).
- (77) Thorogood, R.M., Brit. Chem. Eng., 8, 164, 1963.
- (78) Toor, H.L., and Marcello, J.M., A.I.Ch.E. Journal, 4, 97, (1958).
- (79) Towell, G.D., Strand, C.P., and Ackerman, G.H., A.I.Ch.E.-I. Chem. E., Symp. Ser., 10, 97, (1965).





- (80) Valentin, F.H.H., "Absorption in Gas Liquid Dispersions",  
Ist. Ed., Spon's Chem. Eng. Series 1967.
- (81) van Krevelin, D.W., and Hoftijer, P.J., Chem. Eng. Progr., 46,  
29, (1950).
- (82) Vermeulen, T., Ind. Eng. Chem. ind. (int.) Edn., 45, 1664, (1953).
- (83) Vivian, J.E., and Behrmann, W.C., A.I.Ch.E. Journal, 11, 656,  
(1965).
- (84) Ward, D.M., Träss, O., and Johnson, A.I., Can. J. Chem. Eng.,  
40, 164, (1962).
- (85) Zieminski, S.A., and Raymond, D.R., Chem. Eng. Sci., 23, 17,  
(1968).



## APPENDIX

### A.1 Calibration of Liquid Flow Rotameters

Two rotameters R13M-25-3 and R-10M-25-3 were calibrated to measure liquid velocities ranging from 0 to 2.75 cm./sec. in a column of 20.2 cms. internal diameter.

The calibration data is given in Table 17 and the calibration curves are shown in Figure 13.

### A.2 Calibration of Gas Flow Rotameter

Matheson flowmeter No. 610 was calibrated for air and ammonia separately at 1 atmosphere and 70°F. The calibration curve is shown in Figure 14.

### A.3 Calculations for Determining $k_L$ from CO<sub>2</sub>-Water Data

As an example the data in Table 3 was used for run M8 and the calculations would be done stepwise.

1. The time period data was analysed by a computer program to calculate the sample size. This sample size was used to determine the number of bubbles to be analysed for volume and surface area on the digitizer.

The statistical formula used was,

$$N = \frac{6.61 \times 10^4}{(n - 1) (\bar{x})^2} \cdot \sum_{i=1}^n (x_i - \bar{x})^2$$



Rotameter Reading	Flow Rate	Average Liquid Velocity In Column, cm./sec.
R10M-25-3:		
10	0.5	0.12
20	1.0	0.24
30	1.5	0.35
40	2.0	0.47
50	2.5	0.59
60	3.0	0.71
70	3.5	0.83
80	4.0	0.95
90	4.5	1.06
R13M-25-3:		
10	2.66	0.63
20	5.16	1.22
30	7.65	1.81
40	10.31	2.44
45	11.68	2.75

Table 17: Liquid Flow Rotameters Calibration Data





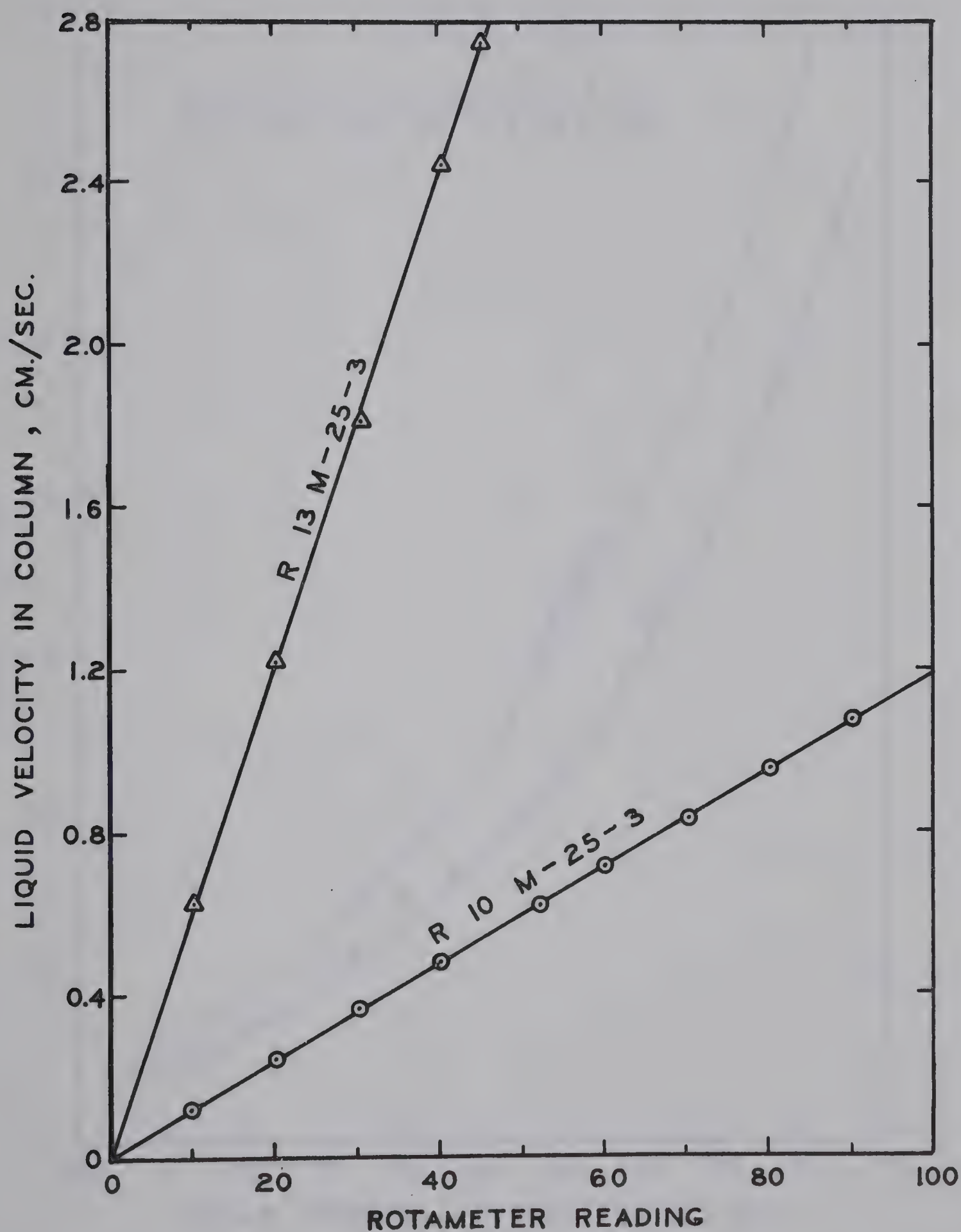


FIG. 13. LIQUID FLOW ROTAMETERS  
CALIBRATION CURVES.



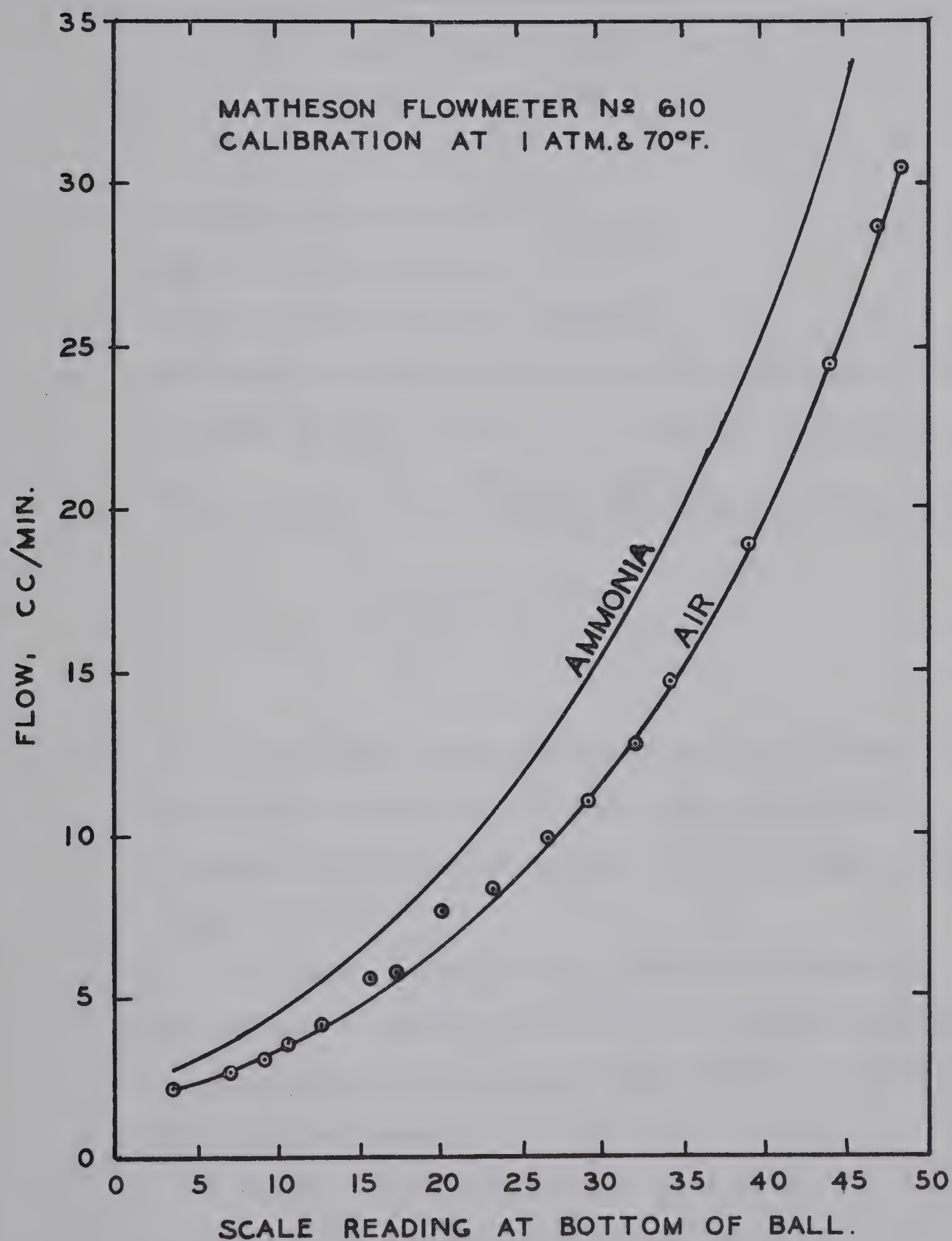


FIG. 14. GAS FLOW ROTAMETER CALIBRATION CURVE



where,  $N$  is the sample size

$n$  is the number of data points

$\bar{x}$  is the arithmetic mean time period

$x_i$  is the  $i^{\text{th}}$  time period

It gives a 99% confidence limit.

e.g. in this case  $N = 13$ .

It was decided to analyse 10 bubbles.

2. The average recorded flow rate of the gas was converted to the flow rate at orifice conditions by using the ideal gas law.

$$\begin{aligned}\text{Flow at orifice} &= \frac{15.52 \text{ (PSIA)}}{14.96 \text{ (PSIA)}} \times \frac{298 \text{ (}^\circ\text{K)}}{295.4 \text{ (}^\circ\text{K)}} \times 0.0822 \text{ c.c./sec.} \\ &= 0.0860 \text{ c.c./sec.}\end{aligned}$$

3. Ten detached bubbles were analyzed on the digitizer and the volumes and surface areas calculated numerically by using a computer program written by Kalra [49] and the mean bubble volume was found.

The bubble having a volume closest to the mean value was analyzed at various points during its formation and the calculated area from the computer was plotted as a function of time as in Figure 5.

The area under this curve was found to be,

$$\int_0^{t_f} A \, dt = 0.446 \text{ cm}^2\text{-sec.}$$





4. The CO<sub>2</sub> concentration at the interface was calculated from the solubility data.

Temperature of water = 25°C.

Assume Henry's law to hold for CO<sub>2</sub>-water.

Henry's constant,  $H = 1.64 \times 10^{-3}$

$$\text{Also, } C_i = \frac{P_A}{H}$$

where,  $C_i$  = CO<sub>2</sub> concentration at the interface,  $\frac{\text{moles CO}_2}{\text{mole soln.}}$

$P_A$  = partial pressure of CO<sub>2</sub>, atm.

The gas CO<sub>2</sub> enters the orifice saturated with water vapour and hence the partial pressure of CO<sub>2</sub> is equal to the pressure at the orifice minus vapour pressure of water at 25°C.

$$P_A = (14.96 - 0.46) \text{ psia}$$

$$= 14.5 \text{ psia}$$

$$= 0.987 \text{ atm.}$$

$$C_i = \frac{0.987}{1.64 \times 10^{-3} \times 18} \frac{\text{gm-moles CO}_2}{\text{c.c. solution}}$$

$$= 0.334 \times 10^{-4} \frac{\text{gm-moles CO}_2}{\text{c.c. solution}}$$

5. CO<sub>2</sub> concentration in the bulk of the liquid was taken as zero since 12.6 c.c. of acid was required for both the blank and water sample.
6. Mass transferred was calculated from the mean bubble volume, time period and gas flow rate at the orifice.



Mean bubble volume = 0.077 c.c.

Mean time period = 0.9604 sec.

Gas flow @ orifice from Step (2) = 0.086 c.c./sec.

$$m_f = \left(0.086 - \frac{0.077}{0.9604}\right) \text{ c.c./sec.}$$

$$= 8.94 \times 10^{-4} \text{ (gm-moles CO}_2\text{/hr.)}$$

7. Average liquid phase mass transfer coefficient,

$$\begin{aligned} k_L &= \frac{m_f t_f}{\left(\int_0^{t_f} A dt\right) C_i} \text{ cm./hr.} \\ &= \frac{8.94 \times 10^{-4} \times 0.9604}{0.446 \times 0.334 \times 10^{-4}} \text{ cm./hr.} \\ &= 57.6 \text{ cm./hr.} \end{aligned}$$

#### A.4 Calculations for Determining $k_G$ From $\text{NH}_3\text{-N}_2\text{-Water}$ Data

Sample data sheet shown in Table 4 for run N2 would be used.

Steps 1, 2, 3 were done in the same manner as for  $\text{CO}_2\text{-water}$ .

Flow at orifice = 0.3026 c.c./sec.

$$\int_0^{t_f} A dt = 0.189 \text{ cm}^2\text{-sec.}$$

Step 4. Taking a mass balance for ammonia gives,



$$\begin{aligned}
 & (\text{NH}_3 \text{ flow in} + \text{NH}_3 \text{ in rest bubble}) \\
 & = (\text{NH}_3 \text{ in detached bubble}) + (\text{NH}_3 \text{ in rest bubble}) \\
 & + \text{mass transfer}
 \end{aligned}$$

Symbolically,

$$G y_i t_f = m_f t_f + v_f y_f$$

where,  $G$  = Gas flow rate @ orifice, c.c./sec.

$y_i$  = Inlet ammonia mole fraction in gas

$y_f$  = Final ammonia mole fraction in gas

$v_f$  = Volume of detached bubble,  $\text{cm}^3$

$m_f$  = Mass transfer, c.c./sec.

$t_f$  = Formation time, sec.

$$\therefore y_f = (G y_i - N_A) / (v_f / t_f)$$

Assuming bulk liquid concentration to remain substantially zero.

Driving force for mass-transfer during bubble formation,

$$y_m = \frac{y_f - y_i}{\ln(y_f / y_i)}$$

$$\begin{aligned}
 \text{here, } y_f &= \frac{0.3026 \times 0.184 - (0.3026 - \frac{0.0805}{0.3231})}{(0.0805/0.3231)} \\
 &= 0.00932
 \end{aligned}$$

$$y_m = 0.0586$$





Step 5. Average overall gas phase mass transfer coefficient,

$$\begin{aligned}
 K_{GC} &= \frac{m_f t_f}{\left(\int_0^{t_f} A dt\right) y_m} \\
 &= \frac{0.0534 \text{ (c.c./sec.)} \times 0.3231 \text{ (sec.)}}{0.189 \text{ (cm}^2\text{-sec)} \times 0.0586} \\
 &= 1.557 \text{ cm./sec.}
 \end{aligned}$$

$$\text{or, } K_{GC} = 5610 \text{ cm./hr.}$$

$$\text{Also } K_G = K_{GC}/RT$$

where,  $K_G$  is in (gm-moles)/(hr)(cm<sup>2</sup>)(atm.)

$R$  is 82.06 (atm.)(cm<sup>3</sup>)/(°K)(gm-mole)

$T$  is in °K

Hence at 25°C.,  $K_G = 0.229 \text{ (gm-moles)/(hr)(cm}^2\text{)(atm)}$

#### A.5 Bubble Area and Volume vs. Time Data for the CO<sub>2</sub>-Water System

The data are presented in Tables 18 to 24.



S. No.	Time During Bubble Formation, Sec.	Surface Area, cm <sup>2</sup>	Volume, cm <sup>3</sup>
1.	0	0.151	0.0064
2.	0.102	0.204	0.0137
3.	0.204	0.291	0.0202
4.	0.306	0.362	0.0283
5.	0.408	0.435	0.0372
6.	0.510	0.505	0.0455
7.	0.612	0.585	0.0545
8.	0.714	0.665	0.0638
9.	0.906	0.871	0.0761
10.	0.926	1.717	0.0819
11.	0.929	1.008	0.0823

Table 18: Bubble Area and Volume vs. Time for Run M6



S. No.	Time During Bubble Formation, Sec.	Surface Area, cm <sup>2</sup>	Volume, cm <sup>3</sup>
1.	0	0.146	0.0063
2.	0.101	0.180	0.0097
3.	0.202	0.215	0.0143
4.	0.303	0.286	0.0211
5.	0.404	0.361	0.0299
6.	0.505	0.534	0.0379
7.	0.606	0.605	0.0499
8.	0.707	0.621	0.0581
9.	0.808	0.721	0.0689
10.	0.949	0.900	0.0804
11.	0.970	1.154	0.0852
12.	0.973	1.020	0.0849

Table 19: Bubble Area and Volume vs. Time for Run M7





S. No.	Time During Bubble Formation, Sec.	Surface Area, cm <sup>2</sup>	Volume, cm <sup>3</sup>
1.	0	0.108	0.0057
2.	0.100	0.173	0.0105
3.	0.200	0.252	0.0174
4.	0.300	0.301	0.0230
5.	0.400	0.384	0.0326
6.	0.500	0.560	0.0407
7.	0.600	0.626	0.0508
8.	0.700	0.623	0.0584
9.	0.800	0.699	0.0670
10.	0.917	0.866	0.0794
11.	0.957	1.056	0.0827
12.	0.960	0.958	0.0827

Table 20: Bubble Area and Volume vs. Time for Run M8



S. No.	Time During Bubble Formation, Sec.	Surface Area, cm <sup>2</sup>	Volume, cm <sup>3</sup>
1.	0	0.117	0.0058
2.	0.107	0.193	0.0116
3.	0.206	0.293	0.0177
4.	0.305	0.318	0.0250
5.	0.404	0.398	0.0337
6.	0.503	0.481	0.0425
7.	0.602	0.590	0.0506
8.	0.701	0.641	0.0610
9.	0.800	0.724	0.0692
10.	0.931	0.914	0.0822
11.	0.953	1.053	0.0834
12.	0.957	0.994	0.0841

Table 21: Bubble Area and Volume vs. Time for Run M9



S. No.	Time During Bubble Formation, Sec.	Surface Area, cm <sup>2</sup>	Volume, cm <sup>3</sup>
1.	0	0.123	0.0056
2.	0.102	0.178	0.0105
3.	0.200	0.286	0.0173
4.	0.297	0.311	0.0244
5.	0.395	0.456	0.0325
6.	0.492	0.521	0.0410
7.	0.590	0.594	0.0500
8.	0.687	0.632	0.0591
9.	0.785	0.719	0.0684
10.	0.931	0.906	0.0827
11.	0.954	1.062	0.0847
12.	0.958	1.000	0.0836

Table 22: Bubble Area and Volume vs. Time for Run M10





S. No.	Time During Bubble Formation, Sec.	Surface Area, cm <sup>2</sup>	Volume, cm <sup>3</sup>
1.	0	0.147	0.0059
2.	0.165	0.159	0.0082
3.	0.331	0.194	0.0119
4.	0.496	0.232	0.0164
5.	0.662	0.289	0.0213
6.	0.827	0.361	0.0282
7.	0.992	0.415	0.0348
8.	1.191	0.574	0.0432
9.	1.389	0.553	0.0525
10.	1.588	0.645	0.0600
11.	1.786	0.719	0.0683
12.	1.985	0.798	0.0768
13.	2.059	0.865	0.0806
14.	2.112	1.035	0.0810
15.	2.116	0.990	0.0816

Table 23: Bubble Area and Volume vs. Time for Run M11



S. No.	Time During Bubble Formation, Sec.	Surface Area, cm <sup>2</sup>	Volume, cm <sup>3</sup>
1.	0	0.143	0.0061
2.	0.214	0.158	0.0077
3.	0.428	0.211	0.0139
4.	0.642	0.310	0.0206
5.	0.856	0.377	0.0280
6.	1.070	0.416	0.0357
7.	1.283	0.603	0.0455
8.	1.497	---	0.0547
9.	1.711	0.674	0.0632
10.	1.925	0.719	0.0724
11.	2.146	0.907	0.0814
12.	2.167	1.159	0.0839
13.	2.170	0.985	0.0825

Table 24: Bubble Area and Volume vs. Time for Run M12



A.6 Mass Transfer Coefficients for the NH<sub>3</sub>-N<sub>2</sub>-Water System

Run No.	$K_G$ gm-moles/hr-cm <sup>2</sup> -atm	$k_L$ cm/hr	$k_G$ gm-moles/hr-cm <sup>2</sup> -atm
N1	0.259	50.0	0.285
N2	0.229	50.0	0.249
N3	0.263	50.0	0.290
N4	0.287	50.0	0.320

Table 25: Mass Transfer Coefficients for the NH<sub>3</sub>-N<sub>2</sub>-Water System









**B29970**